2(mix)

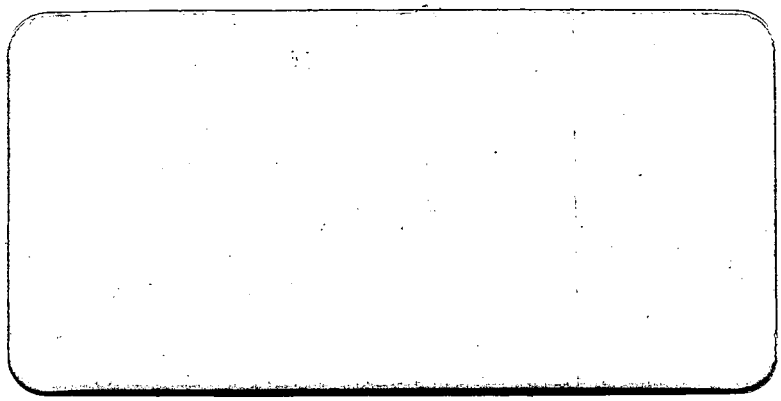

WYLE LABORATORIES
EASTERN OPERATIONS — HUNTSVILLE FACILITY

research

WYLE LABORATORIES - RESEARCH STAFF

REPORT WR 72-6

EFFECTS OF HIGH COMBUSTION CHAMBER PRESSURE ON ROCKET NOISE ENVIRONMENT

By

S. P. Pao

April 1972

Work Performed Under Contract No. NAS8-27298

WYLE LABORATORIES
EASTERN OPERATIONS, HUNTSVILLE, ALABAMA

COPY NO. 10

FOREWORD

This investigation of "Effects of High Combustion Chamber Pressure on Rocket Noise Environment" was conducted by the Eastern Operations Division of Wyle Laboratories for the National Aeronautics and Space Administration, under Contract No. NAS8-27298. Studies in this program were performed under the technical direction of Messrs. S.H. Guest and J.H. Jones of the Unsteady Gasdynamics Branch, Marshall Space Flight Center.

The author wishes to extend his appreciation to Messrs. S. Yam and D.M. Lister for their excellent work of developing computer programs for rocket noise predictions, and to Dr. M.V. Lowson of the University of Technology, Loughborough, England, for his consulting during the course of this program. Most of the technical discussion in Section 4.0 of this report was prepared by Dr. Lowson.

ABSTRACT

In this report, the acoustical environment for the high chamber pressure engine has been examined in detail by using both convention methods and advanced theoretical analysis. The influence of the elevated chamber pressure on the rocket noise environment is established through the increases of exit velocity, flame temperature, and changes of basic engine dimensions. As compared with previous large rocket engines, the overall sound power level is found to be 1.5 dB higher if the thrust is the same. The peak Strouhal number has shifted about one octave lower to a value near 0.01. Other important findings related to apparent sound source location and directivity patterns have also been reached in this study.

TABLE OF CONTENTS

LIST OF FIGURES

LIST OF FIGURES (Concluded)

1.0 INTRODUCTION

The high chamber pressure engine is one of the advanced propulsion systems which meets the requirements of the Space Shuttle booster and orbiter stages. At elevated chamber pressures, the combustion process is permitted to proceed at a higher temperature, and more thermal energy in the combustion produces can be recovered as mechanical energy. For engine operations in the atmosphere, the high chamber pressure further permits a higher expansion ratio across the nozzle without penalties of over-expansion.

The engine performance parameters for the high p_c engine are significantly different from those of the large rocket engines currently in use. With these changes in performance, corresponding changes in the acoustic characteristics of the exhaust flow can be expected. The principal objectives of this investigation are to predict the high p_c engine noise environment and to compare it with those of conventional rocket engines.

According to the conventional methods of rocket noise prediction, the overall noise environment depends only on parameters such as the exit velocity, exit diameter, and overall mechanical power. Several key properties of rocket exhaust noise can be represented in nondimensional form:

- The spectral function of overall noise emission,
- The apparent sound source location as a function of frequency,
- Directivity patterns, and
- Acoustic power as a function of overall mechanical power.

Previous experimental measurements have verified that these nondimensional properties of the noise environment collapsed quite well over a large collection of large and small rockets.

There are several reasons that the accuracy of these nondimensional properties of rocket noise should be reexamined. Firstly, according to theories of aerodynamical noise radiation, the noise environment of a high speed jet exhaust is mainly governed by the convection velocity of the turbulent flow. Temperature of the jet is also known to have some effects on the characteristics of the noise field. For the liquid or solid fuel rocket engines developed prior to the high p_c engine, the exit velocity is limited mainly in the 7000 fps to 9000 fps range. The Mach number is normally in the order of 3 to 3.5. However, the high p_c engine has a typical exit velocity of approximately 13,000 fps, which is almost twice the lower speed limit for previous rocket engines. Furthermore, the flame temperature and the local speed of sound in the exhaust flow are also much

higher for the high p_c engine. Secondly, the Space Shuttle is a reusable system which may experience 50 to 100 missions during its service life time. For an economical standpoint, it is necessary to define the acoustical environments as accurately as possible such that the vehicle system will not be penalized by excessively conservative designs owing to the uncertainties in the dynamical excitation levels. In addition to the above practical requirements, it seems also timely to undertake a basic study to identify the key mechanisms of rocket noise generation, and their trends of variation with changes of the turbulent exhaust flow parameters. Analysis related to this problem is rather scarce in the literature, and increased knowledge in understanding the basic rocket noise mechanisms is definitely required for accurate predictions of the shuttle vehicle noise environment.

In this report, the immediately expected characteristics of the high p_c engine noise environment have been established through conventional methods. Following this initial analysis, an extensive numerical study, based on the generalized aerodynamical noise theory, has been undertaken to evaluate the fundamental characteristics of high p_c noise environment. Important conclusions have been arrived at in the following areas:

- Overall noise spectrum
- Sound source location
- Directivity patterns, and
- Source strength distribution along the exhaust flow.

In this report, Section 2.0 is a discussion of the performance characteristics of the high p_c engine and the mean flow characteristics of the rocket exhaust. Section 3.0 is an initial analysis of the characteristics of the overall noise environment by using conventional methods of rocket noise predictions. In Sections 4.0 through 6.0, a theoretical analysis of the high p_c engine noise characteristics is reported. It begins with a discussion of turbulence structures in a turbulent jet in Section 4.0, followed by the presentation of the numerical results of noise prediction in Section 5.0, and finally, the conclusions are summarized in Section 6.0. Various tabulated numerical results are documented in the Appendix.

2.0 CHARACTERISTICS OF THE HIGH CHAMBER PRESSURE ENGINE AND THE FLOW STRUCTURE

Advanced propulsion systems with a high combustion chamber pressure have some clear advantages for uses in the booster stage of the Space Shuttle vehicles. An important effect of increased chamber pressure is to elevate the heat of reaction and the adiabatic flame temperature through inhibition of endothermic decomposition (Reference 1). The higher pressure of combustion and expansion reduces losses associated with energy trapped in dissociated species. This effect favors mixture ratios close to the stoichiometric value and combustion at higher temperatures (see Figures 1 and 2). Without the higher pressure, the gain in combustion temperature will be penalized by excessive and unrecoverable deposition of energy in dissociated species. The undesirable increase in molecular weight of the combustion product is not of sufficient importance to override the advantages associated with the decreased endothermic decompositions or increased exothermic recombinations.

If the rocket is to operate within an atmosphere, increased chamber pressure will premit an increase in expansion ratio without the losses owing to overexpansion which would be encountered at lower chamber pressures. For a fixed vehicle diameter and thus a maximum nozzle exit area, higher area ratios are obtained at higher pressures simply because the throat area decreases for fixed mass flow. This effect indeed contributes to increased performance for both atmospheric and space operations.

In reviewing the effects of chamber pressure upon propellant performance, in this case as expressed in terms of specific impulse, one must be careful to identify those parameters which are held constant. If the pressure ratio across the nozzle is a constant, the effect of chamber pressure is a minor one. Increasing the chamber pressure from 100 to 10,000 psia produces less than a two second change in the theoretical specific impulse for the hydrogen/oxygen system. A more meaningful presentation of the effect of chamber pressure is obtained by examination of sea level specific impulse at a fixed expansion ratio in terms of the area ratio rather than the pressure ratio of the nozzle. The advantage of increasing chamber pressure is pronounced. To summarize, the advantage of high chamber pressure at a fixed area ratio in terms of specific impulse is obtained only in operating under atmospheric conditions, that is, with a significant ambient pressure. Under vacuum ambient conditions, any apparent increase in specific impulse associated with increased chamber pressure must be associated with increasing the nozzle expansion ratio and is in reality independent of the chamber pressure.

The enthalpy is dependent upon both the temperature and the pressure through composition changes. Large enthalpy increases at moderate temperatures are associated with decomposition reactions. The value of increasing the propellant temperature to produce dissociation for the purpose of taking advantage of large propellant enthalpies will be great if the enthalpy so invested can be recovered in the expansion process. In a high p_c engine, such recovery is greatly enhanced.

A chamber pressure effect of probable significant importance but as yet ill-defined is related to the acceleration of reaction kinetics at elevated pressure. Increased pressures in the combustion chamber should speed reaction kinetics and favor production of equilibrium combustion products which in turn yields increased performance. Similarly, the gases in the nozzle will be at higher pressures and, thus, the exothermic three body recombination reactions will be accelerated. The transition from equilibrium to frozen flow in the nozzle should thereby be delayed and specific impulse increased. Although the transition zone in a high p_c engine will be located significantly further downstream from the throat, it will still be inside the nozzle. Under the accelerated recombination conditions, most of the available energy in the combustion process becomes available to the flow as mechanical energy. Residue thermodynamical and chemical kinetic fluctuations in the exhaust flow will be at a minimum.

It is precisely this latter property that simplifies the conditions under which the noise predictions are to be made for the high p_c engines. The temperature or entropy fluctuations in a high p_c engine exhaust flow should actually be no stronger than those in a conventional rocket exhaust. Hence the change in acoustical environments as produced by the rocket engine should be mainly associated with Mach number, exit velocity, temperature profile, and the evolution of the jet structure along the axis of the jet.

The engine performance data for the high chamber pressure engine are given in Table I. Those corresponding parameters for the F-1 engine are also given in the same table for direct comparison. In reference to the F-1 engine, the chamber pressure for the high p_c engine has been elevated three-fold to 3000 psia. The exit velocity has been increased from 9320 fps to 13,890 fps. For both engines, the stagnation temperature and the mass flow per unit area at the nozzle exit remain approximately the same. The overall performance of the high p_c engine is significantly higher. For the same given thrust, the exit area and the exit diameter of the high p_c engine are only 0.662 and 0.814 times the corresponding values of the F-1 engine, respectively. The specific enthalpy for the high p_c engine is much higher. Since the mass flow per unit exit area remains the same, the overall temperature in the downstream regime of the exhaust plume for the high p_c engine should also be much higher.

According to the given engine performance parameters, the structure of the turbulent exhaust plume can be predicted with reasonable accuracy by using existing methods. In Reference 2, Donaldson and Gray have developed a general method of predicting the mixing flow structure for high temperature, supersonic jet exhaust flows. The analysis is based on a mixing hypothesis where the integral effect of the turbulent mixing process is described by a so-called mixing parameter K. It was found experimentally that this mixing parameter depends only on the local Mach number in the exhaust flow, and it varies very little with the local temperature or the molecular

TABLE I. ROCKET ENGINE PERFORMANCE CHARACTERISTICS

	F-1	High p_c
Chamber Pressure	1090 psia	3000 psia
Velocity	9320 fps	13890 fps
Mass Flow Rate	5690 lb/sec	1375 lb/sec
Mach Number	3.7	4.05
Diameter at Exit	139.5 in.	68.8 in.
Expansion Ratio	16	34.6
Thrust	1,500,000 lbs	550,000 lbs
Specific Impulse	264 sec	420 sec
Nozzle Exit Area	106.1 ft^2	25.80 ft^2
Area per 10^6 lb Thrust	70.8 ft^2	40.90 ft^2
Exit Temperature	1461 K	1385 K
Stagnation Temperature	3460 K	3640 K
Exit Molecular Weight	24.8	12.5
Exit Density	0.00565 lb/cu ft	0.00388 lb/cu ft
Enthalpy Ratio (Reference to ambient air enthalpy sea level)	24	49.5

weights of the mixing species. Detailed descriptions of this method can be found in References 2, 3 and 4.

By using the Donaldson and Gray method, the exhaust flow structures for both the high p_c and the F-1 rocket engines have been calculated. The local Mach number U/c, the convection Mach number U/c_0, and the local speed of sound ratio c/c_0 along the centerline of these exhaust flows are shown in Figures 3 and 4. The spreading of the jet boundary, which is defined here as the 10% velocity point, is shown in Figure 5. Other aerodynamical parameters such as the local specific heat ratio, local molecular weight of the mixing gases, local temperature, etc., have been computed at 16 stations along the flow axis with six radial locations at each station. These values have been presented in the Appendix in tabular form.

There are a number of important differences between the structures of these two exhaust flows. For the high p_c engine, the laminar core length is about 25 D, as compared to a core length of 20 D for the F-1. Along the axis of the flow, the sonic point is located at 55 D downstream of the nozzle exit, while the convection Mach number reaches 1.0 at approximately 88 D. These locations are both further downstream from the nozzle exit than the corresponding points in the F-1 rocket exhaust flow. The above differences are quite significant from the standpoint of noise environmental studies. In previous experimental investigations, the strongest noise radiation region was found to correspond closely with the sonic point of the mixing jet flow. Hence, a change of the location of the sonic point will probably affect the noise source distribution along the axis of the exhaust flow. Furthermore, the apparent sound source location and the directivity pattern in the near-field and far-field are also dependent upon the velocity and temperature distributions in the flow domain. As the flow structure changes, corresponding changes in the sound field can be expected.

Along the entire length of the exhaust flow, the local speed of sound is much higher for the high p_c engine. In the mixing region of the flow, the higher value of the local speed of sound is caused almost entirely by the smaller molecular weight of the combustion products of the high p_c engine. Owing to the turbulent mixing mechanisms, the local molecular weight of the gas mixture in the developed portion of the exhaust flow approaches rapidly the value of the ambient air. This is true for both the high p_c and the F-1 engines. Nevertheless, the local speed of sound at $x/D = 200$ for the high p_c engine is still 40% higher than the corresponding value for the F-1 engine. This is because the specific enthalpy of the high p_c flow is twice as much as the specific enthalpy of the F-1 exhaust, while the mass flow per unit exit area remains approximately the same for both engines.

Figure 5 shows that the divergence of the flow boundary for the high p_c engine is somewhat slower than the F-1 rocket. Within the first 100 D of the exhaust plume, the flow is approximately 20% narrower. However, computations indicate that the jet boundaries for these two engines approach a common asymptotic value at stations further downstream.

In the conventional techniques of rocket noise predictions, the parameters of rocket engine performance as given in Table I would provide sufficient information for the evaluation of acoustical environment for the launch vehicle. The overall sound power, the frequency characteristics, and noise spectra at specific locations can be directly estimated. However, all these calculations depend upon predetermined spectral function of noise intensity, the apparent sound source location at given Strouhal numbers, and the directivity patterns at various frequencies. The accuracy of these empirical functions is directly related to the precision and relevance of the experimental data from which the empirical functions are derived. For the high p_c engine, parameters such as convection Mach number and local temperature are significantly different from the large rockets currently in use. Hence, there is a compelling need to examine the possible changes in these empirical standards.

In Reference 5, applications of the generalized aerodynamical noise theory to rocket noise prediction have been discussed in detail. By using this theory, the characteristics of the acoustic environment for hot, supersonic jets can be computed provided that the mean flow parameters of the exhaust flow and the characteristics of the turbulence structure are assumed known. By means of the Donaldson and Gray method of free jet mixing computation, the mean flow parameters for the rocket exhaust flows can be predicted in great detail. However, there is no satisfactory way to define the turbulence structure in a supersonic free jet. In Reference 5, a model of the turbulence structure has been assumed. It is interesting to note that the general noise radiation characteristics have been reproduced with considerable accuracy.

In the present study, a detailed computer program has been developed for rocket noise calculations. The entire rocket exhaust flow is divided into a large number of small volume elements. Noise radiation from each volume element is then computed. The summation over a given set of the volume elements or over all the volume elements will then represent the noise radiation from a certain segment of the jet, or the overall noise radiation from the entire flow. The results of computation and the associated discussions will be given in the later portion of this report.

3.0 ESTIMATION BY CONVENTIONAL METHODS

A number of methods have been developed in the past decades for practical applications of rocket noise predictions (References 6 to 10). One of the most useful and detailed approaches of rocket noise prediction was first developed by I. Dyer (Reference 6), and later refined by Wyle Laboratories (Reference 9) and Wilhold, et al. (Reference 10). In this approach, four basic characterisitcs of the rocket noise environment are considered to be universal nondimensional functions:

The Spectral Function — The spectral function represents the spectrum of overall noise produced by the entire rocket exhaust flow. The frequency coordinate is normalized in the form of Strouhal number. The sound power density can be represented in several forms. Both constant bandwidth and one-third octave band spectral density may be used. The magnitude of the spectral density can be normalized against the overall acoustical power or to the mechanical power of the rocket exhaust flow itself. In the method of Wyle Laboratories, the spectral function is given in terms of one-third octave band level relative to overall sound power, while in the Wilhold method, the spectral function is given in terms of sound power density per unit Strouhal number per total mechanical power of the rocket propulsion system. The shape of the spectral function is determined empirically from data of rocket noise measurements.

Apparent Sound Source Locations — For noise radiation at a given Strouhal number, most of the acoustical power comes apparently from a fixed location in the exhaust flow. The assignment of such locations along the exhaust flow has been studied extensively by dimensional analysis and experimental measurements. Results from various investigations vary greatly, as can be seen from Figure 6 . Since the actual sound source at a given Strouhal number is distributed rather than concentrated as a point source, the apparent source location can not be uniquely defined. Hence, in each method of rocket noise prediction, the assignment of sound source location is highly arbitrary.

Directivity — The spectral function represents only the total sound power density which is a sum of acoustical energy radiated into all directions. The directivity pattern indicates the distribution of acoustical energy as a function of direction, and it varies with frequency. In most rocket noise prediction methods, the directivity patterns are given for specific ranges of frequencies instead of Strouhal numbers. This is rather unfortunate because such representation would only be valid for a pre-determined class of rockets. The directivity pattern in the Wyle method, which is derived from the work of Cole (Reference 7), is given in Figure 7.

Overall Sound Power — According to the Lighthill theory, the acoustical power of a supersonic jet should be directly proportional to the mechanical power of the jet exhaust flow itself. However, the proportional constant

does vary within a small range. The acoustical power can be 0.002 to 0.0048 times the mechanical power of the rocket exhaust flow. For most of the large operational rockets, this ratio is very close to 0.003. For small rockets, the acoustical power efficiency tends to decrease with the decrease of the overall mechanical power. A typical curve is shown in Figure 8 .

At any given location on the vehicle, the sound pressure level spectrum can be computed by using the above nondimensional functions and appropriate scaling factors. Other effects such as shielding, ground effect, deflector configuration, and air absorption must also be taken into account.

By using the above approach, some of the basic characteristics of the high p_c engine noise environment become immediately evident. For convenience, the engine performance parameters and the acoustical properties of the F-1 rocket engine are chosen as the basis for comparison in the following discussion.

The mechanical power of a rocket exhaust flow is half of the product of the thrust and the exit velocity. For the high p_c engine, the exit velocity has been increased by a factor of 1.47. Hence, if both the thrust and the acoustic efficiency were kept constant, the acoustic power level will be higher by the same factor. A factor of 1.47 is equivalent to an increase of 1.6 dB.

According to Table I, the high p_c engine is also much more efficient in terms of thrust per unit nozzle exit area. Here, if the thrust were kept constant, the nozzle exit area of the high p_c engine will be smaller by a factor of 0.662, and the effective nozzle diameter will be smaller by a factor of 0.814. By taking into account both the change in exit velocity and effective nozzle diameter, the peak frequency of a high p_c engine propulsion system, which has the same thrust as the propulsion system of the F-1 engines, will be higher by a factor of 1.8. This is slightly less than an increment of one octave.

According to experimental data obtained so far on the high p_c engine and other jets with very high velocities, changes in the basic rocket noise characteristics have been observed. First of all, the one-third octave band spectrum of the overall noise radiation from the high p_c engine peaks at above $Sn = 0.01$. This is clearly lower than the peak Strouhal number for the conventional rockets. Furthermore, the peak region of the spectrum is broader, and beyond the peak the PWL declines with frequency at a much smaller rate. The shift of peak Strouhal number toward lower values is consistent with previous measurement. In the early rocket noise measurements, the exit velocity of a typical rocket engine is approximately 7600 fps (Reference 7). The nondimensional one-third octave band sound power spectrum peaks at a Strouhal number greater than 0.030. Later measurement for rocket engines, such as F-1, the peak Strouhal number was found to be near 0.020. It is not too surprising to find that the high p_c engine has yet a lower peak Strouhal number.

In earlier rocket noise measurements, the directivity has a highly directional radiation pattern for the higher frequencies. Most of the acoustic energy is in the direction between 60 to 80 degrees from the downstream flow axis. It is surprising to find from Saturn and other high speed jet experiments (References 10 and 11) that the directivity pattern for high frequencies tends to be less directional and more uniformly distributed in all directions.

As far as the scaling laws are concerned, there are only two important considerations: the definition of Strouhal number, and the overall acoustic power as a function of the total mechanical power of the propulsion system. In the class of large rockets, the power efficiency will probably not change by any significant amount. On the other hand, there have been many ways to define the Strouhal number:

- Normalization against the jet exit velocity fD/U
- Normalization against the ambient speed of sound fD/c_0
- Normalization against the true Mach number at the nozzle:

  $$\left\{ fD/U \right\} \cdot \left\{ c_e/c_0 \right\} = fD/c_0 M$$

- Normalization against the speed of sound in the exhaust flow fD/c_e.

Each definition is intended for a better data collapsing for the spectral function. In the author's opinion, the first definition is perhaps most convenient. It is interesting to note that the third definition seems to agree quite well with the analysis of the generalized aerodynamical noise theory (Reference 5).

4.0 CHARACTERISTICS OF JET TURBULENCE

The noise radiation from a high speed jet exhaust is dependent on the nature of turbulent flow field. In turn this turbulent field arises from, and governs the development of, the mean flow. The principal objective of the present report has been to specify the relationship between noise and the exhaust parameter. Hence for practical application to the study of high p_c engine it is necessary to define accurately both the mean flow and the turbulence.

A substantial body of work is now available on the mean flow characteristics of jet exhausts. Calculation of the mean flow invariably requires assumptions as to the nature of the turbulent transfer mechanisms within it, and a wide range of models have now been tested against the available mean flow data, although rather little comparison of compressible flow cases has been accomplished. Only relatively simple integral parameter descriptions are necessary for these mean flow predictions. Although some properties of the turbulence related to noise predictions can also be represented in terms of simple functions of mean flow properties, the degree of refinement of description of the turbulence structure for noise prediction purposes is considerably higher. Inspite of extensive experimental efforts devoted to the measurement of jet turbulence structures, data is only available in the subsonic range. As far as supersonic jet turbulence is concerned, one can only infer some of its properties by using hypotheses (Reference 12); by comparison with the turbulence structure measured in related flow conditions such as boundary layer and wake flow; and, ironically, by deriving simple integral properties of the turbulence from the mean flow developments of supersonic jet exhausts.

Hence in this section, the first part reviews the various possible assumptions on the nature of turbulent mixing, with emphasis on their implications for noise prediction. Based on a somewhat small collection of work on jet turbulence measurements, the second part of this section therefore reviews the existing data. The discussions in this latter part will be concentrated mainly in the definition of the integral spatial and time scales of the turbulence structure and the magnitude of the turbulent intensity.

4.1 The Turbulent Mixing Assumption

It is probably worthwhile to give the primary equations governing the flow of a compressible turbulent jet, through which various parameters of turbulent mixing are defined. For the axisymmetric case, the continuity equation is

$$\frac{r\partial \rho u}{\partial x} + \frac{\partial r \rho v}{\partial r} = 0 \qquad (1)$$

and the momentum equation is

$$\rho u r \frac{\partial u}{\partial x} + \rho v r \frac{\partial u}{\partial r} = \frac{\partial \tau r}{\partial r} \tag{2}$$

where a cylindrical coordinate system is used. Equations (1) and (2) may be integrated with respect to r to give

$$\tau_1 = \frac{\partial}{\partial x} \int_0^{r_1} \rho u^2 r dr - u_1 \frac{\partial}{\partial x} \int_0^{r_1} \rho u r dr \tag{3}$$

In Equation (2) τ is the Reynolds stress given by

$$\tau = - \overline{\rho u v}$$

and in Equation (3) τ_1 is the value of the Reynolds stress evaluated at the location r_1. The key to the solution of this equation is to establish a method for the prediction of $\tau = \overline{\rho u v}$. It is noteworthy that $\rho u v$ also appears as the principal quadrupole source strength in the noise generation equations. Thus calculations of both noise and mean flow require evaluation of virtually the same dynamic quantities. There are two subtle differences between these cases, however. Firstly, the noise case requires evaluation of $\rho u_i u_j$ and thus includes the diagonal terms of the Reynolds stress tensor like ρu^2 as well as $\rho u v$. Secondly, the shear stress affects the mean flow only through its mean, while it affects the noise through its mean square value.

Nearly all methods of calculating shear flows rely on some form of the momentum transfer theory. As shown in Reference 17, the assumption that momentum is a transferable quantity allows the expression for shear stress to be written as

$$\tau = - \overline{\rho u v} = \ell' v \frac{\partial \rho u}{\partial y} \tag{4}$$

where ℓ' is a "mixture length". An extension of these arguments leads to the possibly more familiar form of Prandtl's mixing length

$$\tau = \rho \ell^2 \left| \frac{\partial u}{\partial y} \right| \frac{\partial u}{\partial y} \tag{5}$$

where the mixing length ℓ is not equal to the mixture length ℓ' .

It is worth noting that the form derived for Equation (4) includes a density term in the differential. In all the formulae derived hereafter the density term is taken outside the differential. To the writer's knowledge no momentum transfer theory has used the density differential even for compressible cases, and this may justify further study.

An alternative approach is to model the turbulence stress system in the same way as the viscous stress system, by defining

$$\tau = \rho \nu_T \frac{\partial u}{\partial y} \tag{6}$$

where ν_T is an "eddy viscosity". Eddy viscosity models for turbulent flows have tended to be rather inaccurate predictions, but are often used because of their simplicity. For example, Prandtl suggested putting

$$\nu_T = K b \Delta u \tag{7}$$

where b is a width scale, Δu is the velocity difference across the shear layer and K is an empirical constant of order 0.01. This formulation has the advantage that eddy viscosity is assumed constant across any jet station, and thus only varies with axial position. Several other models for eddy viscosity have been put forward. Useful evaluation and reviews are presented by Harsha (Reference 14) and Rotta (Reference 15).

For much of the work in the present report the method of Donaldson and Gray (Reference 2) is used to predict the rocket exhaust profiles. Donaldson and Gray used an eddy viscosity model of the Prandtl form, Equations (6) and (7), for the turbulent shear stress:

$$\tau = K \rho b u_5 \frac{\partial u}{\partial r} \tag{8}$$

The value of u_5 is taken to be half the difference between centerline and external flow velocities, and b equals to the radial distance between the centerline (or the edge of the core r_i) and the half velocity point r_5 . A Gaussian form for the velocity profile was assumed for the developed region of the jet. For the core region, similar assumption was made. At the edge of the core, a discontinuity in the slope of the profile was allowed. Hence, there may be some objections as to the assumptions made by Donaldson and Gray about the flow profiles. On the other hand they did allow a full evaluation of the effects of compressibility and for a full range of possible exhaust gas parameters. Reasonably acceptable agreement of the prediction with experiment

was found. It is worth noting that the computation and the comparison with experiment showed that the effects of compressibility and heat transfer in the equations are dominant, with details of the turbulent exchange model being of lesser importance. Extensions to the work of Donaldson and Gray would appear to be valuable at least because the detailed flow parameters required for noise prediction are extremely difficult to measure in a real rocket exhaust flow.

4.2 Details of the Turbulence Structure

Virtually all jet noise calculation models have assumed the turbulence to be isotropic. Indeed the major part of all theoretical work on turbulence is based on isotropic assumptions. The resulting simplifications are normally a prerequisite to further calculation. However, the isotropic assumption is violated by shear flows. Lateral and longitudinal turbulent intensities are not found to be equal. The isotropic assumption also implies zero mean Reynolds stress, but it is just the stress effects of the turbulence which dominate the development of the mean flow. The ratio of mean Reynolds stress to turbulent energy has been found by Harsha (Reference 14) to be 0.3. One of the first estimates of Reynolds stress, by von Karman as reported in Reference 13, indicated a ratio $\overline{\rho u v} / \overline{\rho u^2}$ of 0.33.

However, there is some evidence that the subsonic jet turbulence is isotropic. Turbulence scale measurements from a number of publications are summarized in Table II. The isotropic model requires that all longitudinal scales (that is, those measured in the same direction as the velocity component), are equal. The isotropic model also requires that the lateral scale to be one-half of the longitudinal. These conditions are approached by the data rather well.

For supersonic flows, isotropic structure for the turbulence is much less evident. It has been reported that the ratio of longitudinal to transverse scale can be as high as 10 to 18, which far exceeds a value of two for the isotropic assumption (References 16 and 17).

Analytically, prediction of jet noise requires knowledge of the turbulence in such great details as the space-time-correlation functions or the wavenumber-frequency-spectra of the turbulent fluctuations. Such measurements have been undertaken by Chu (Reference 18) for a subsonic jet. In that case, the correlation function can be represented as an analytical function by curve fitting. In Reference 19, it is found that the noise prediction for quantities such as spectrum, source location, etc., are not particularly sensitive to the details of the turbulence. The most important parameter is, rather, the integral spatial and time scales. Recently, it is found in Reference 5 that the directivity of sound radiation does depend on the source spectrum. However, satisfactory prediction of directivity can be obtained if the source structure were specified within reasonable limits. A moderate amount of data is now available on the length scale of the axial velocity component, and this is plotted on Figures 9 and 10.

TABLE II. LONGITUDINAL AND TRANSVERSE INTEGRAL SPATIAL SCALES OF JET TURBULENCE

Bradshaw, Ferriss, and Johnson $x/r_0 = 4$ M = 0.3 D = 2" y/r = 1				
	r, 0, 0	0, +r, 0	0, -r, 0	0, 0, r
R_{11}	0.0445	0.033	0.024	0.0064
R_{22}	0.015	0.044	0.048	0.038
R_{33}	0.012	0.016	0.024	0.087

Chu $x/r_0 = 8$ M = 0.127 D = 4" y/r = 1			
	r, 0, 0	0, r, 0	0, 0, r
L_x/D	0.191	0.138	0.023
L_{45}/D	0.168	0.187	0.025
L_{60}/D	0.144	0.223	0.048
L_x/D	0.0477	0.0345	0.0057
L_{45}/D	0.042	0.0467	0.0062
L_{60}/D	0.038	0.0557	0.012

Data from several experiments (References 20 through 22) indicates that the ratio L_x/x reduces with axial distance. Typically beyond the end of the core region ($x/D = 5$). Against this must be set the data of Bradshaw, Ferris and Johnson (Reference 23), and of Chu, who both found a substantially lower value of scale than the other workers, around $L_x/x = 0.5$. Furthermore, data taken by Wygnanski and Fiedler (Reference 24) indicates a value of L_x/x somewhat larger than 0.05. (Wygnanski and Fiedler also found a variation of scale across the jet.) Laurence's data was some of the first taken and there are obvious inconsistencies in his data beyond $x/D = 5$. However, the differences between the other two groups of experimenters are less easy to explain. The Davies, Fisher and Barrett results were based on a one inch diameter jet and may suffer from a scale effect due to boundary layer development in the nozzle. However, Sami's results were taken on a 12 in. diameter jet. Nevertheless the data of Bradshaw, et al., and Chu apparently represent the results of considerable care and have been given more weight here. Thus it is concluded that turbulent scale L_x is equal to about $0.065\,x$ over the whole length of the jet. The variation with radius is unimportant and is ignored.

Turbulent intensities in the jet flow are a strong function of position. Many workers have presented data on the fluctuating velocities, but the most useful data for the present purposes was taken by Tu (Reference 25). Curves taken from his report (Figures 40, 41 and 42) give the magnitude of the three components of turbulent intensity at various stations down the jet.

It will be observed that the curves have peak intensity in line with the nozzle lip at $x_2/D = 0.5$ over almost the whole length of the jet exhaust flow. Near the end of the jet core ($x_1/D = 4.0$) the u component turbulent intensity reaches a maximum of $0.16\,u_j$, while the v component reaches around $0.12\,u_j$ and the w component reaches $0.13\,u_j$. There is a weak tendency towards increased isotropy further away from the jet axis, but the data of Wygnanski and Fiedler reveals no tendency toward increased isotropy along the jet axis. Wygnanski and Fiedler's data is of value because it was taken very far down the jet, and therefore provides a good basis for interpolation. In the initial region of the jet the turbulence is a maximum at the point of maximum shear in the jet, while far downstream it is at a maximum on the centerline. It is of particular interest that in each case the maximum intensity is around 27% of the local velocity at that point.

Thus a useful empirical method for predicting peak turbulence intensity is to assume that it is simply 0.27 of the velocity at a point in line with the nozzle lip ($x/D = 0.5$). This simple model is found to hold with remarkable accuracy over the whole length of a subsonic jet. The rather minor variations of the v and w components of intensity from this model can probably be ignored.

From this point of view of noise radiation, an important role is played by the moving axis time scale L_t, which appears to the fourth power in the Pao-Lowson analysis based on the Lighthill jet noise model. Lighthill suggested that this time scale was inversely proportional to the turbulence intensity, and thus is found on a reinterpretation of the results of Davies, Fisher and Barrett, as shown by Lowson and Pao (Reference 19). It was found there that

$$L_t = 0.76\, L_x/u_0$$

The data of Wygnanski and Fiedler for the jet far downstream suggests that, approximately

$$L_t = 0.25\, L_x/u_{rms}$$

so that there is some experimental indication that time scales involve rather more complex parameters than turbulent intensities alone. However, in the absence of any more complex experimental information little more can be said.

Theoretically, the most useful hypothesis appears to have been advanced by Morkovin (Reference 12) who assumed that the turbulent structure was essentially unchanged in high speed flow unless the local turbulent velocities were themselves supersonic. For the characteristic jet exhaust flows studied here this would correspond to exit convection Mach numbers of around 7.0.

Some indication of the possible effects can be found by returning to the mean flow models considered at the beginning of this chapter. The shear stress models essentially involve assuming that turbulent intensity is proportional to a typical velocity divided by a typical (transverse) scale. One of the simplest models was used by Eldred (Reference 26), who assumed a full mixing length expression of the form

$$\tau = \rho k c^2 b^2 \left| \frac{\partial u}{\partial r} \right| \frac{\partial u}{\partial r}$$

where b is a local transverse scale parameter appearing in the Gaussian shape, assume k is a mixing coefficient to be determined, and $c = \ell/b$ where ℓ is a "mixing length".

Eldred indicates that ℓ is two-thirds of the lateral scale, which is just one-third of the longitudinal scale L_x for isotropic turbulence. Thus

$$c = L_x/3b$$

Also, Eldred finds that, on solution of the momentum equation

$$\frac{x_c}{r_e} = \frac{0.32}{k c^2}$$

where x_c is core length, r_e is exit radius, and $k = 0.88$.

Using these results gives:

$$L = 1.8\, b \sqrt{\frac{r_e}{x_c}}$$

For a low speed jet exhaust, at the core tip $b = r_e$ and $x_c/r_e \approx 10$, so that scale there is predicted to be $0.57\, r_e$, in comparison with the $0.65\, r_e$ predicted from the empirical formula $L_x = 0.065\, x$ given earlier. Thus some agreement between theory and experiment is found.

But the significance of the result is less in the absolute magnitudes predicted than in the general trend. Core length increases markedly with increasing Mach number, and the model above indicates that scale will vary as the inverse square root of this, causing a reduction in scale at supersonic speeds. It appears that a similar interpretation applied to the Donaldson and Gray eddy viscosity model would result in a variation of scale as the inverse first power of core length. Certainly shadowgraph pictures suggest a finer grained structure to the supersonic turbulence, but it is shown that such indications cannot necessarily be taken literally.

Donaldson and Gray's model takes:

$$\tau = K \rho r_5 \frac{U}{2} \frac{\partial u}{\partial r}$$

and essentially includes a single power of scale L in the K term. Donaldson and Gray's results do show a reduction in K by a factor of as much as 2, and this could be taken to indicate an equivalent reduction in scale in the compressible case.

The value of $\alpha = L_x/U\, L_t$ would not show an equivalent reduction following the argument that time and space scales are related through turbulent intensity. But again little information on turbulent intensity is available, so that this conclusion cannot be relied on absolutely.

To summarize then, the effect of compressibility on turbulent intensity, and on the ratio of time to space scales is not expected to be great, but there is evidence that scale is somewhat reduced. For the present work in which the Donaldson and Gray work is used extensively, it is recommended that L_x be taken proportional to K.

5.0 NUMERICAL PREDICTION OF THE HIGH p_c ENGINE NOISE CHARACTERISTICS

One of the most important objectives of this report is to determine the high p_c engine noise characteristics through analytical calculations. At the present time, data collected from the high p_c engine is not in sufficient quantity to clearly define its differences with conventional rocket exhaust flows. Without knowing the trends of noise characteristics as a function of exhaust speed, flame temperature, or chamber pressure, it is not feasible to extrapolate the existing rocket noise data to predict the high p_c engine noise with sufficient accuracy.

In this report, the generalized aerodynamical noise theory is employed to predict the noise environment. The required formulae and details of this method have been reported recently in Reference 5 , and these discussions will not be repeated here. As discussed in earlier parts of this report, an accurate noise prediction requires the knowledge of mean flow and turbulence properties of the entire rocket exhaust. The mean flow properties can be computed by the Donaldson and Gray method with reasonable accuracy. The following assumptions have been made for the turbulence structure:

- The local turbulent integral spatial scale is 0.6 of the local turbulent jet thickness. The thickness is defined as the width of the mixing zone in the core region, and the radius of the jet in the transition and developed regions.

- The wavenumber-frequency spectrum of the turbulence structure is assumed to follow a power law, as given in Reference 5. The non-dimensional ratio of spatial to time scale α , is assumed to be 0.30. It remains constant throughout the exhaust flow. In the high supersonic sections of the exhaust, the turbulence structure is assumed to be anisotropic with a longitudinal to transverse scale ratio of 2. In the downstream regions, the structure is assumed to be isotropic.

- The turbulent intensity of velocity fluctuations is the most difficult quantity to define, since no experimental indication is available. It is therefore defined arbitrarily for given axial stations:

$$(\overline{u_1^2})^{\frac{1}{2}} = 0.16\, c \qquad \text{if} \qquad M \geq 1$$

$$(\overline{u_1^2})^{\frac{1}{2}} = 0.16\, U_1 \qquad \text{if} \qquad M < 1$$

where $(\overline{u_1^2})^{\frac{1}{2}}$ represents the local maximum of turbulent intensity, c is the local speed of sound, U_1 is the local maximum axial velocity, and M is the true Mach number at the same axial station.

The profile of the local turbulent intensity across the jet is assumed to be a Gaussian distribution. Furthermore, the source intensity is modified also by a factor $(K/K_0)^{\frac{1}{2}}$, where K is the local mixing parameter, and K_0 is the mixing parameter at zero convection Mach number.

The inability to define the turbulent intensity of velocity fluctuations precludes the prediction of overall sound power from the jet. However, an indicative sound source distribution along the exhaust flow can be computed. Detailed discussions will be given later in this section.

A comprehensive noise prediction program has been developed in the present study. The entire rocket exhaust flow is divided into many small volume elements for which the mean flow properties are first computed. By using the computed mean flow properties and the assumed properties of the turbulence, noise radiation from each volume element is computed. Calculations have included the following properties of noise radiation

- Directivity
- Local spectrum of radiation
- Relative magnitude of overall sound power

The program permits summation of noise contribution from volumes in a section of the jet, or a summation over all the volume elements in the jet. In the former case, the following information can be obtained:

- Characteristic frequency at a given section
- Noise spectrum from a section of the jet
- Spectrum as a function of direction
- Sound source location - overall noise
- Apparent source location as a function of direction
- Source strength distribution along the jet axis.

In the latter case, the following can be obtained:

- Directivity as a function of frequency
- The far-field noise spectrum

These results will be discussed in the remainder of this report, calculations have been made for both the high p_c engine and the F-1.

5.1 Local Noise Radiation Characteristics

At a given station along the exhaust flow, the cross-section of the jet is divided into six annular volume elements. Noise radiation from each element is computed according to the local mean flow and turbulent properties, and the results are summed over these six elements. In the core region, volume of the core is excluded from the calculation, and the region between the edge of the core to the boundary of the jet is divided into six parts.

Sound radiation intensity at a given Strouhal number is computed from 0 to 180 degrees at 2 degree intervals, and the integrated acoustic power over all directions has also been computed. The directional pattern of the acoustical intensity is given in the computer output only at 60, 90, 120 and 150 degrees. The computed results are given in tabular form in the Appendix. A total of thirteen frequencies are investigated at each station, and a total of 16 stations are studied for both the high p_c and F-1 rocket exhaust flows. The ranges of computation are summarized in Table III.

The overall noise spectra and the spectra at 150° are presented for the F-1 exhaust flow (Figure 11) and the high p_c exhaust (Figure 12). A number of important conclusions can be observed from these figures. Firstly, the shape of the spectrum changes with the characteristic convection velocity at each section. For sections with very large convection Mach numbers, the spectrum has a "plateau" region which spans across frequencies of over a decade. The peak frequency location is rather sensitive to a small change of the slope in the plateau region. For smaller convection Mach numbers, the width of the peak region decreases. The spectral shape of the local noise radiation resembles the spectrum of low speed jet exhaust flows. Secondary, it is interesting to note that the upstream radiation spectrum has a very large shift toward lower frequencies in relation to the overall spectrum. Although this phenomenon is expected from a theoretical standpoint, it is the first time that such spectra are computed.

The local spectra for the high p_c exhaust and the F-1 flow do not appear to be much different at a casual review. However, along the main noise production region of these flows, the high p_c exhaust flow has a larger number of "flat top" spectra than the F-1 exhaust flow. This is mainly because the characteristic velocity in the high p_c exhaust flow is much higher. Since the overall noise spectrum is a sum of all the local spectra, it is expected that the overall noise spectrum for the high p_c engine has a broader peak region than the F-1 engine noise. This is, indeed, the result of the overall noise computation which will be given later in this section.

According to the peak frequency at each station, the sound source location can be established, as presented in Figure 13. It is surprising to find from this figure that the computed sound source location for the high p_c and the F-1 engines are extremely close

TABLE III. RANGES OF COMPUTATION

Frequencies $2\pi Sn$	0.00125, 0.0025, 0.005, 0.010, 0.020, 0.040 0.080, 0.160, 0.320, 0.640, 1.280, 2.560, 5.120
Axial Stations x/D	5, 10, 15, 20, 25, 30, 35, 40, 50, 60, 80, 100, 120, 160, 200, 240
Directional Pattern at: Degrees	OVERALL, 60, 90, 120, 150.

together. Indeed, the source locations for radiations in the 150 degree direction actually coincide for these two cases. Source locations as defined by this method are actual source location. If the wave propagation path through the jet exhaust flow were also taken into account, then the observed, or "apparent" source location should lie further downstream. The source locations as given in Figure 13 are re-plotted in Figure 14. The derived apparent source locations are shown in dashed curves. On the same graphs, two sets of experimental curves are also shown. The first is taken from Mull, et al. (Reference 27) and the second set is taken from Smith (Reference 11). The predicted source location agrees extremely well with these experimental evidences.

The directivity at the peak frequency of each section have been computed for both engines. The results are shown in Figures 15 and 16. The comparison of these directivity patterns with experimental data in the high frequency and the very low frequency ranges has been found to be very favorable (Reference 5). This is perhaps a good indication that noise emission at such Strouhal number ranges comes mainly from the neighborhood of the apparent source location.

The sound source location in the 150 degree direction has very important practical implications. The acoustical pressure fluctuations received at the space vehicle itself are mainly upstream radiations. The 150 degree angle is quite typical. Hence, the apparent sound sources should appear to be much further upstream than the measured apparent source locations. Furthermore, one must keep in mind that the 150 degree source location can not be measured by techniques such as the traversing microphone method. In such measurement, the results are always dominated by the downstream radiations at the same frequency but a much higher intensity. The 150 degree source locations will be completely masked. It is interesting to note that the source location assignment in the Wilhold method is quite close to the 150 degree curve in the low Strouhal number range, and it is close to the overall predicted curve in the higher Strouhal number range. This would have been also a logical choice if the above arguments are taken as the basis.

In spite of the inadequate definitions of the intensity of turbulence, the computed sound source strength distributions are shown in Figure 17. In both cases, the sound source strength per unit length of the jet increases initially with the distance from the nozzle exit. A maximum is reached near the sonic point of the exhaust flow. Beyond the peak source location, the acoustic power drops rapidly. The rate of decline is much larger than x^{-7}. This is mainly because the mean flow velocity along the centerline of the jet decays at a rate much faster than the x^{-1} relationship, which is commonly assumed in previous analytical studies. In view of the excellent agreement of source location predictions, the fast rate of decline of the source strength distribution, as predicted here, is perhaps very close to reality.

The prediction of sound source strength in the core region is perhaps too low. For example, it could have been excessively penalized by the factor $(K/K_0)^{\frac{1}{2}}$ in the definition of the turbulence intensity. By removing this factor, the relative power level in this region will probably increase by a factor of 4, in relation to the peak.

However, this change should not alter the tendency of sound power increase as a function of the distance from nozzle exit.

5.2 Predicted Overall Noise Characteristics

The following properties of the overall noise environment have been computed for both the high p_c and the F-1 rocket engines:

- The sound power spectrum
- The overall noise directivity, and
- Directivity patterns at given Strouhal numbers.

Comparisons with data have been made. It is worthwhile to review here the restrictions of the computation. In this study, only a very simple model of turbulent intensity distribution in the exhaust flow is assumed. Figure 17 indicates that the contribution from the initial section of the exhaust flow may be underestimated. Consequently, the spectral density prediction in the high frequency end will not be accurate. The effect on directivity patterns at very high Strouhal numbers is more drastic. With an underestimation of sound power in the core region, the predicted directivity pattern at a large Strouhal number will not be dominated by radiations in the neighborhood of the apparent source location, but the "residue" radiation from the strong source region further downstream. Directivity patterns in the low Strouhal number range are also influenced to some extent by radiations from the strong source region.

Figure 18 shows the predicted one-third octave sound power spectra for the high p_c engine peaks at a Strouhal number of 0.01, and the peak Strouhal number for the F-1 engine is slightly higher at 0.020. Hence, the increase in frequency of the high p_c engine owing to a smaller diameter and a higher exit velocity is partially neutralized by a downward shift of the basic spectral function. If the noise source strength in the core region were increased to a higher value, the predicted spectrum for either rocket would become slightly broader in shape, and the levels in the high frequency range will increase by approximately one or two dB.

The predicted overall noise directivity curves are shown in Figure 19. For both engines, the upstream noise radiation patterns are almost the same. They are slightly different in the forward direction. The effect of higher convection velocity cause the peak of noise radiation to be shifted to a higher angle. Some experimental data for these rocket engines are given on the same figure (Reference 28). The agreement with the Saturn noise data is good between 30 to 90 degrees while agreement in upstream directions is rather poor. Comparison with the high p_c engine data is only fair for all directions. Further investigation in both analytical and experimental aspects of noise directivity is definitely necessary.

The directivity patterns for a range of Strouhal numbers have been predicted for the case of high p_c engines. These patterns are shown in Figure 20. Corresponding measured directivity patterns from Reference 11 are shown on the same figures. The agreement between prediction and experiment in the peak frequency range is very good. The difference is generally less than two dB. However, comparison in the mid-frequency range is not conclusive. Differences are often between 3 to 5 dB.

For Strouhal numbers smaller than approximately 0.002, the experimental data actually agrees very well with the predicted directivity in the neighborhood of the apparent source location (Figure 16). Such comparison has been made previously in Reference 5. This is perhaps an indication that the contribution from the peak source region is overestimated in the present calculation such that the true directivity for the lower frequencies have been partially masked. Further refinement of the prediction method is necessary for an accurate prediction of the detailed noise directivity characteristics.

6.0 CONCLUSIONS

In this report, the acoustical environment for the high combustion chamber pressure engine has been examined in detail by using both conventional methods and advanced theoretical analysis. The major conclusions are summarized as follows:

a) The principal influence of the high chamber pressure on the rocket noise environment is established through increases of exit velocity, flame temperature, and changes of basic engine dimensions.

b) If the thrust were held constant, the overall sound power of the high p_c engine will be approximately 1.5 dB higher than the conventional rocket sound power level.

c) The one-third octave sound power spectrum is expected to have a broad peak frequency region, and the peak Strouhal number is expected to be approximately 0.01, which is slightly lower than the observed peak Strouhal number for propulsion systems such as F-1 engines for the Saturn vehicle.

d) The sound source location for the high p_c engine has been investigated by theoretical predictions. No significant change is detected between the F-1 and high p_c engines. These computed results agree very well with the experimental data.

e) The apparent sound source locations for noise emission in the 150° direction have been computed. This is considered to have great practical significance.

f) The noise directivity patterns at various given Strouhal numbers have been computed. Excellent agreement has been obtained near and above the peak frequency range. Comparison in the lower frequencies is not conclusive. However, the numerical computations indicate that it is feasible to obtain better prediction through a refinement of the method.

REFERENCES

1. Glassman, I. and Sawyer, R.F., The Performance of Chemical Propellants, AGARDograph No. 129, 1970. Library of Congress Card No. 74-82418

2. Donaldson, C. DuP. and Gray, K.E., "Theoretical and Experimental Investigation of the Compressible Free Mixing of Two Dissimilar Gases," AIAA Journal, Vol. 4, pp. 2017-2025, 1966.

3. Radcliffe, S.W., "An Experimental Program for the Investigation of Shock-Turbulence Interaction Phenomena," Wyle Laboratories Technical Memorandum TM 68-5, 1968.

4. Gray, K.E. and Woodrow, P.J., "A.R.A.P. Turbulent, Two Gas, Compressible, Free Jet Program Documentation," Aeronautical Research Associates of Princeton, Inc., Princeton, N.J., 1971.

5. Pao, S.P., "Applications of the Generalized Jet Noise Theory," Wyle Laboratories Research Report WR 72-5, March 1972.

6. Dyer, I., "Estimation of Sound Induced by Missile Vibration," Random Vibration, (ed. S.H. Crandall), Chapter 9, MIT Technical Press, 1958.

7. Cole, J.N., et al., "Noise Radiation from Fourteen Types of Rockets in the 1000 to 130,000 Pound-Thrust Range," WADC TR 57-354, December 1957.

8. Franken, P.A. and Wiener, F.M., "Estimation of Noise Levels at the Surface of a Rocket-Powered Vehicle," Shock and Vibration Bull. No. 31, Pt. 3, pp. 27-31, 1963.

9. Sutherland, L.C., "Sonic and Vibration Environments for Ground Facilities - A Design Manual," Wyle Laboratories Research Report WR 68-2, March 1968.

10. Wilhold, G.A., et al., "Prediction of Blast and Acoustic Environments of Large Space Vehicles," Hazards Manual - The Interagency Chemical Rocket Propulsion Group, Unsteady Gasdynamics Branch, NASA/MSFC, 1968.

11. Smith, E.B., "Acoustic Scale-Model Tests of High Speed Flows," Martin-Marietta Corporation, Denver, Contract Report Martin CR-66-13, 1966.

12. Morkovin, M.V., "Effects of Compressibility on Turbulent Flows," Proceedings of the Marseille Conference on Turbulence CNRS Report No. 108, Paris, 367-380, 1962.

13. Goldstein, S., "Modern Developments in Fluid Mechanics," Oxford University Press, 1938.

14. Harsha, P.T. and Lee, S.C., "Analysis of Coaxial Free Mixing Using the Turbulent Kinetic Energy Method," AIAA Journal, Vol. 9, pp. 2063-2066, 1971.

15. Rotta, J.C., "Aerodynamics of Turbulent Shear Flow," AGARD CPP, 1971.

16. Demetriades, A., "Turbulence Measurements in an Axisymmetric Compressible Wake," Phys. of Fluids, Vol. 11, p. 1841, 1968.

17. Phillips, O.M., "Shear Flow Turbulence," Article in Annual Review of Fluid Mechanics, (ed. W.R. Sears), Vol. 1, pp. 245-264, Annual Review Inc., Palo Alto, California, 1969.

18. Chu, W.T., "Turbulence Measurements Relevant to Jet Noise," University of Toronto, Institute of Space Studies, UTIAS Report 119, 1966.

19. Lowson, M.V. and Pao, S.P., "Some Applications of Jet Noise Theory," Wyle Laboratories Research Report WR 70-4, 1970.

20. Laurence, J.C., "Intensity, Scale and Spectra of Turbulence in Mixing Region of Free Subsonic Jet," NACA Report 1292, Lewis Center, Flight Propulsion Laboratory, 1956.

21. Davies, P.O.A.L., et al., "The Characteristics of the Turbulence in the Mixing Region of a Round Jet," J. Fluid Mech., Vol. 15, pp. 337-367, Corrigendum, p. 559, 1963.

22. Sami, Sedat, "Balance of Turbulence Energy in the Region of Jet Flow Establishment," J. Fluid Mech., Vol. 29, Pt. 1, pp. 81-92, 1967.

23. Bradshaw, et al., "Turbulence in the Noise Producing Region of a Circular Jet," AGARD Rep. 450, 1963.

24. Wygnanski, I.J. and Fiedler, "Some Measurements in the Self-Preserving Jet," J. Fluid Mech., Vol. 38, pp. 577-612, 1969.

25. Tu, B.J., "On the Measurement of Turbulent Velocities u_0, u_{45}, u_{90}, u_{135}, and w in a Circular Jet," Wyle Laboratories Research Report WR 70-2, 1970.

26. Eldred, K.McK., et al., "Suppression of Jet Noise with Emphasis on the Near Field," ASD-TDR-62-578, Flight Dynamics Laboratory, Wright-Patterson AFB, Ohio, 1963.

27. Mull, H.R., et al., "Effects of Jet Structure on Noise Generation by Supersonic Nozzles," J. Acoustic. Soc. Am., February 1959.

28. Guest, S.H., Preliminary Data; Unsteady Gasdynamics Branch, NASA, Marshall Space Flight Center, 1972.

FIGURES

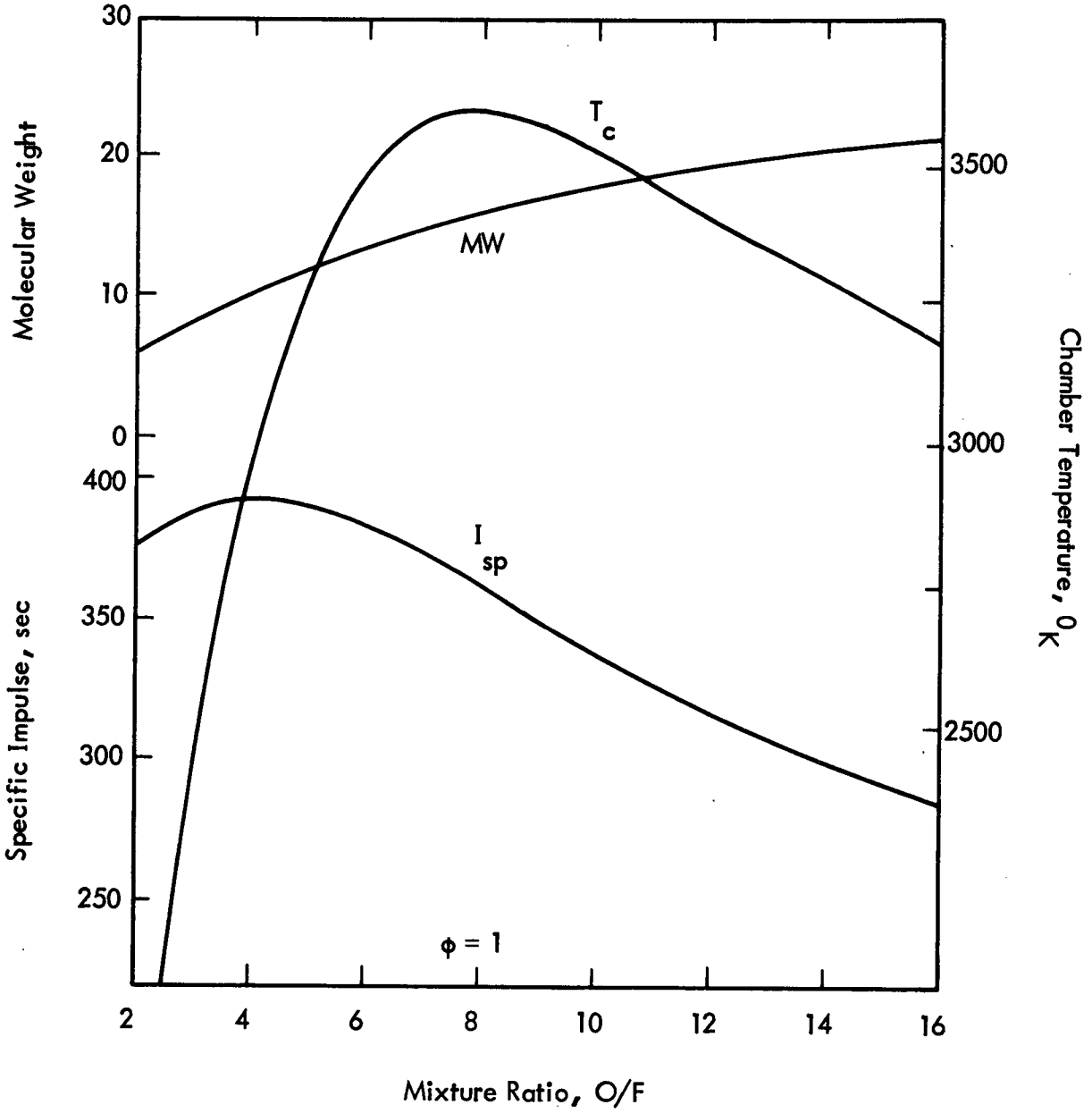

Figure 1. Hydrogen/oxygen combustion products characteristics and propellant performance. The maximum specific impulse lies at a mixture ratio between the mixture ratios of minimum molecular weight and maximum combustion temperature. p_c = 1000 psia, optimum equilibrium expansion to one atmosphere ambient pressure. (Reference 1)

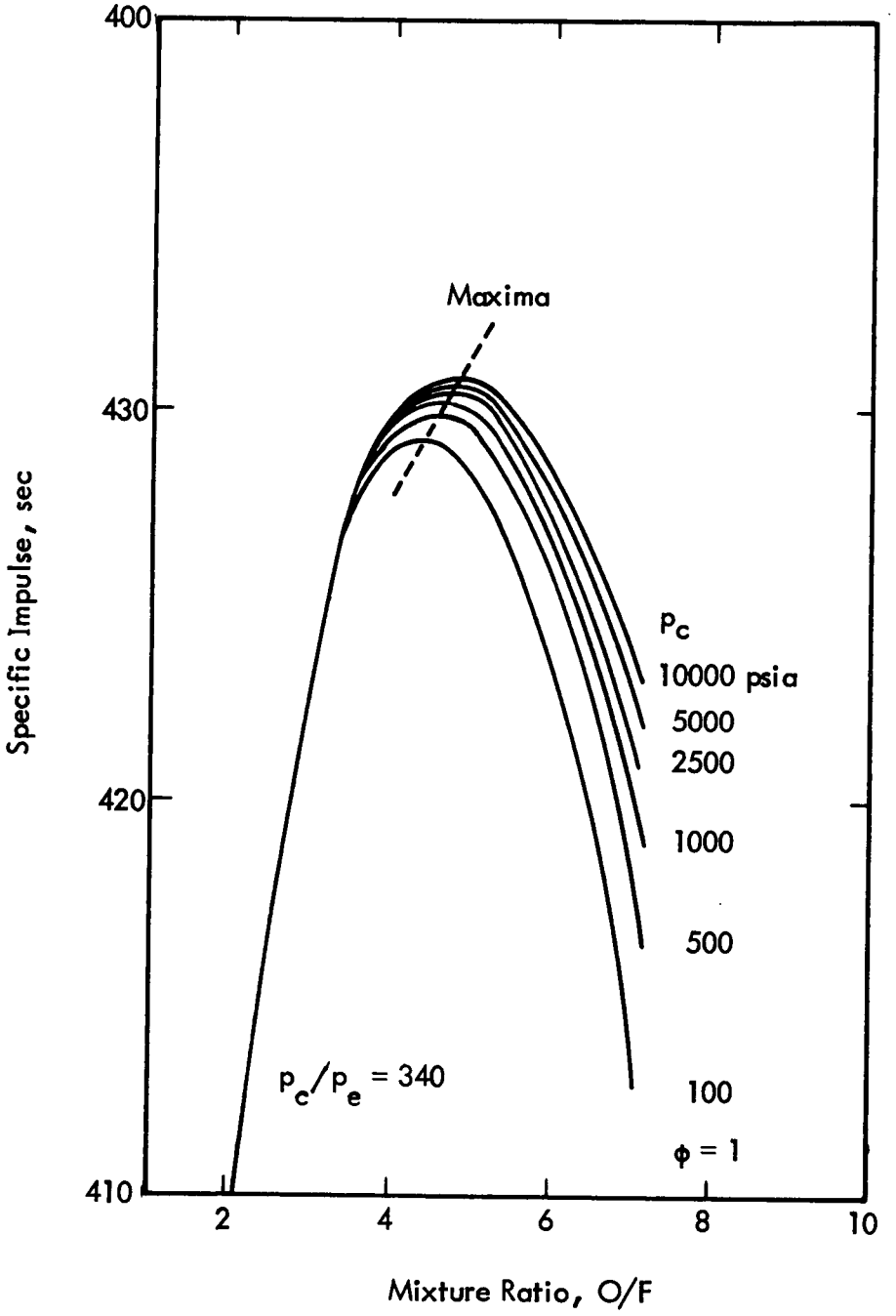

Figure 2. Theoretical equilibrium expansion performance of hydrogen/oxygen showing the effect of chamber pressure, p_c, on optimum mixture ratio. (Reference 1)

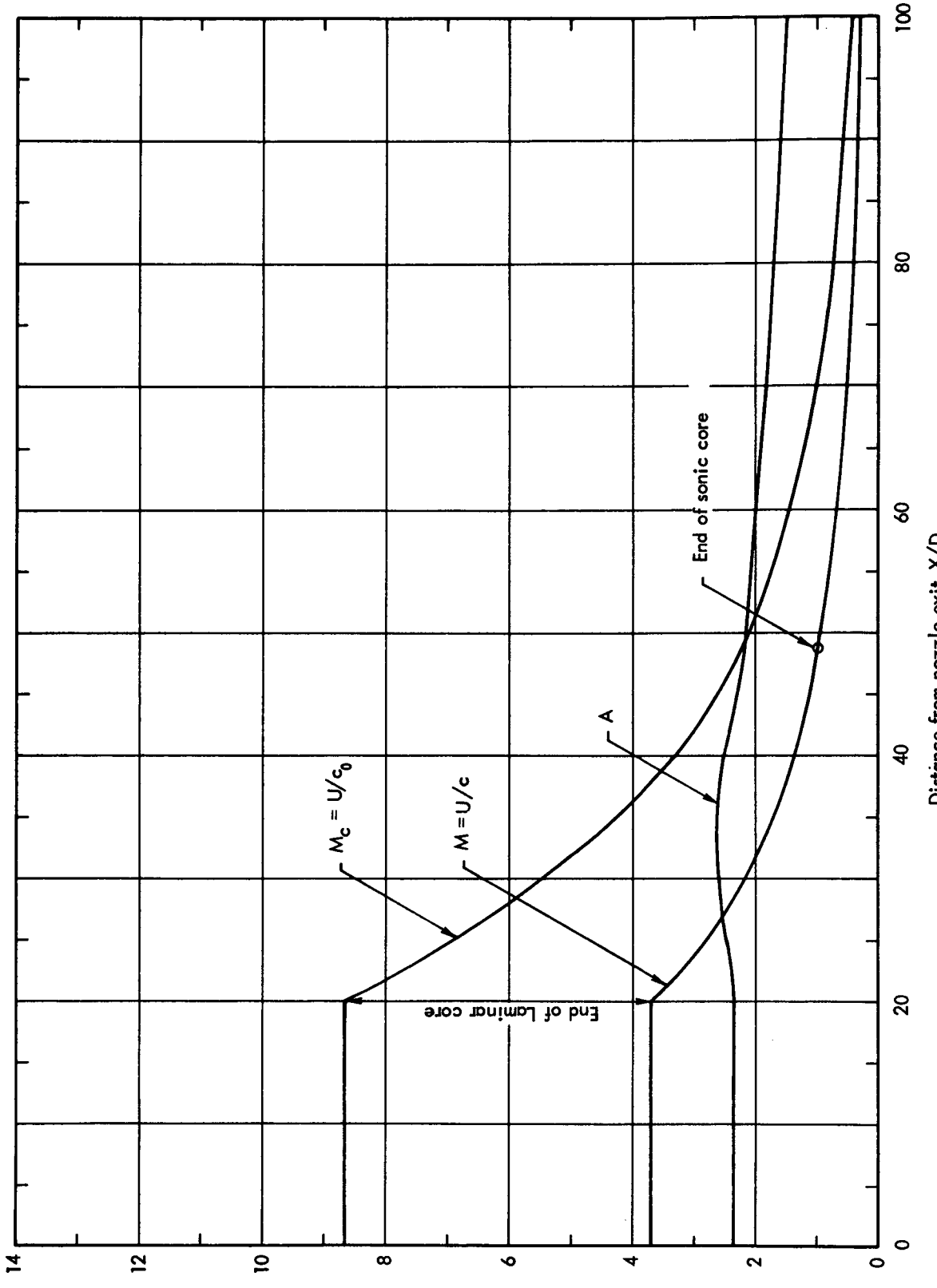

Figure 3. Important Flow Parameters for the F_1 Engine

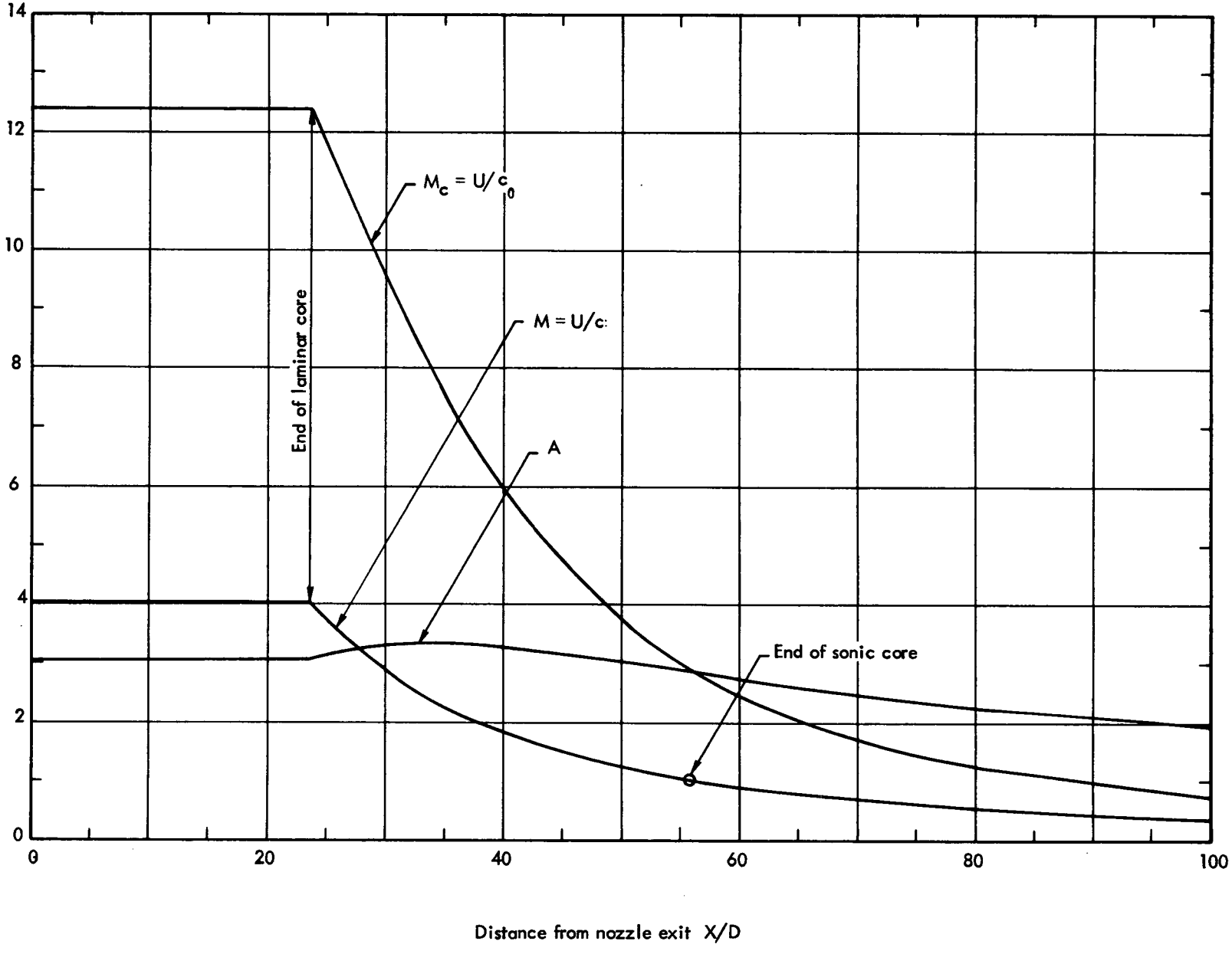

Figure 4. Important Flow Parameters for the High Chamber Pressure Engine

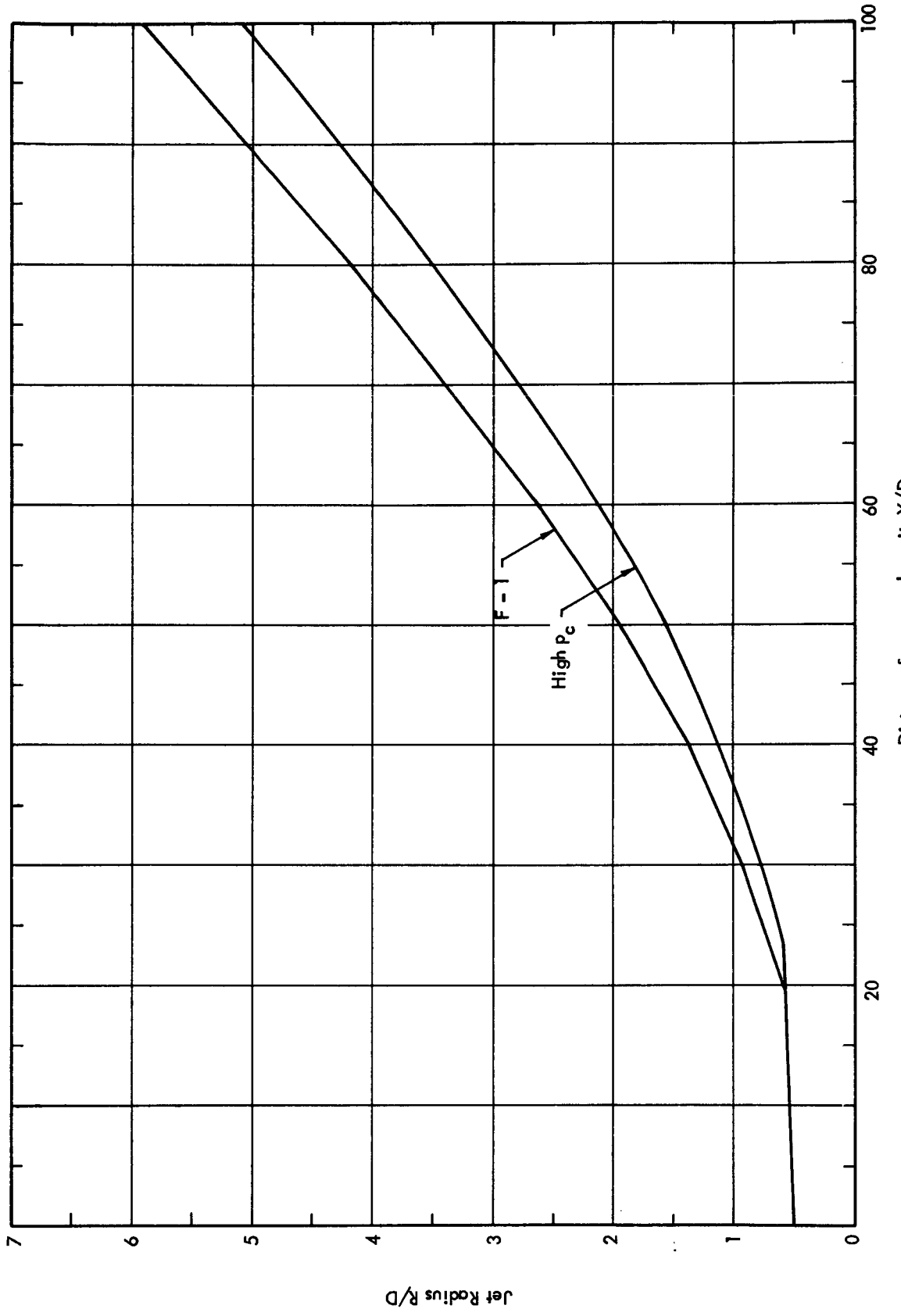

Figure 5. Expansion of Rocket Exhaust Flow Boundary

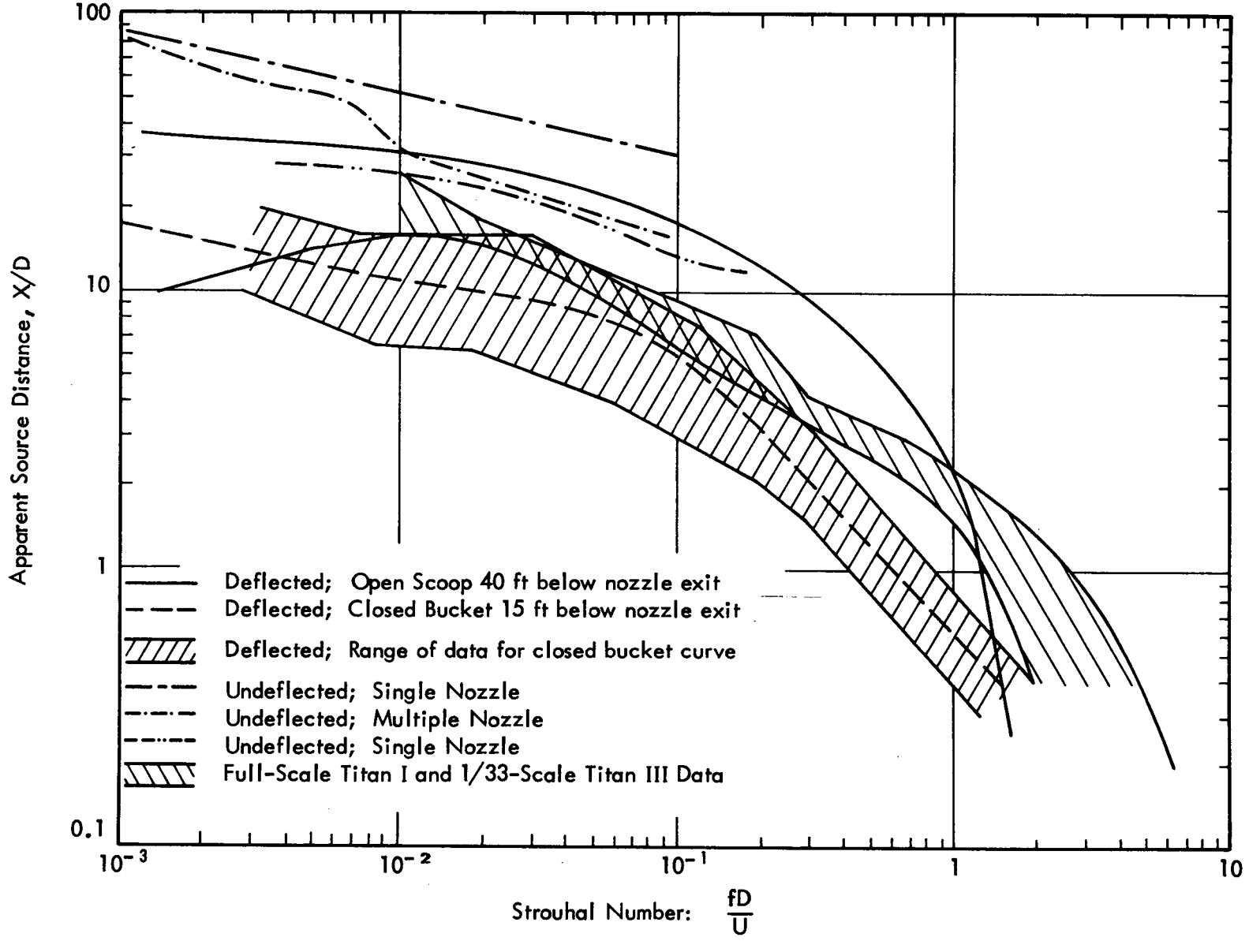

Figure 6. Apparent Source Distribution in a Rocket Exhaust Flow

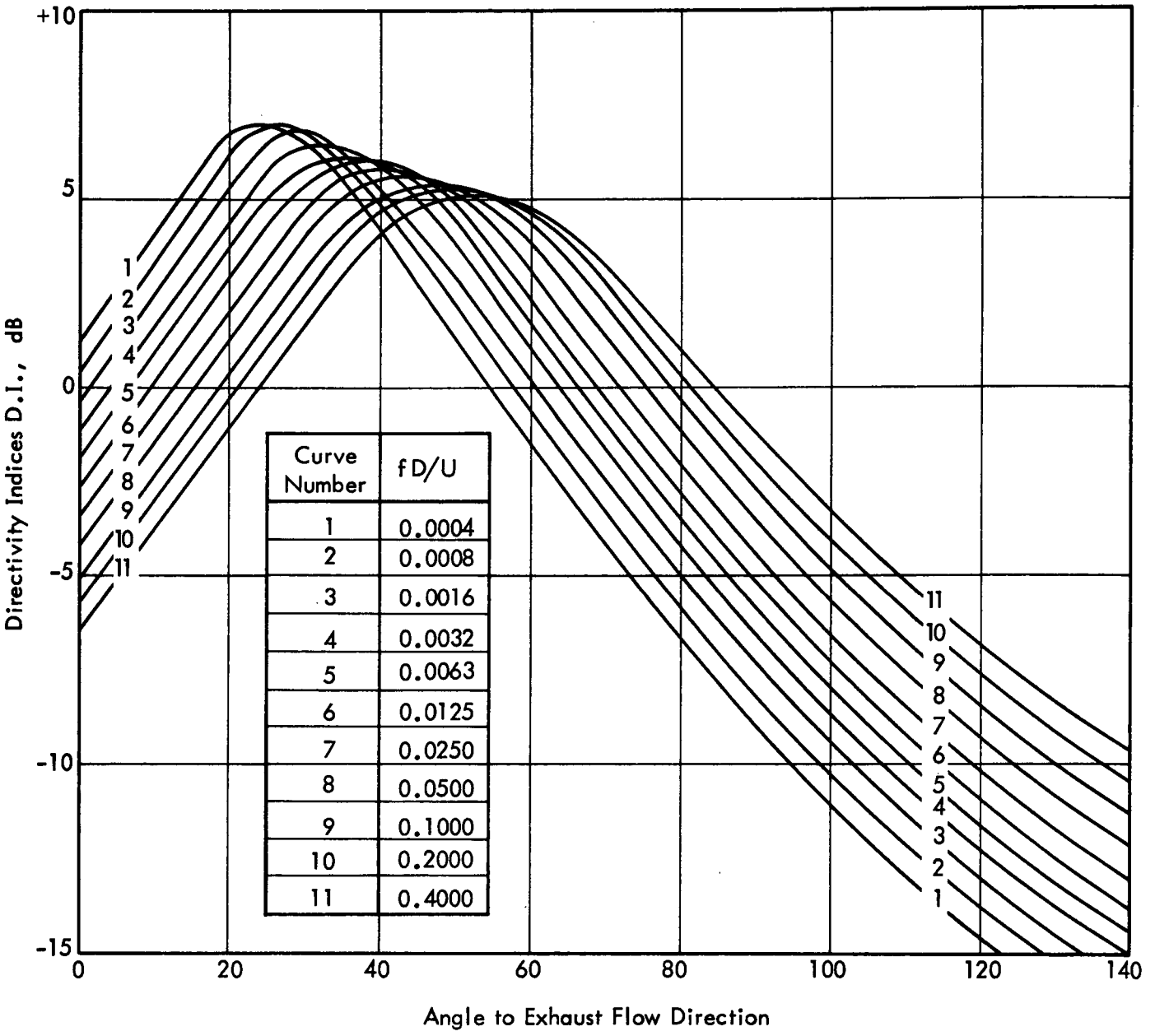

Figure 7. Far-Field Directivity Curves

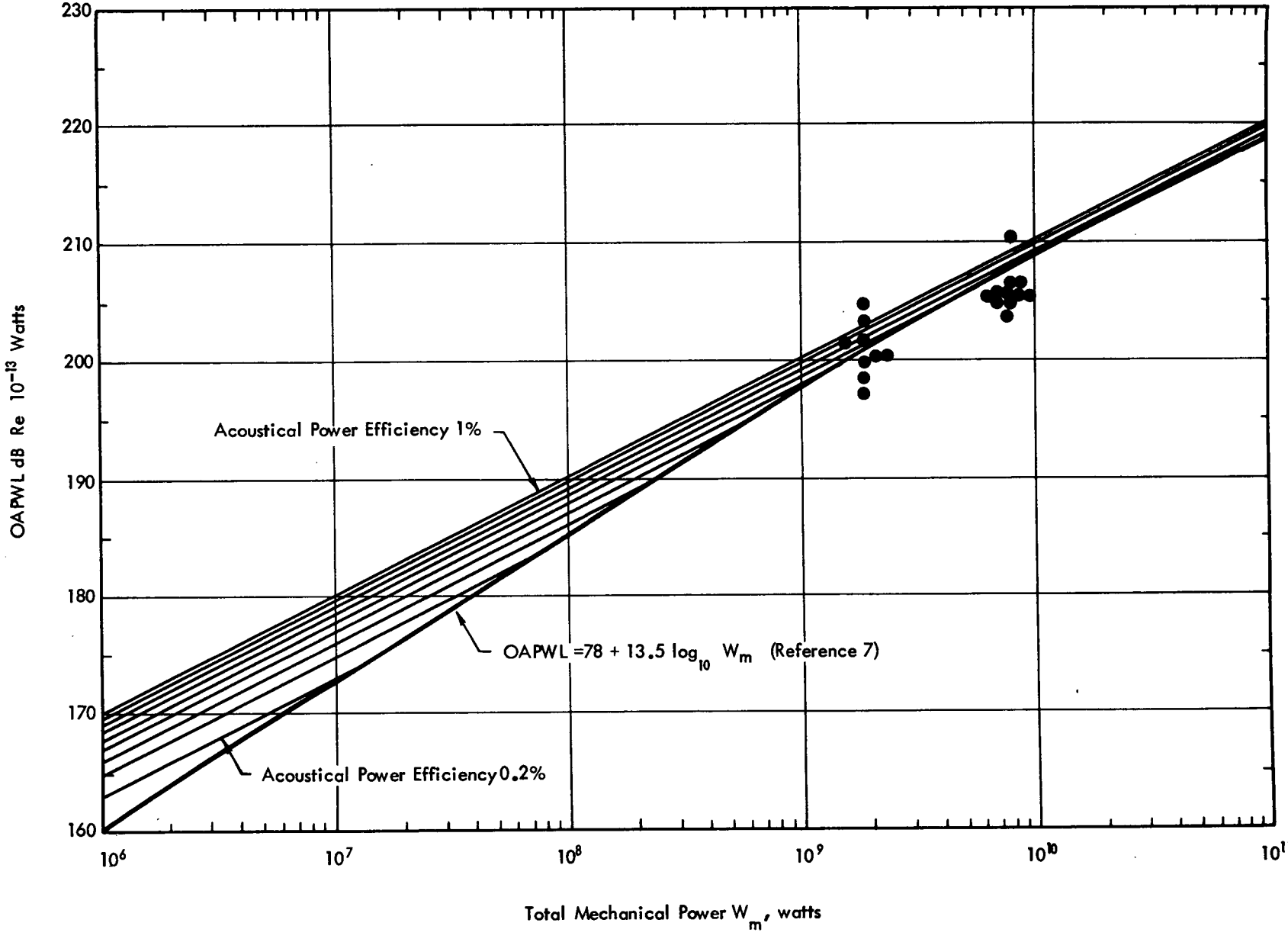

Figure 8. Overall Acoustical Power Level as a Function of Total Mechanical Power of the Rocket Exhaust Flow

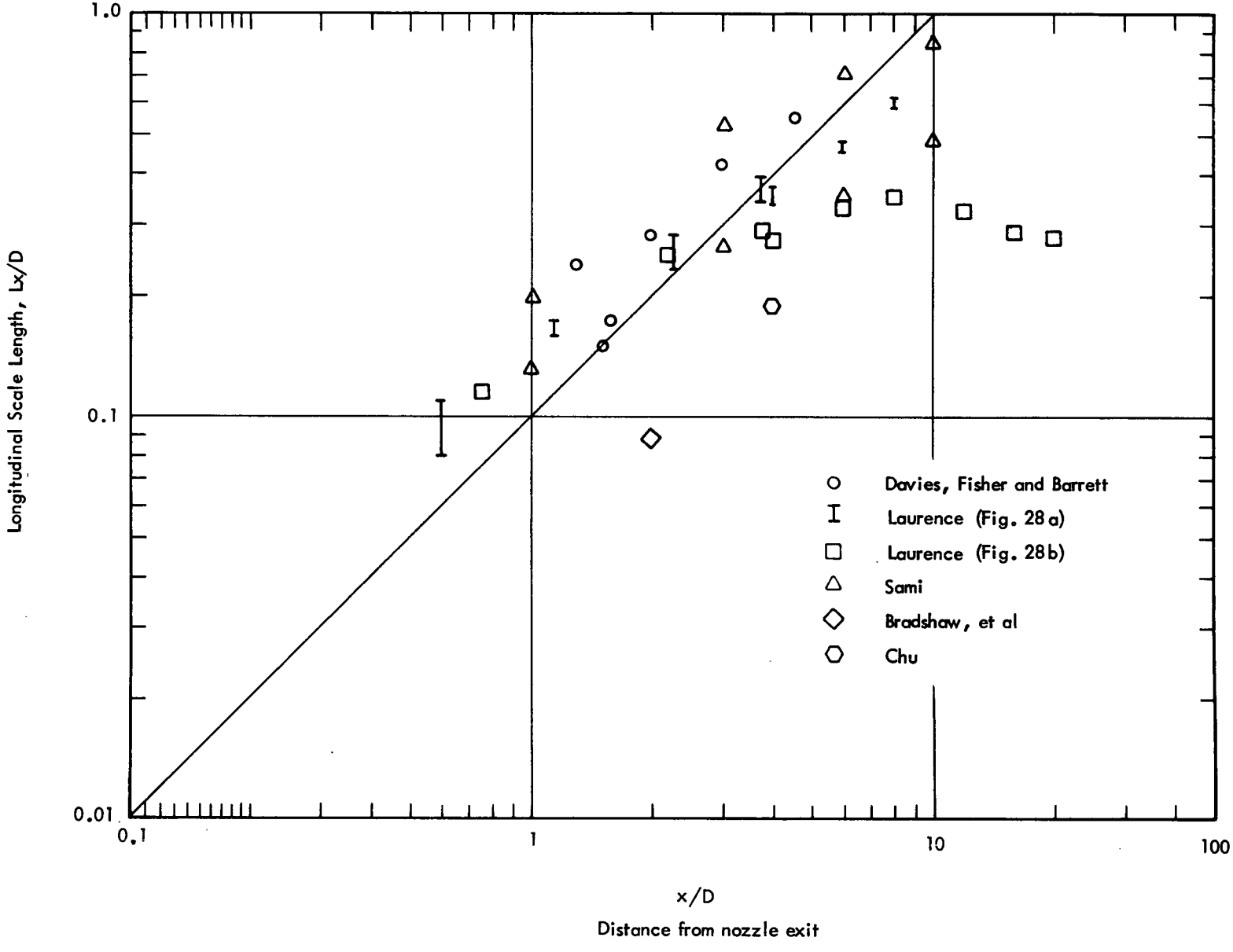

Figure 9. Longitudinal Integral Spatial Scale in the Axial Direction

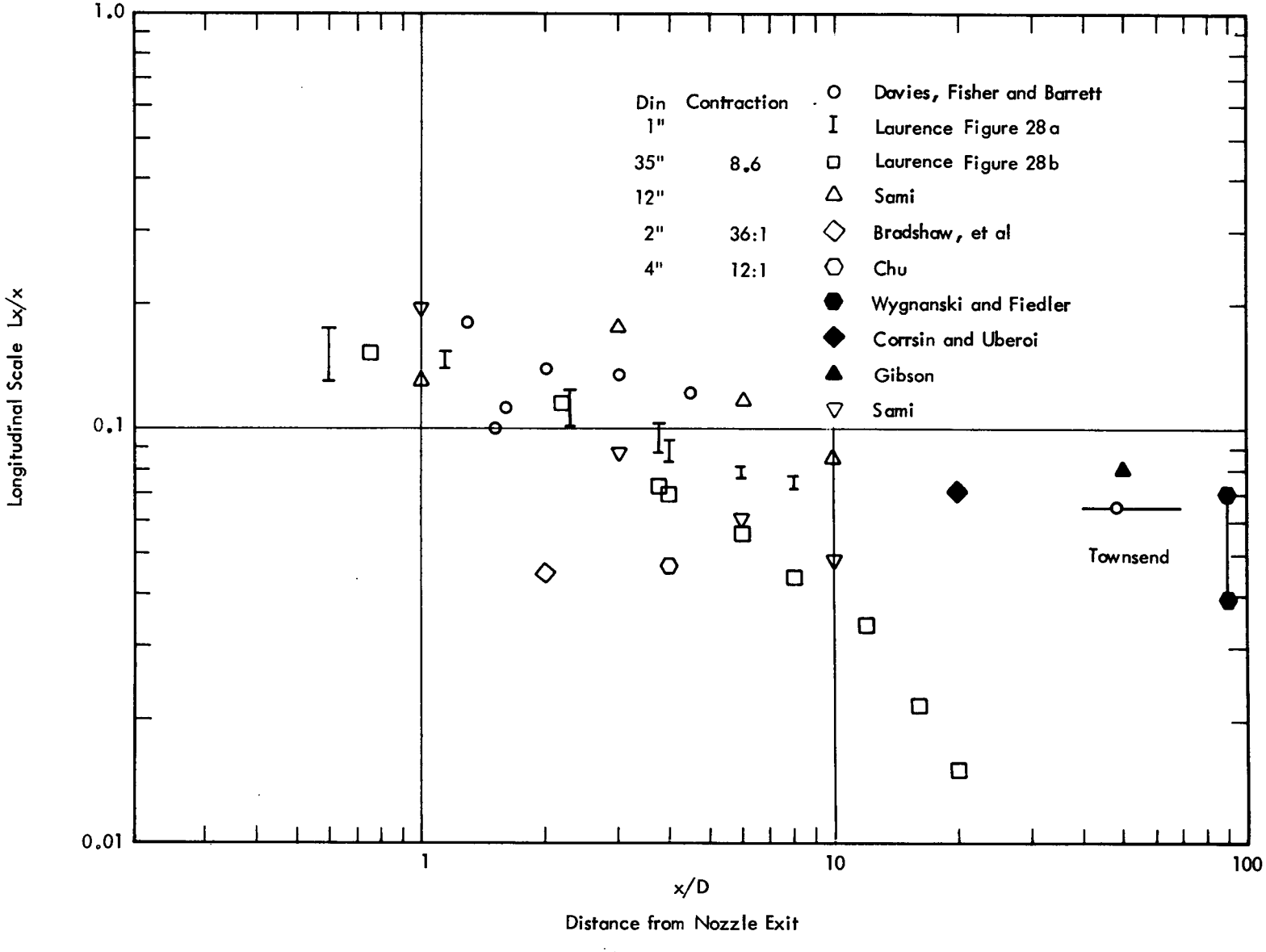

Figure 10. Longitudinal Integral Spatial Scale in the Axial Direction

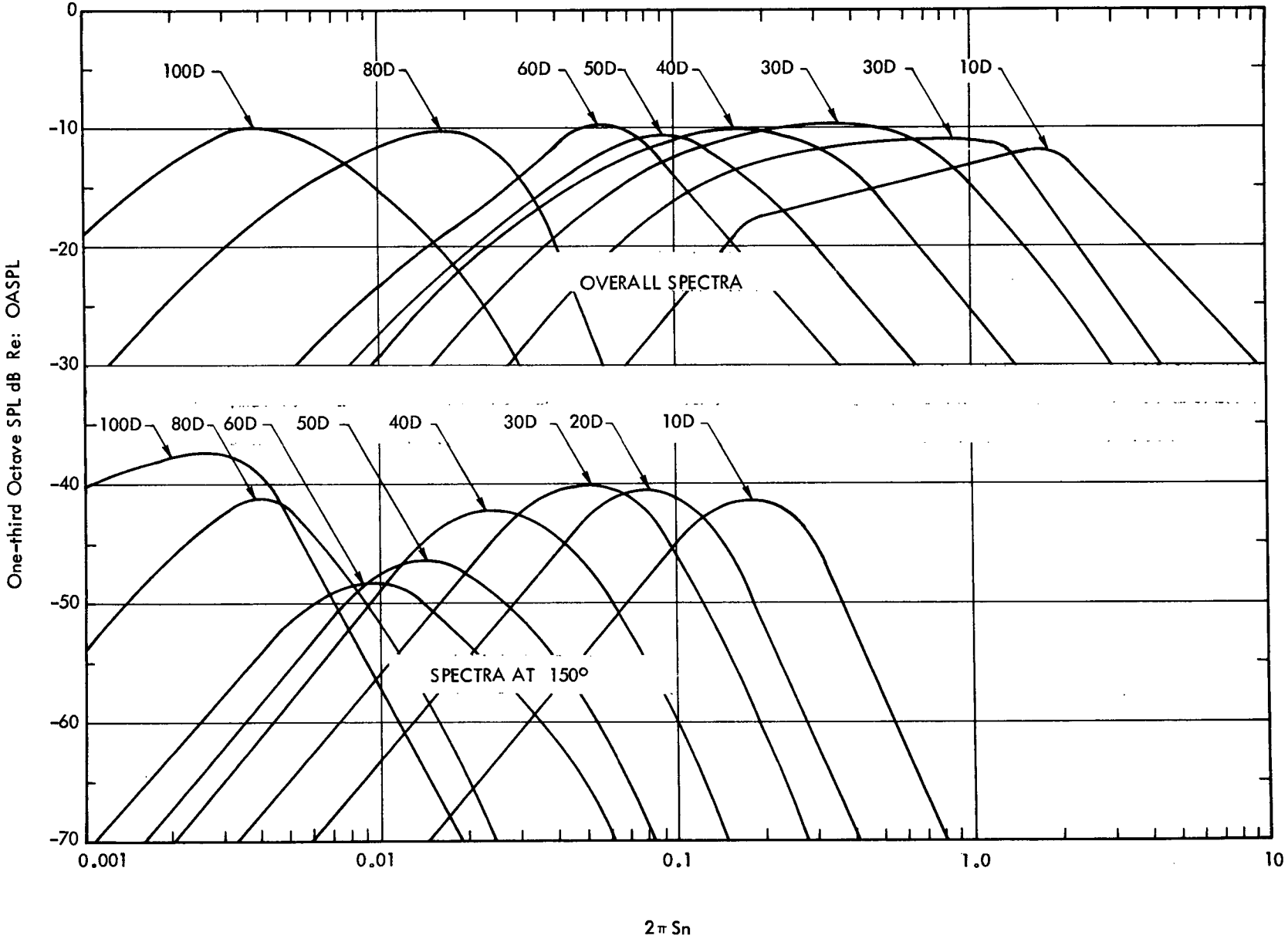

Figure 11. Local Noise Emission Spectra at Various Axial Stations for the F - 1 Exhaust Flow

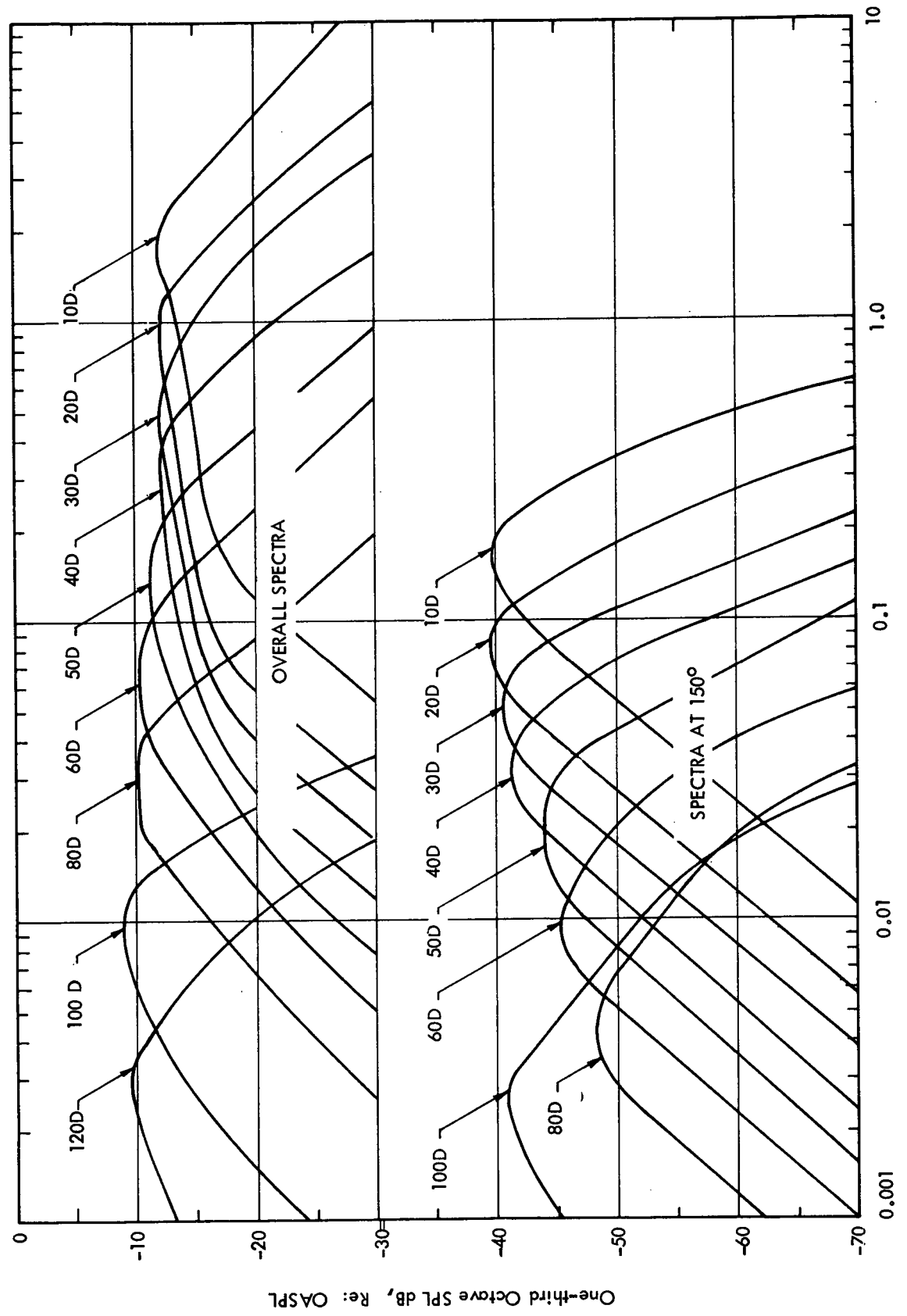

Figure 12. Local Noise Emission Spectra at Various Axial Stations for the High Chamber Pressure Engine

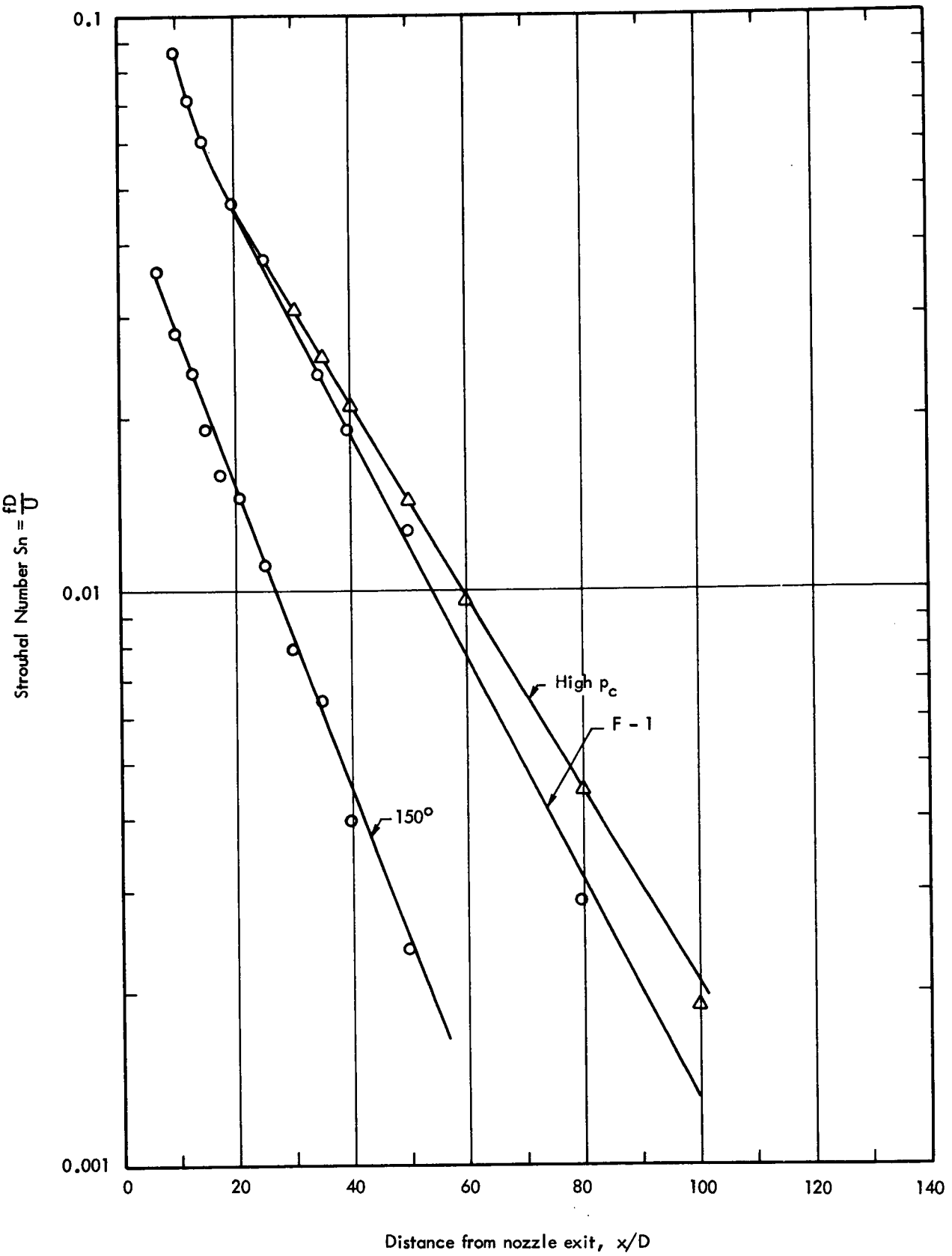

Figure 13. Predicted Real Sound Source Location

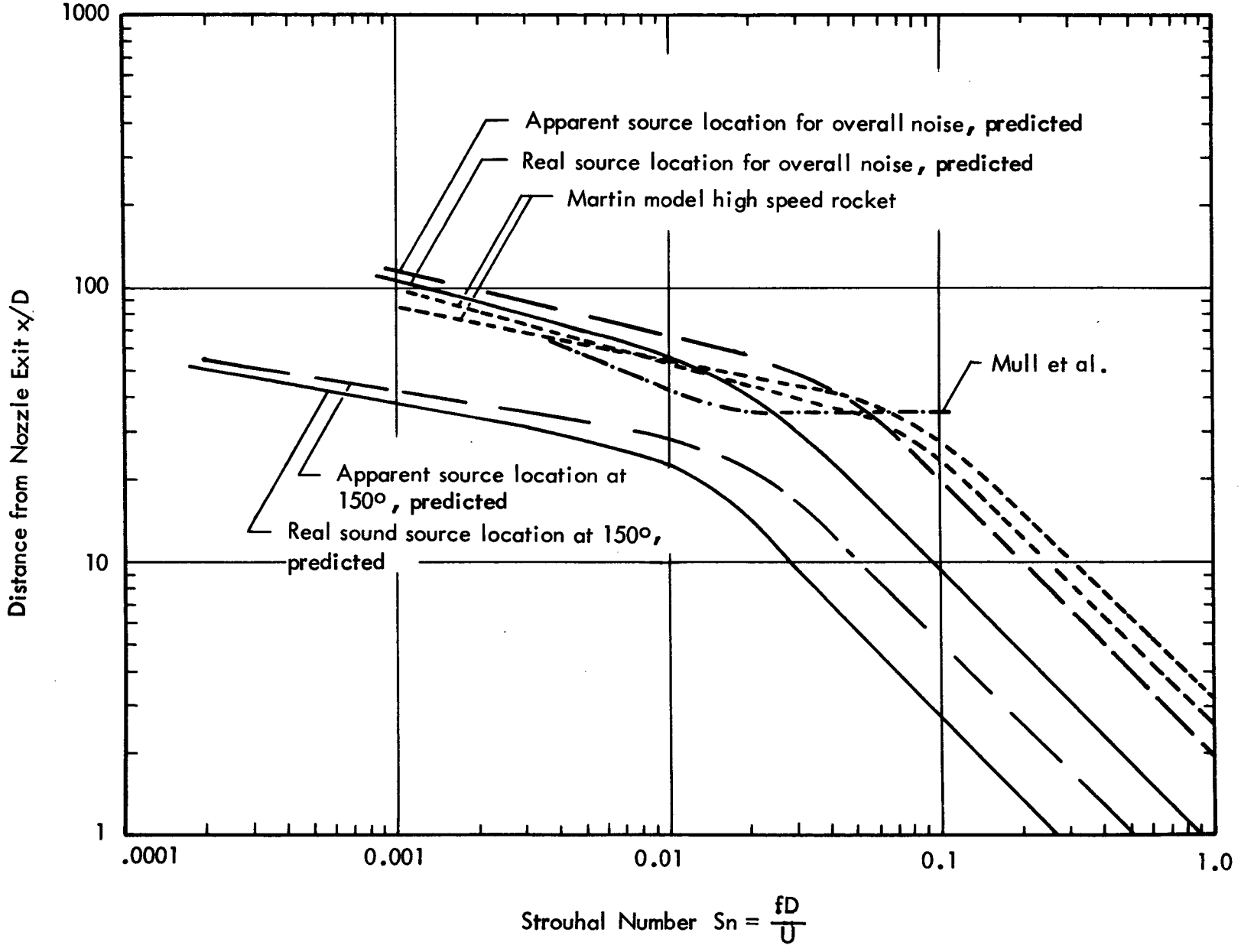

Figure 14. Predicted and Measured Sound Source Locations

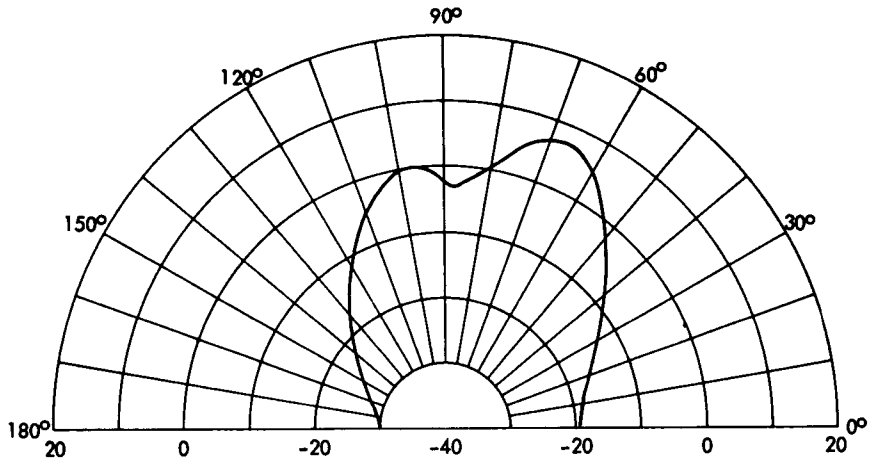

Sn = 0.068 x/D = 10 Mc = 5.2

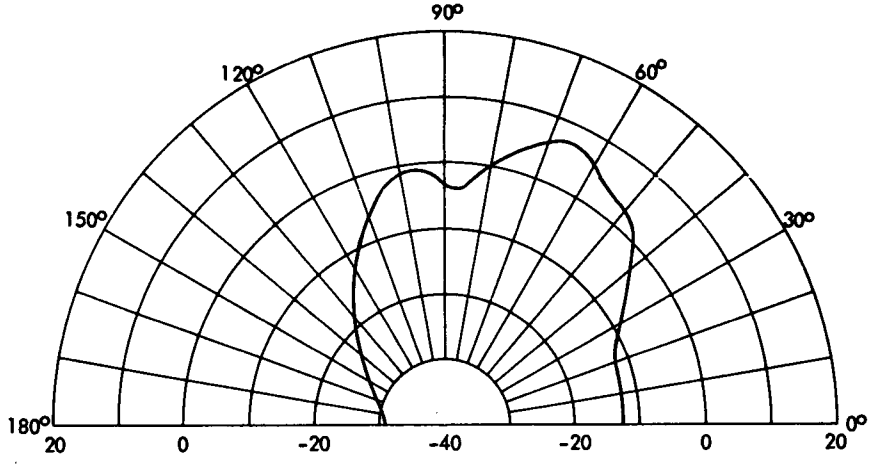

Sn = 0.038 x/D = 20 Mc = 5.2

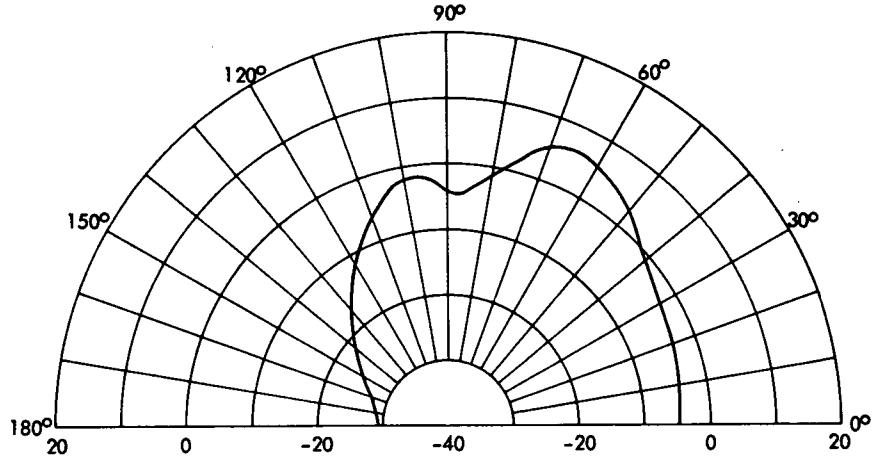

Sn = 0.022 x/D = 30 Mc = 4.2

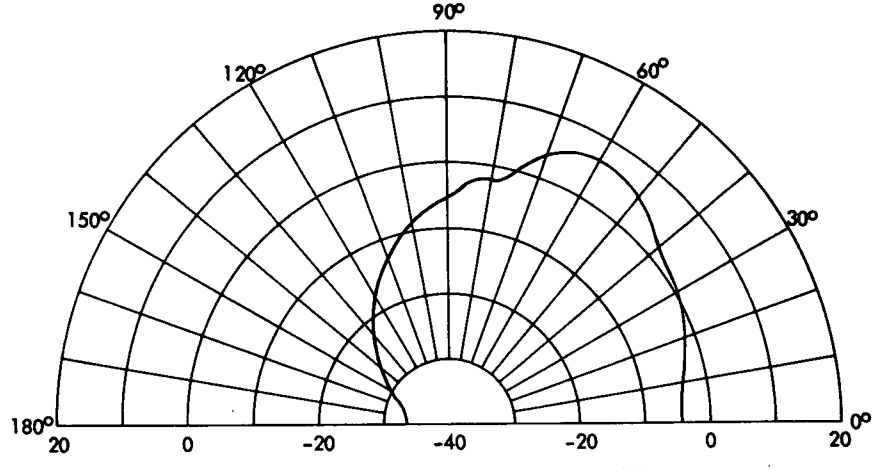

Sn = 0.015 x/D = 40 Mc = 3.1

Figure 15. Noise Directivity Patterns at Different Sections of the Exhaust Flow of the F-1 Rocket Engine. M = 3.7

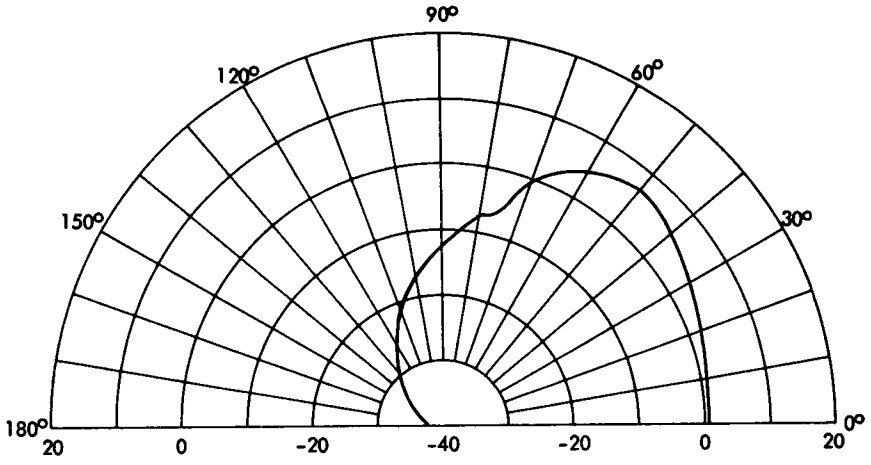

SPL, dB - Relative to Spherical Average SPL

Sn = 0.011 x/D = 50 Mc = 2.2

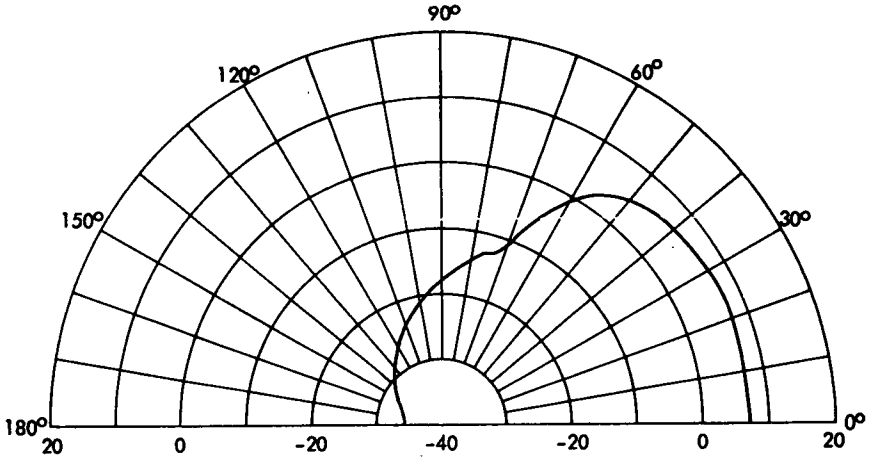

SPL, dB - Relative to Spherical Average SPL

Sn = 0.0062 x/D = 60 Mc = 1.6

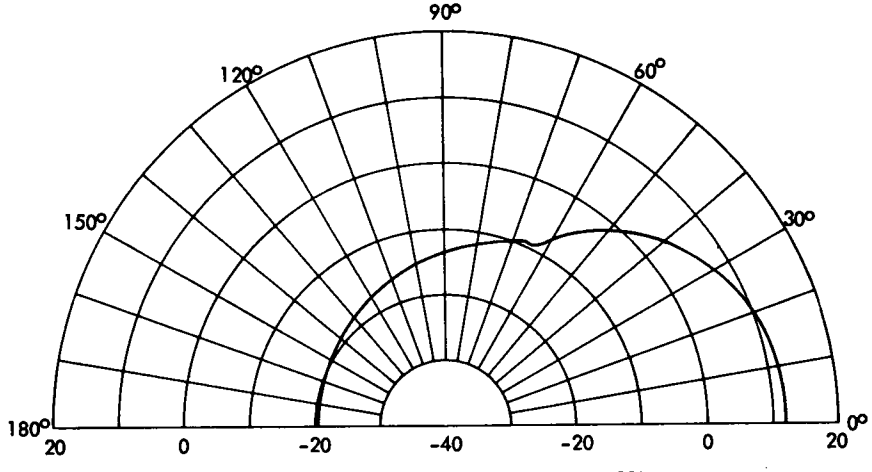

SPL, dB - Relative to Spherical Average SPL

Sn = 0.0025 x/D = 80 Mc = 0.8

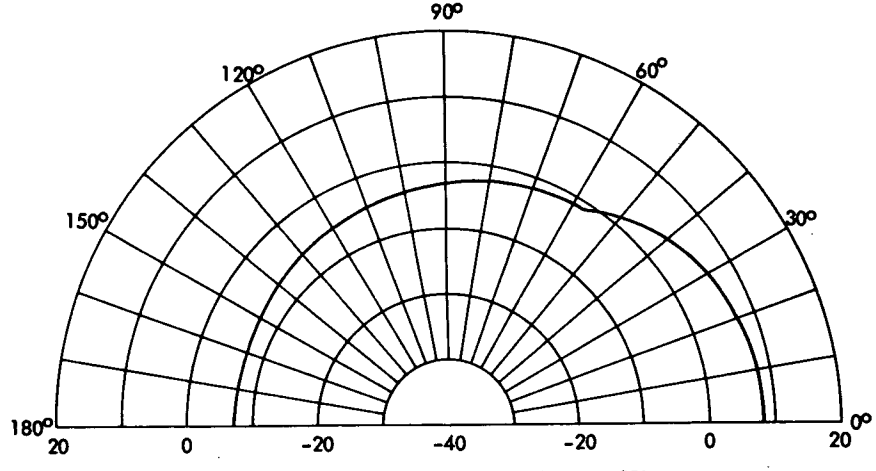

SPL, dB - Relative to Spherical Average SPL

Sn = 0.0010 x/D = 100 Mc = 0.4

Figure 15 (Concluded)

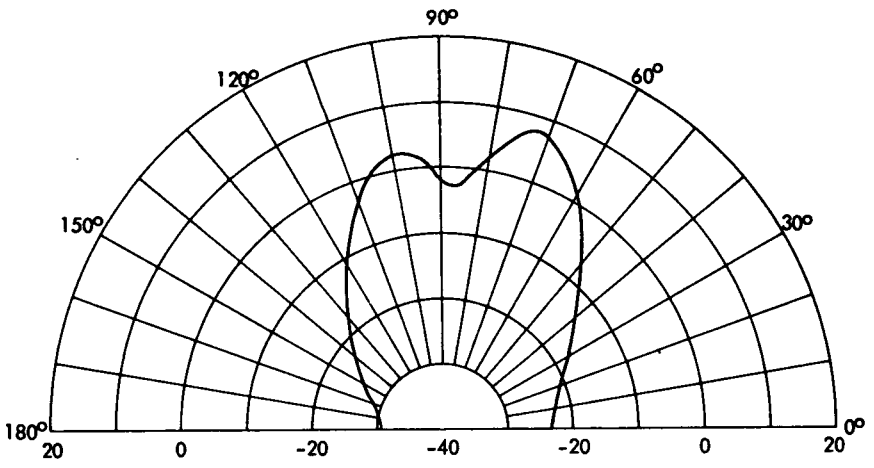

Sn = 0.035 x/D = 20 Mc = 7.4

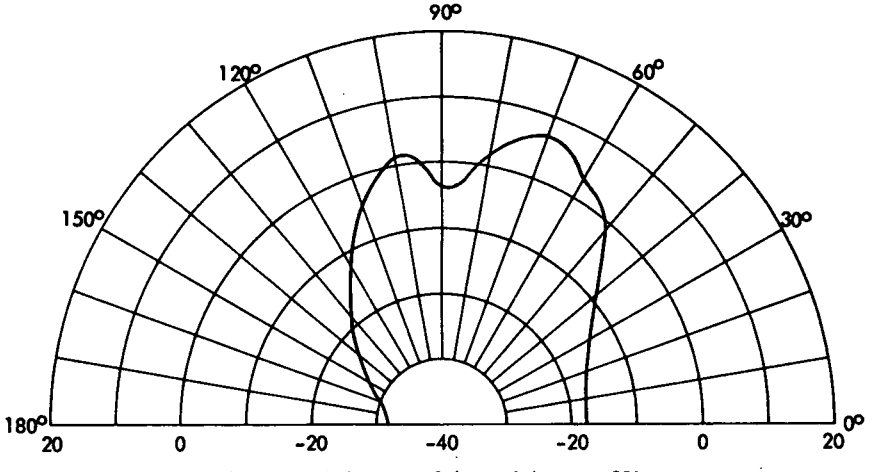

Sn = 0.024 x/D = 30 Mc = 6.6

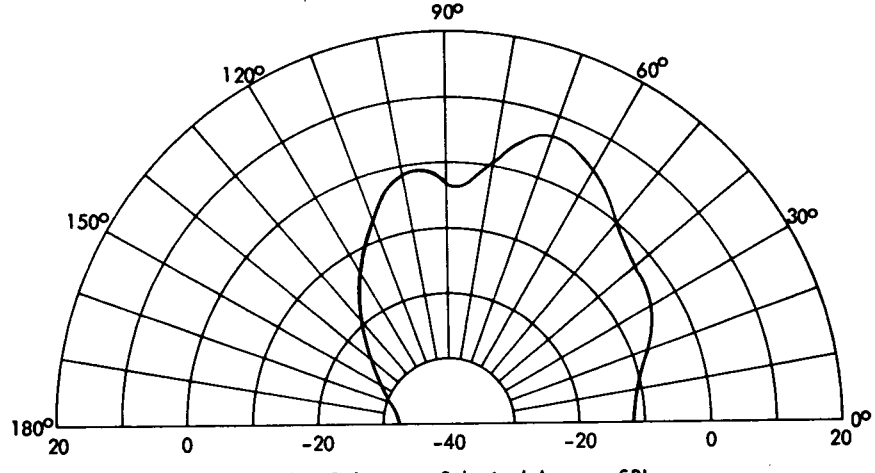

Sn = 0.017 x/D = 40 Mc = 5.5

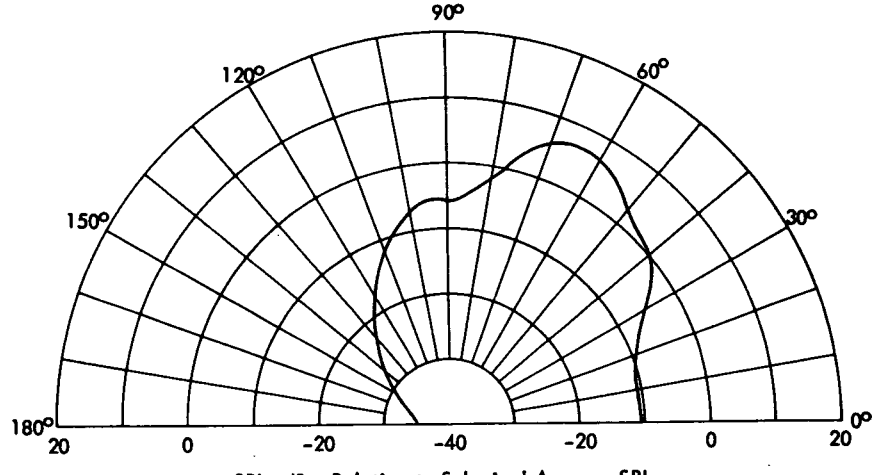

Sn = 0.012 x/D = 50 Mc = 3.8

Figure 16. Noise Directivity Patterns at Different Sections of the Exhaust Flow of the High P_c Rocket Engine. M = 4.05

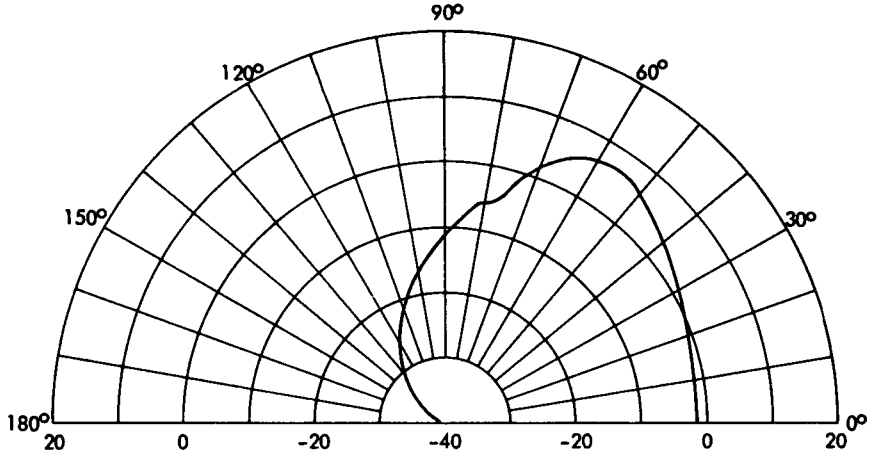

SPL, dB - Relative to Spherical Average SPL

Sn = 0.0078 x/D = 60 Mc = 2.4

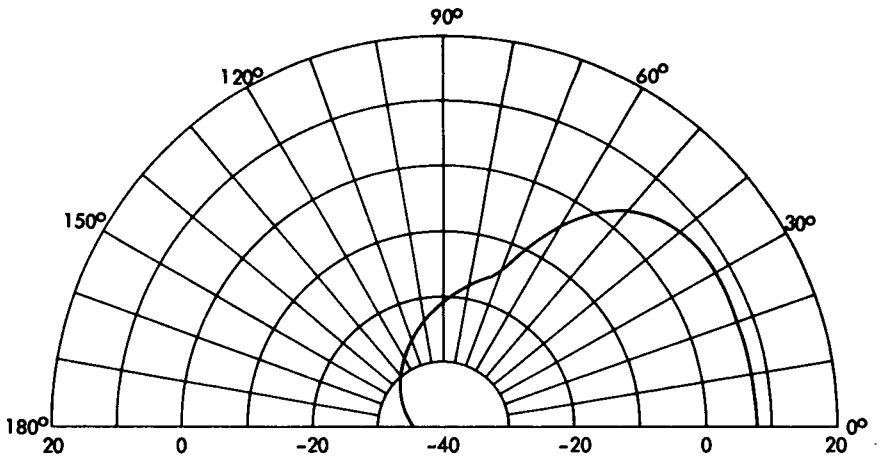

SPL, dB - Relative to Spherical Average SPL

Sn = 0.0036 x/D = 80 Mc = 1.2

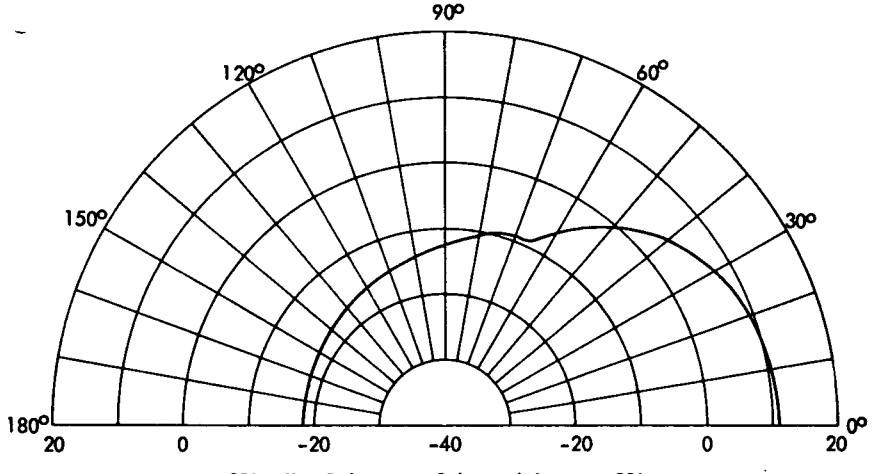

SPL, dB - Relative to Spherical Average SPL

Sn = 0.0016 x/D = 100 Mc = 0.7

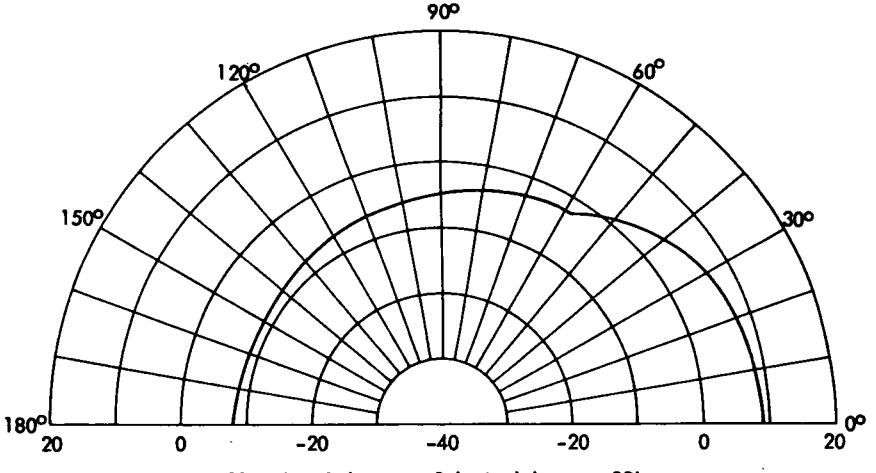

SPL, dB - Relative to Spherical Average SPL

Sn = 0.0008 x/D = 120 Mc = 0.4

Figure 16 (Concluded)

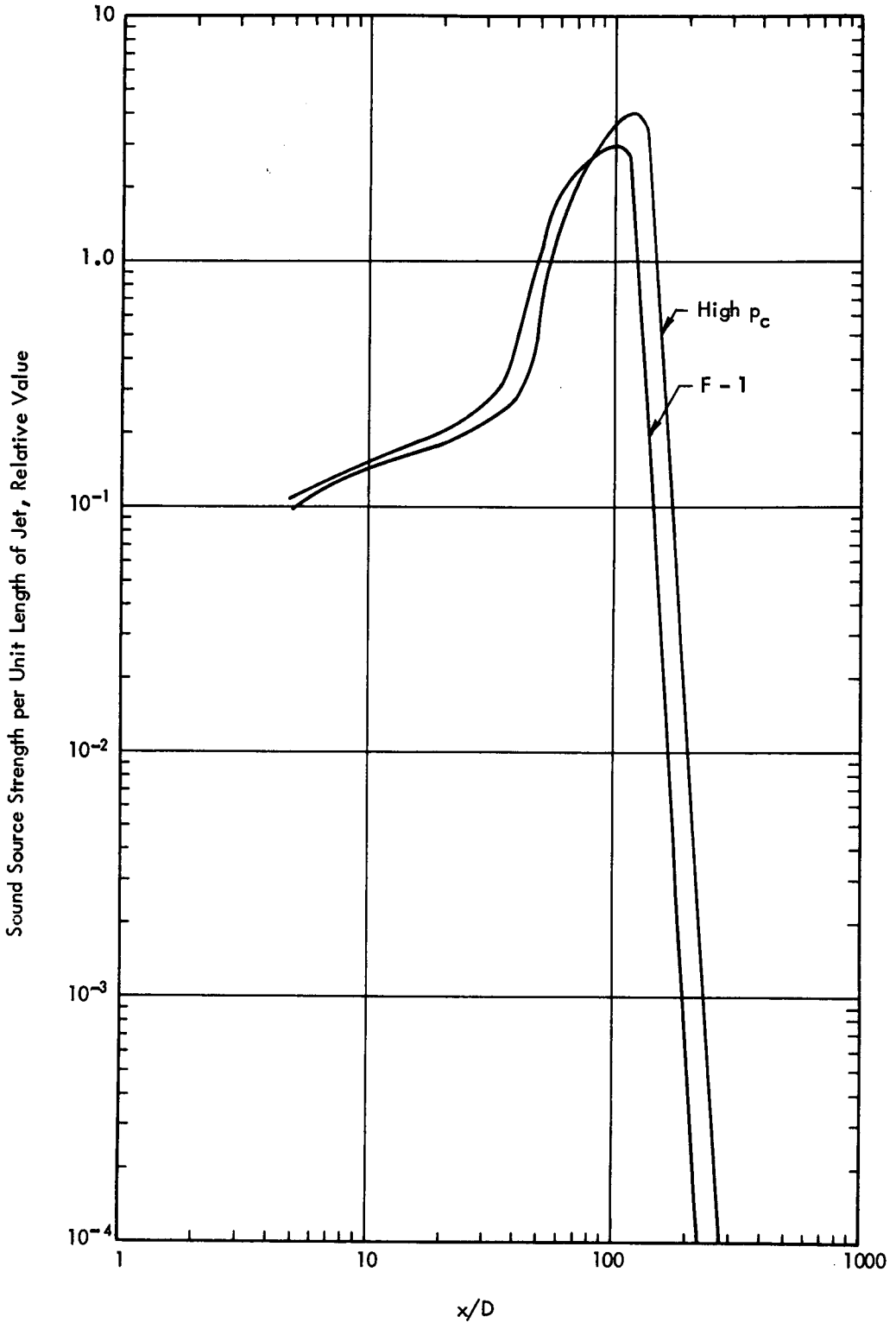

Figure 17. Computed Sound Source Strength Distribution Along the Rocket Exhaust Flow

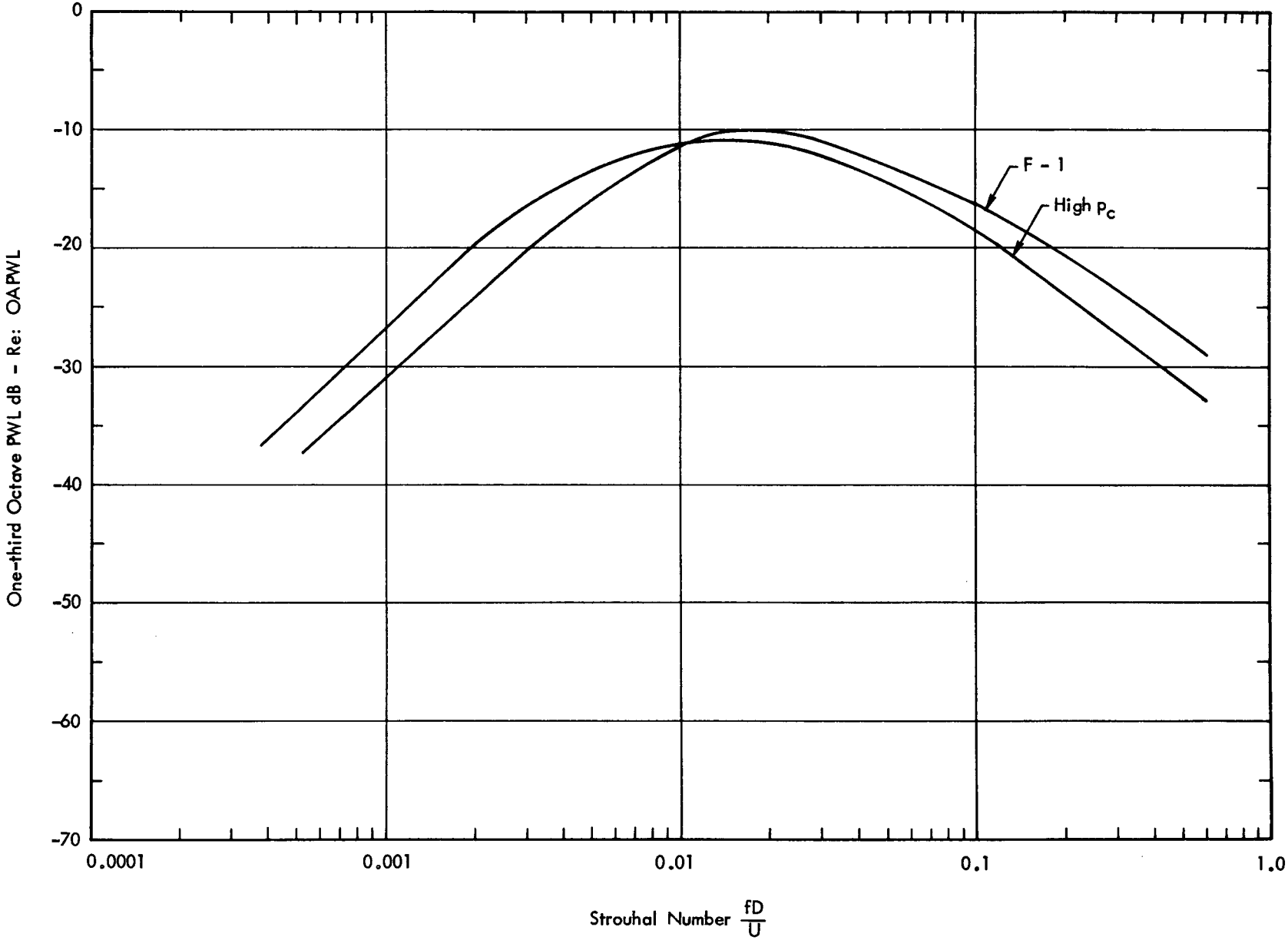

Figure 18. Predicted Overall Sound Power Spectrum for the High p_c and F - 1 Rocket Engines

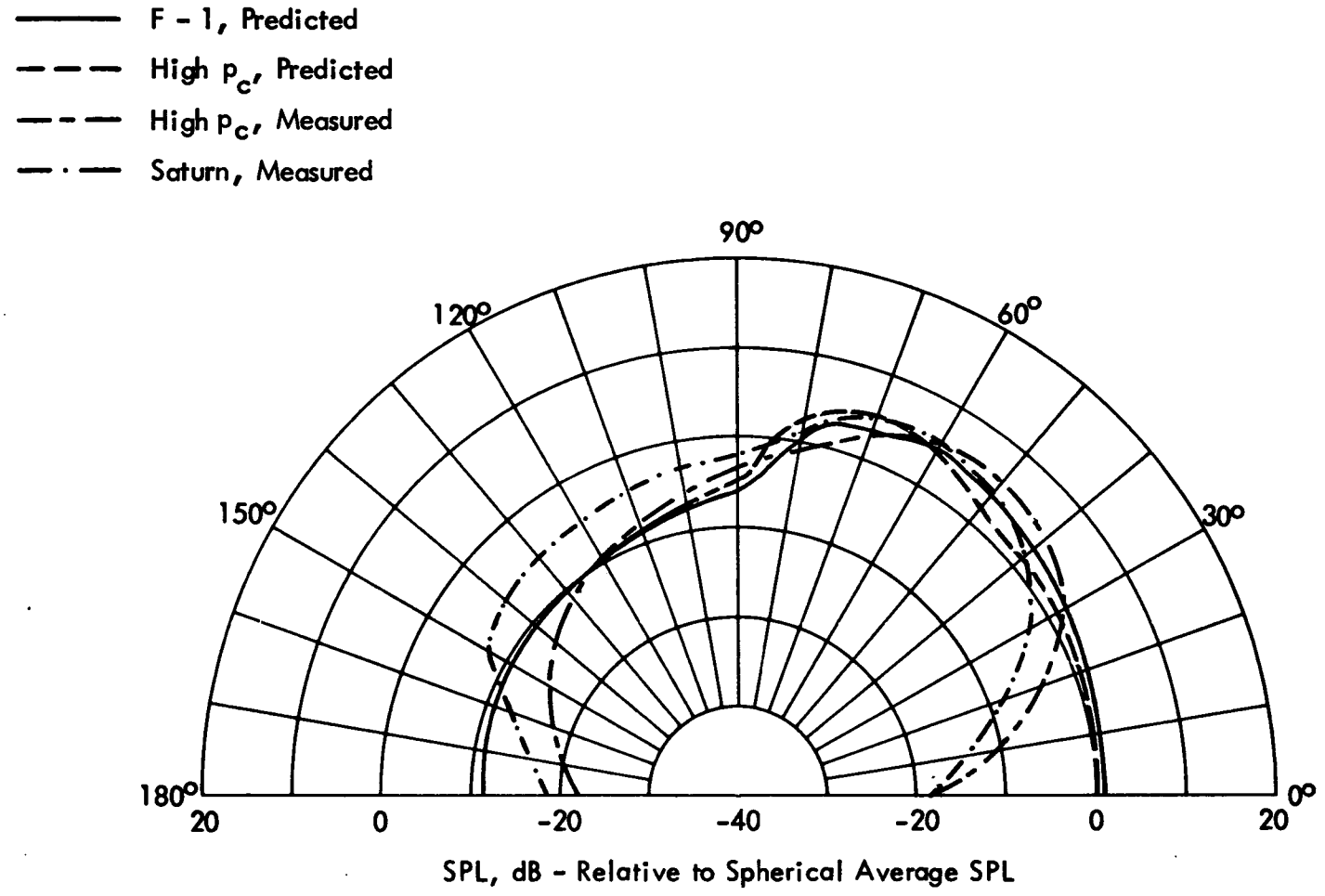

Figure 19. Theoretical and Experimental Directivity Patterns for the Overall Noise of the High Chamber Pressure and the F - 1 Rocket Engines

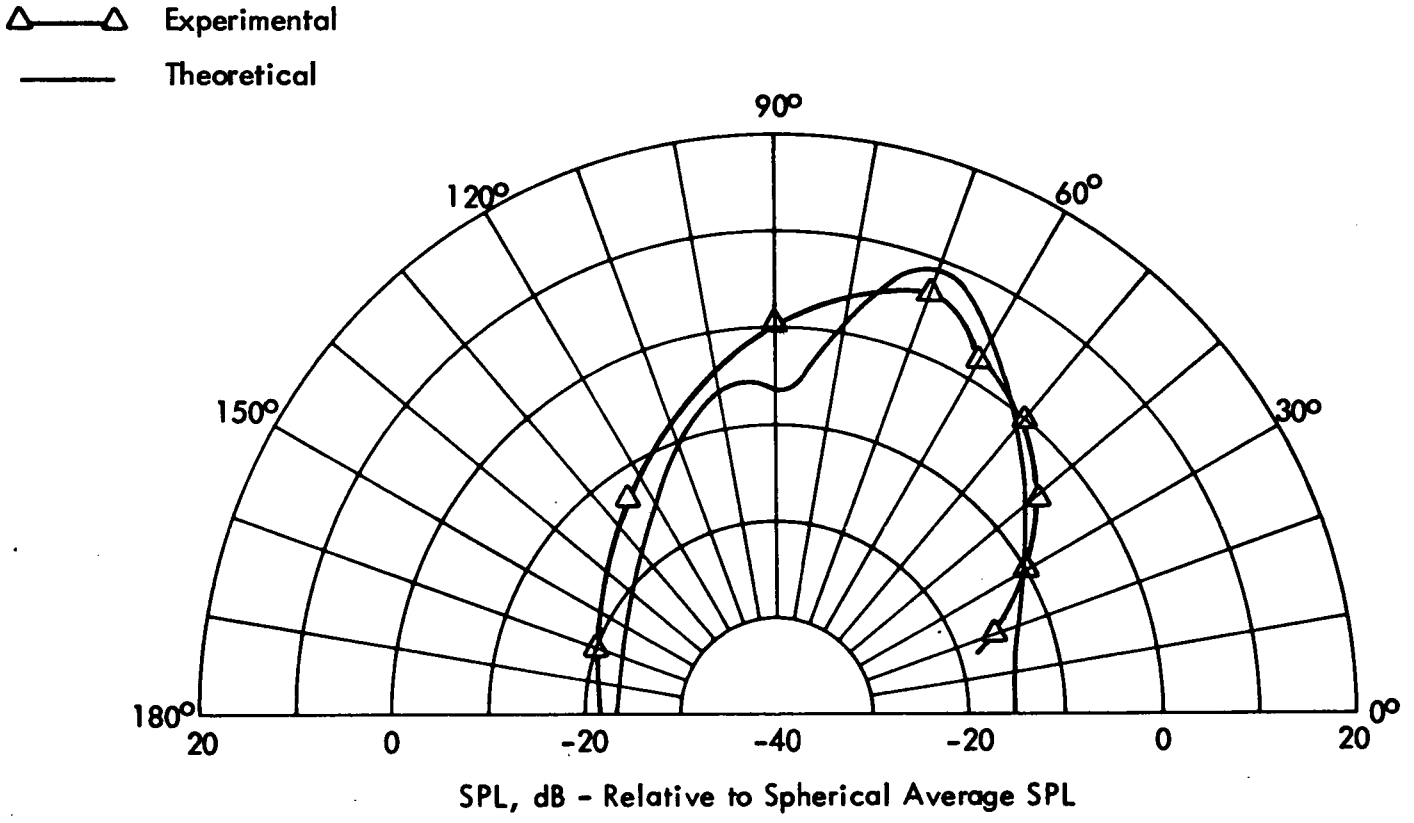

Sn = 0.0204

Figure 20a. Theoretical Directivity Patterns of the High p_c Engine and the Corresponding Experimental Data for a High Velocity Model Rocket

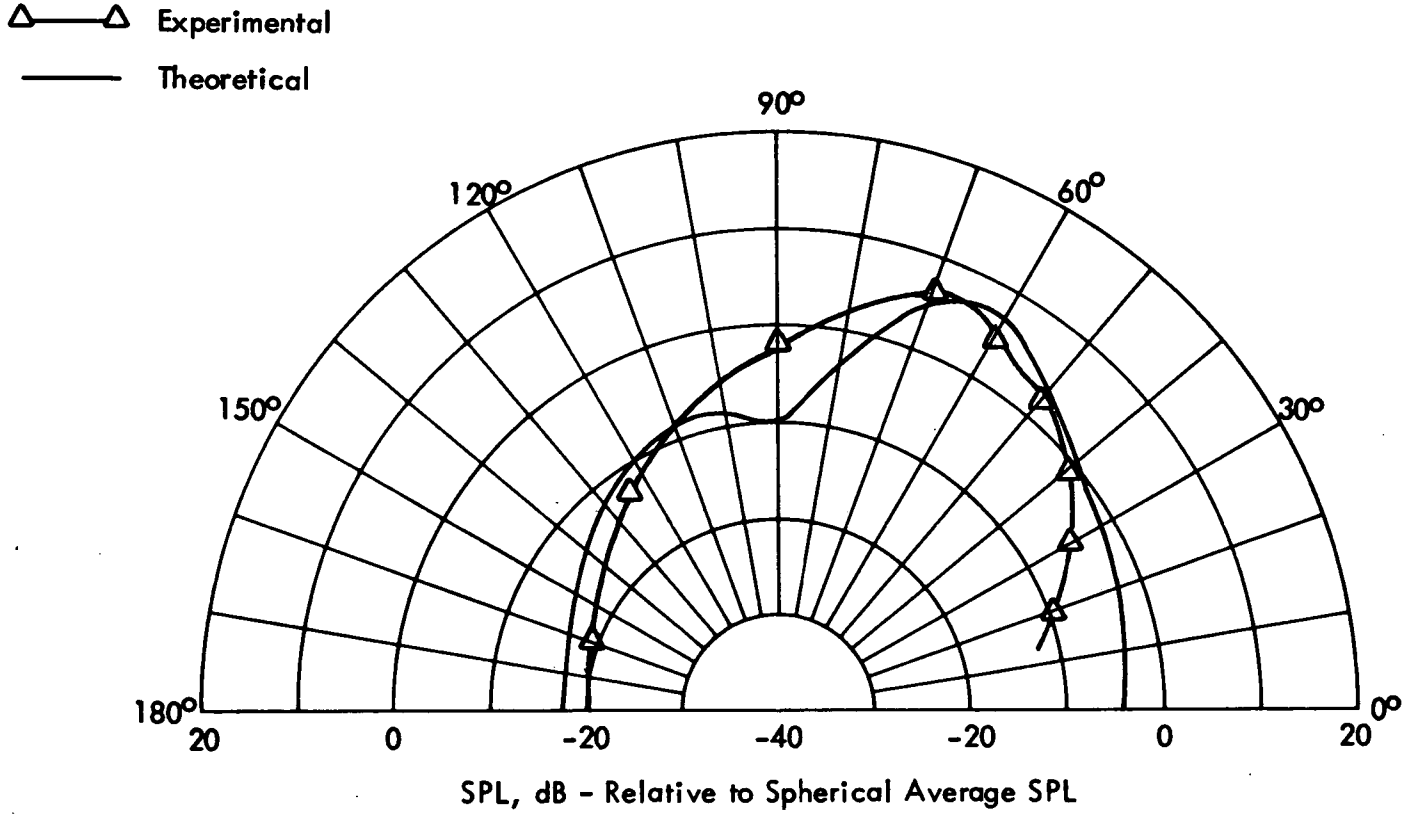

(b) $S_n = 0.0102$

Figure 20 (Continued)

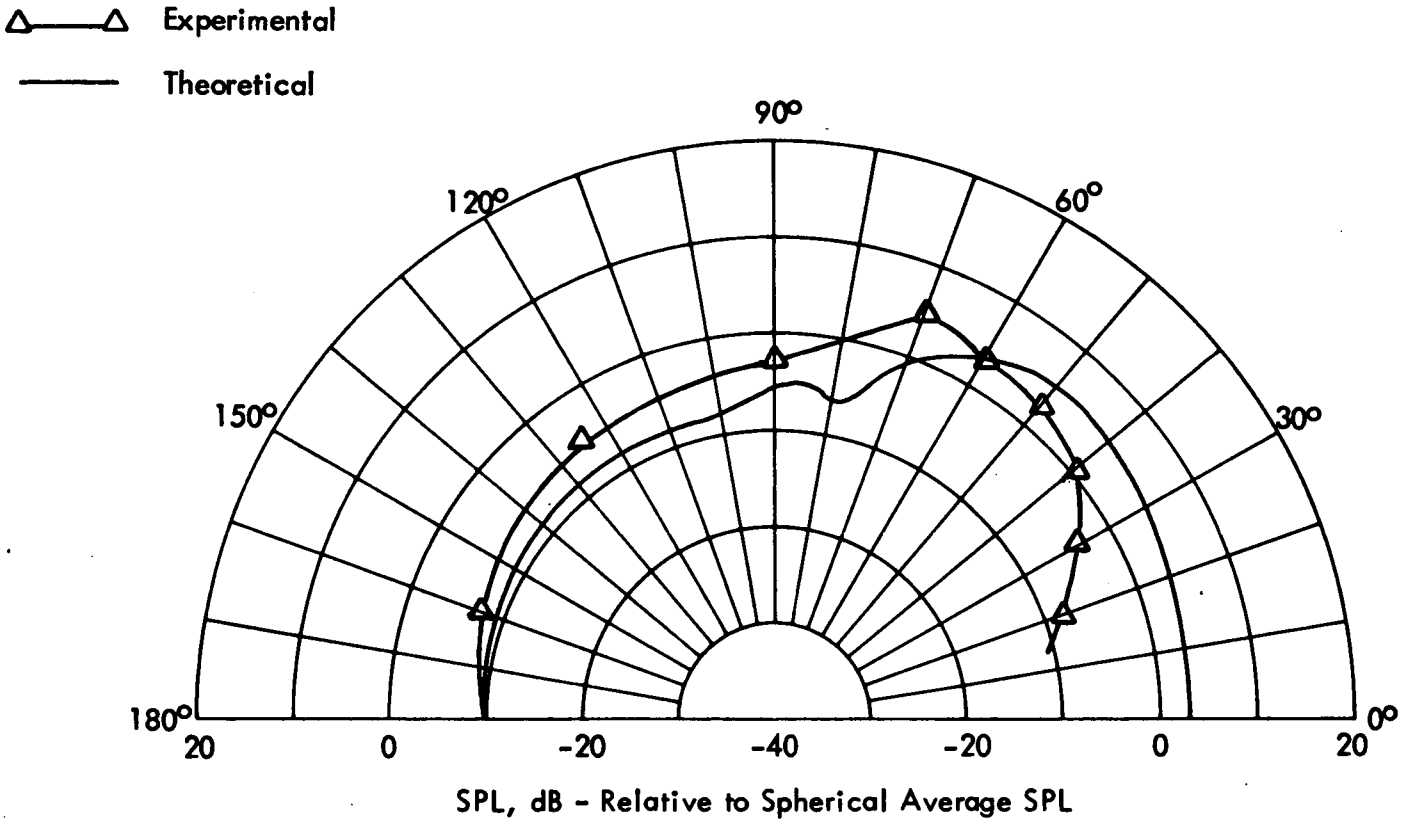

(c) Sn = 0.0051

Figure 20 (Continued)

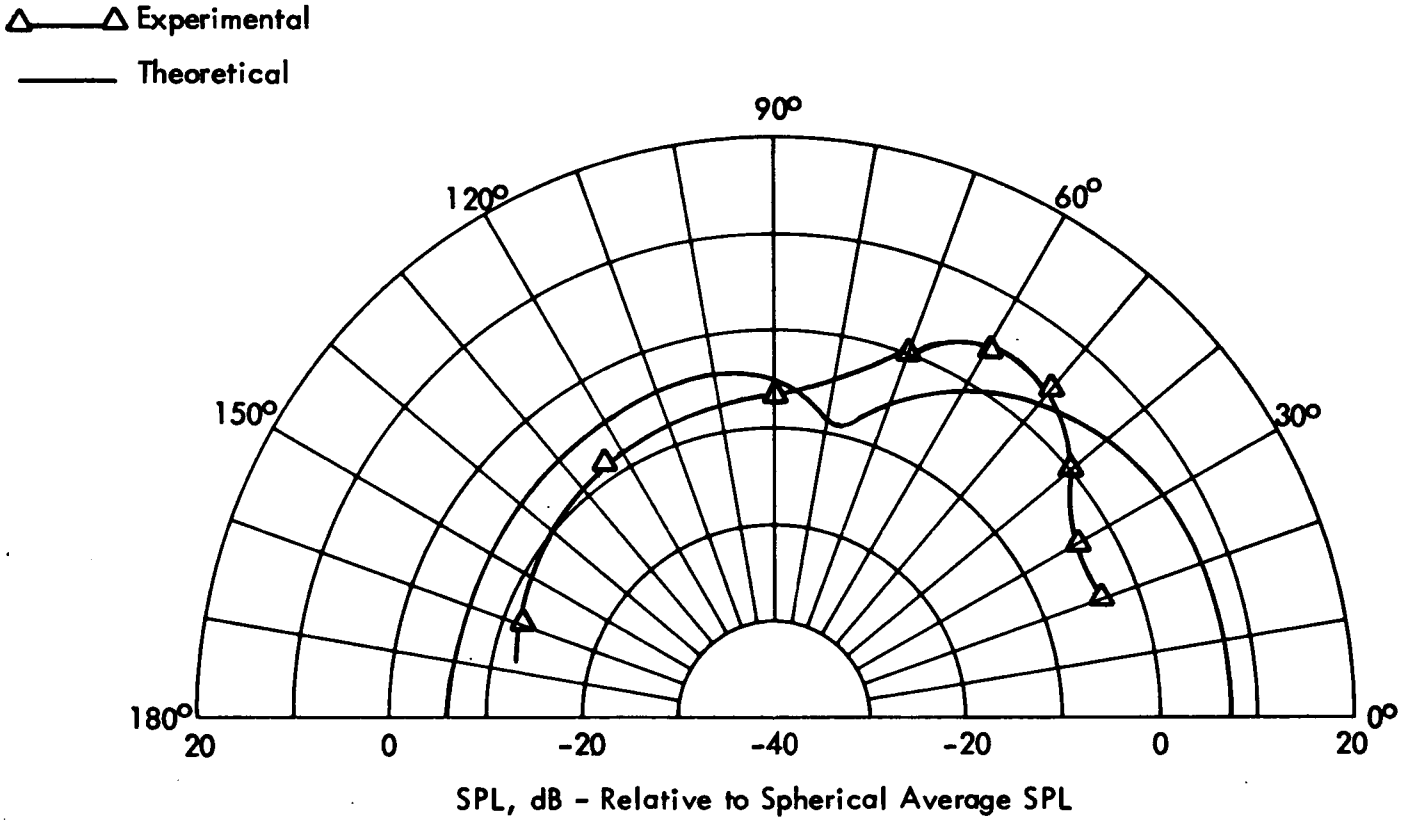

(d) Sn = 0.0026

Figure 20 (Continued)

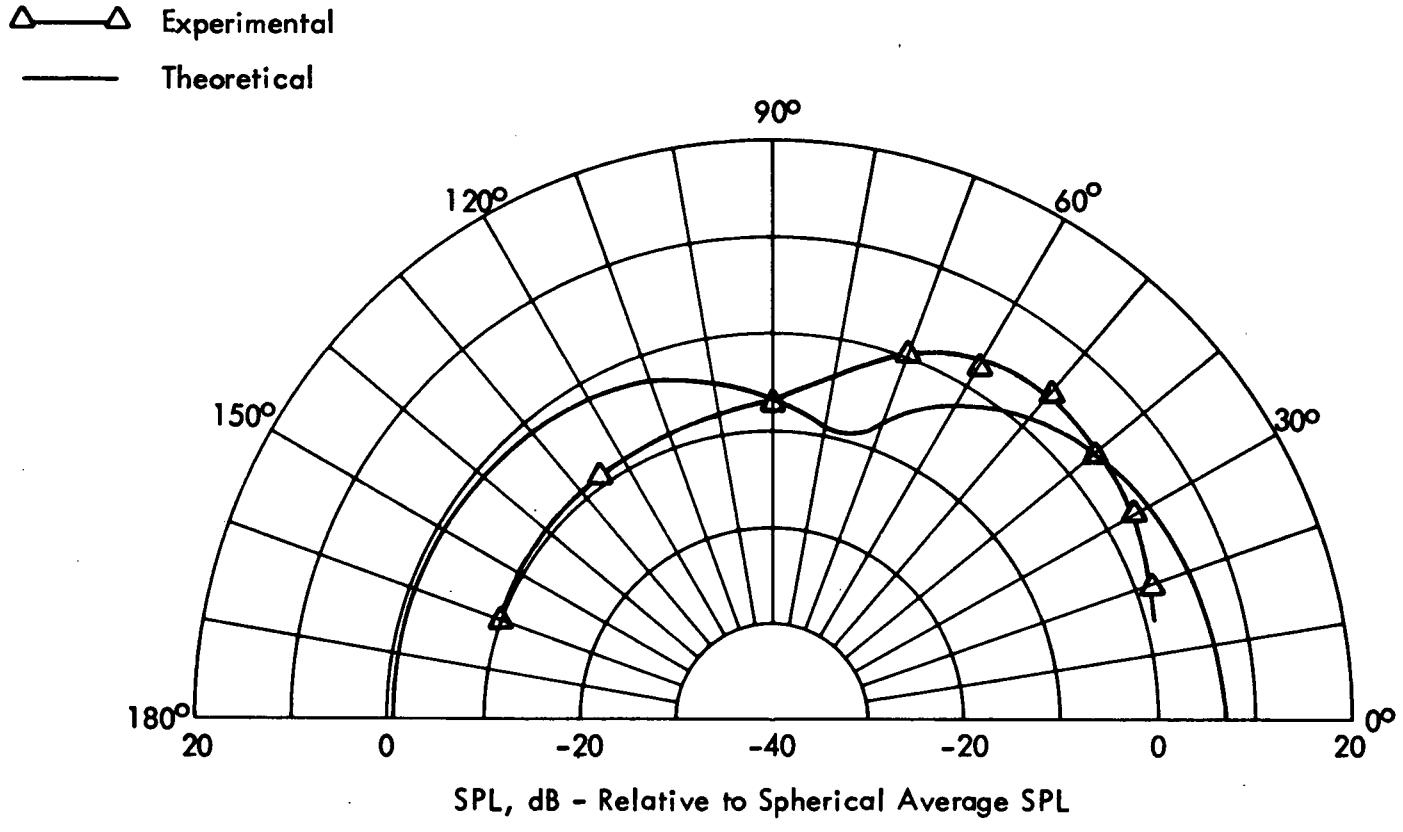

(e) Sn = 0.0013

Figure 20 (Continued)

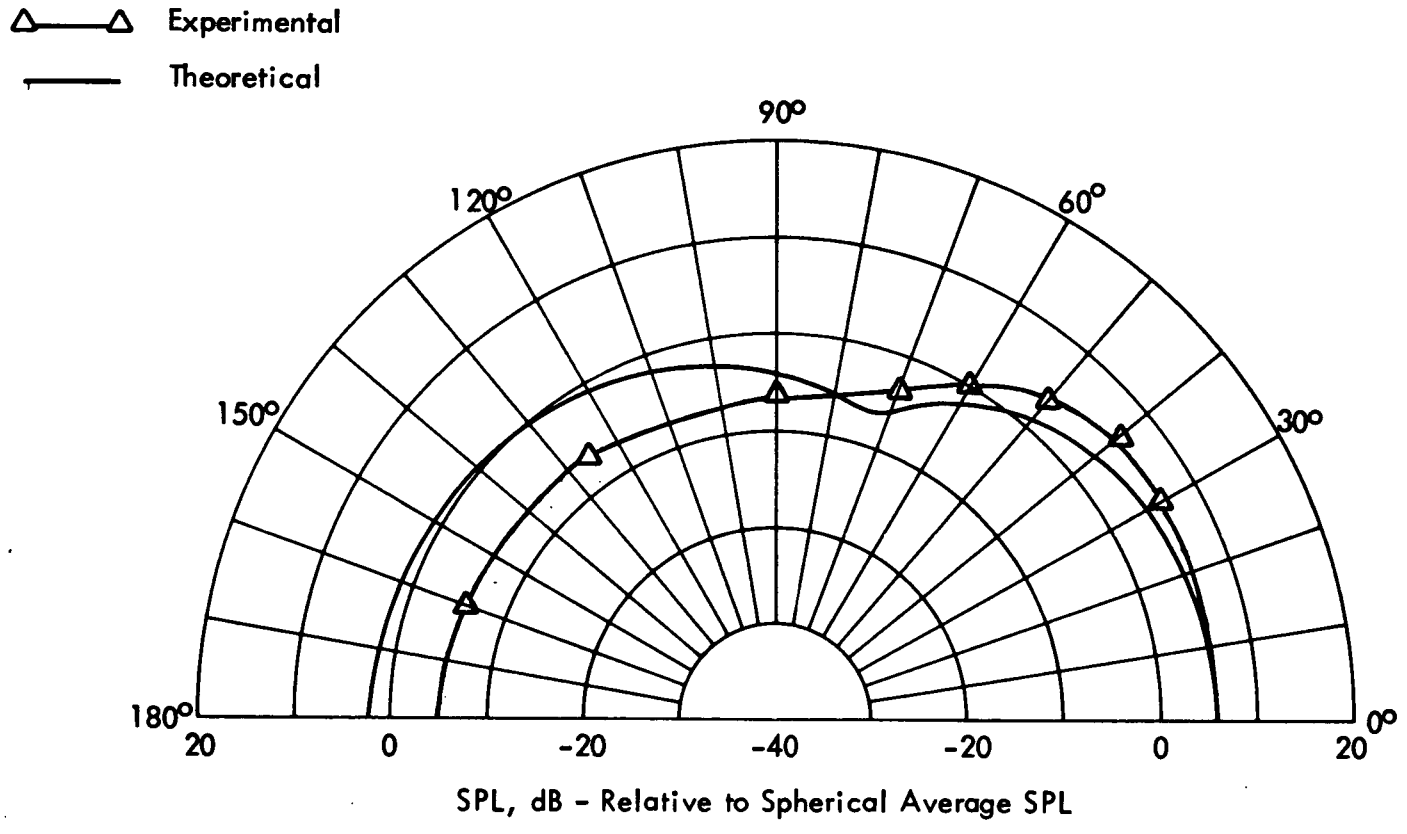

(f) Sn = 0.0007

Figure 20 (Concluded)

APPENDIX

TABLES FOR
THE MEAN FLOW PARAMETERS OF
THE F-1 ROCKET ENGINE

AERONAUTICAL RESEARCH ASSOCIATES OF PRINCETON, INC. -- GENERAL TURBULENT EXHAUST MIXING PROGRAM --
TEST RUN (SET 8) (APRIL 6 72)

BASIC INPUTS -	M 1	GAMMA 1	GAMMA INF	M 1/M INF	H'1/H INF	XC	PHI BREAK	M* BREAK
	3.700000	1.181999	1.400000	0.855000	24.000000	40.549301	0.010000	0.010000
RUN CONSTANTS -	(U 1)2/2H 1	H'1/H 1	P*	M*	A	B	KC*XC	SOLUTION
	1.245784	2.245784	1.170267	0.169590	23.000000	13.313304	0.617099	X
OUTPUT AT X=	5.000000	10.000000	15.000000	20.000000	25.000000	30.000000	-35.000000	0.000000
OUTPUT AT R/RS=	0.167000	0.500000	0.830000	1.167000	1.500000	-1.830001	0.000000	0.000000

INTEGRATION DATA	DX MINIMUM	DX INITIAL	DX MAXIMUM	DX MAX RATIO	RI ERROR	UC ERROR
	0.001000	0.010000	10.000000	2.000000	0.000100	0.000100

TABLE OF POLYNOMIALS USED FOR INTERPOLATION

INDEX	IND. VARIABLE	A0	A1	A2
1	0.000000	0.47450E-01	0.20080E-02	-0.50024E-01
2	0.200000	0.46873E-01	0.77651E-02	-0.62529E-01
3	0.300000	0.49951E-01	-0.14511E-01	-0.24984E-01
4	0.400000	0.53989E-01	-0.34948E-01	-0.56980E-04
5	0.500000	0.56886E-01	-0.47103E-01	0.12368E-01
6	0.600000	0.65719E-01	-0.77073E-01	0.37365E-01
7	0.700000	0.60075E-01	-0.60026E-01	0.24686E-01
8	0.800000	0.48654E-01	-0.31897E-01	0.75283E-02
9	0.900000	0.56962E-01	-0.50371E-01	0.17722E-01
10	1.000000	0.48903E-01	-0.33938E-01	0.94003E-02
11	1.099998	0.40455E-01	-0.18803E-01	0.26543E-02
12	1.200000	0.39909E-01	-0.17800E-01	0.22010E-02
13	1.299998	0.31001E-01	-0.41294E-02	-0.30254E-02
14	1.400000	0.31550E-01	-0.50842E-02	-0.26257E-02
15	1.500000	0.41048E-01	-0.17876E-01	0.16708E-02
16	1.599998	0.51620E-01	-0.31080E-01	0.57814E-02
17	1.700000	0.27603E-01	-0.25530E-02	-0.26701E-02
18	1.799998	0.27220E-01	-0.24546E-02	-0.26066E-02
19	1.900000	0.93207E-01	-0.72162E-01	0.15771E-01
20	2.000000	0.58643E-01	-0.38185E-01	0.74519E-02
21	2.200000	0.33152E-01	-0.15344E-01	0.23576E-02

AERONAUTICAL RESEARCH ASSOCIATES OF PRINCETON, INC. -- GENERAL TURBULENT EXHAUST MIXING PROGRAM --
TEST RUN (SET B) (APRIL 6 72)

CORE REGION

X/R 1	RI	R/R 5 GAMMA	R/R 1 M/M INF	U/U 1 CP/CP INF	M RHO/RHO INF	P1/P INF PTN/P INF	T T INF T1/T INF	H/H INF H1/H INF
10.000000	0.897813							
		0.914844	0.950953	0.780249	2.710514	27.146255	5.666582	10.840735
		1.203526	0.883141	1.913099	0.155851	8.936579	9.903157	18.945724
		0.948906	0.986360	0.656131	2.248211	11.609818	5.859961	10.359521
		1.218918	0.899869	1.767848	0.153562	6.364336	9.102028	16.091003
		0.982969	1.021767	0.548276	1.883136	6.236854	5.852895	9.608284
		1.234912	0.914929	1.641629	0.156321	4.664343	8.290760	13.610354
		1.017031	1.057173	0.455258	1.587884	3.936692	5.683571	8.711625
		1.251243	0.928327	1.532773	0.163335	3.506938	7.483784	11.470942
		1.051093	1.092580	0.375633	1.344969	2.791947	5.391151	7.761050
		1.267607	0.940112	1.439590	0.174380	2.705806	6.696042	9.639559
		1.085155	1.127987	0.307978	1.142480	2.156805	5.013701	6.820718
		1.283679	0.950363	1.360415	0.189553	2.150414	5.941926	8.083488
20.000000	0.766778							
		0.805648	0.871828	0.814952	2.850077	35.445465	5.580100	10.901901
		1.199693	0.878574	1.953711	0.157448	9.804847	10.105837	19.743881
		0.883389	0.955955	0.678809	2.328892	13.405411	5.839355	10.478067
		1.215889	0.896765	1.794388	0.153573	6.779554	9.258084	16.612595
		0.961130	1.040081	0.555977	1.908298	6.498619	5.859658	9.672190
		1.233674	0.913836	1.650640	0.155954	4.772073	8.352798	13.787468
		1.038670	1.124207	0.447773	1.564730	3.804297	5.662322	8.629457
		1.252679	0.929422	1.524014	0.164141	3.424595	7.413835	11.298785
		1.116611	1.208334	0.354611	1.281818	2.568447	5.287614	7.481914
		1.272366	0.943274	1.414989	0.178393	2.521055	6.470755	9.156044
		1.194351	1.292460	0.276145	1.047477	1.929885	4.788618	6.336123
		1.292065	0.955264	1.323163	0.199486	1.929626	5.555887	7.351345

AERONAUTICAL RESEARCH ASSOCIATES OF PRINCETON, INC. -- GENERAL TURBULENT EXHAUST MIXING PROGRAM --
TEST RUN (SET 8) (APRIL 6 72)

CORE REGION

X/R 1	RI	R/R 5 GAMMA	R/R 1 M/M INF	U/U 1 CP/CP INF	M RHO/RHO INF	P1/P INF PIN/P INF	T T INF T1/T INF	H/H INF H1/H INF
30.000000	0.579836							
		0.649863	0.733952	0.861215	3.044575	51.719833	5.445415	10.933581
		1.194860	0.872560	2.007851	0.160237	11.085538	10.363289	20.807938
		0.789918	0.892128	0.712332	2.451059	16.730682	5.796317	10.628234
		1.211597	0.892217	1.833618	0.153928	7.435486	9.480502	17.383621
		0.929973	1.050304	0.567828	1.947275	6.929643	5.868065	9.767457
		1.231800	0.912161	1.664511	0.155445	4.941678	8.446958	14.060053
		1.070026	1.208481	0.436230	1.529169	3.611657	5.627134	8.499813
		1.254932	0.931117	1.510505	0.165469	3.300492	7.304371	11.033288
		1.210081	1.366657	0.322981	1.187242	2.277955	5.108779	7.039762
		1.279920	0.948070	1.377974	0.185577	2.263710	6.116634	8.428561
		1.350136	1.524835	0.230463	0.910209	1.663815	4.405386	5.593532
		1.305175	0.962387	1.269703	0.218457	1.663815	4.962296	6.300642
40.549301	0.015218							
		0.167000	0.198659	0.980854	3.602026	157.037155	5.005557	10.751245
		1.163641	0.857381	2.147861	0.171286	15.212911	10.968885	23.559647
		0.500000	0.594787	0.840896	2.957899	43.669937	5.507196	10.926680
		1.196945	0.875192	1.984073	0.158918	10.504669	10.251945	20.340607
		0.830000	0.987347	0.620327	2.123798	9.340891	5.877633	10.144486
		1.223923	0.904813	1.725947	0.153942	5.751969	8.845876	15.267516
		1.167000	1.388232	0.389074	1.385515	2.949538	5.451276	7.933348
		1.264667	0.938101	1.455319	0.172088	2.829675	6.836087	9.948691
		1.500000	1.784361	0.210225	0.848615	1.564491	4.210848	5.246795
		1.311435	0.965576	1.246018	0.229307	1.564491	4.683051	5.835169
		1.830001	2.176922	0.098148	0.482327	1.166679	2.806772	3.129155
		1.352345	0.983628	1.114859	0.350448	1.166679	2.921808	3.257403

AERONAUTICAL RESEARCH ASSOCIATES OF PRINCETON, INC. -- GENERAL TURBULENT EXHAUST MIXING PROGRAM --
TEST 5

DEVELOPED REGION

X/R 1	K	R/R 5 GAMMA	R/R 1 M/M INF	U/U 1 CP/CP INF	M RHO/RHO INF	P'/P INF P'N/P INF	T T INF T'/T INF	H/H INF H'/H INF
60.000000	0.022237							
		0.167000	0.303680	0.614565	2.104097	9.029370	5.878702	10.106694
		1.224755	0.905614	1.719205	0.154050	5.658180	8.803489	15.135002
		0.500000	0.909223	0.526873	1.813825	5.577250	5.828576	9.422372
		1.238439	0.917977	1.616582	0.157496	4.374986	8.114701	13.118080
		0.830000	1.509309	0.388673	1.384305	2.944671	5.449551	7.928281
		1.264753	0.938162	1.454850	0.172154	2.825926	6.831958	9.939476
		1.167000	2.122125	0.243778	0.950416	1.734996	4.524848	5.815720
		1.301213	0.960299	1.285285	0.212228	1.734996	5.140417	6.606901
		1.500000	2.727668	0.131718	0.599099	1.262693	3.291215	3.798540
		1.338840	0.978150	1.154145	0.297200	1.262693	3.491347	4.029523
		1.830001	3.327756	0.061496	0.339947	1.081387	2.205343	2.364054
		1.368574	0.989679	1.071966	0.448764	1.081387	2.252311	2.414401
70.000000	0.025086							
		0.167000	0.371364	0.478646	1.660750	4.392374	5.742263	8.958750
		1.246881	0.924921	1.560143	0.161073	3.774239	7.697276	12.008849
		0.500000	1.111867	0.410348	1.450028	3.225509	5.537187	8.196234
		1.260167	0.934937	1.480216	0.168847	3.035025	7.051671	10.437998
		0.830000	1.845698	0.302712	1.126775	2.116558	4.978701	6.742425
		1.285027	0.951170	1.354254	0.191048	2.112033	5.879538	7.962386
		1.167000	2.595097	0.189863	0.785846	1.474347	3.998506	4.886938
		1.318043	0.968805	1.222191	0.242292	1.474347	4.391177	5.366858
		1.500000	3.335601	0.102587	0.498340	1.178384	2.874319	3.219391
		1.350489	0.982901	1.120053	0.341959	1.178384	2.999412	3.359502
		1.830001	4.069434	0.047895	0.280425	1.055137	1.961125	2.071046
		1.375038	0.991943	1.056049	0.505803	1.055137	1.990046	2.101586

AERONAUTICAL RESEARCH ASSOCIATES OF PRINCETON, INC. -- GENERAL TURBULENT EXHAUST MIXING PROGRAM --
TEST E

DEVELOPED REGION

X/R 1	K	R/R 5 GAMMA	R/R 1 M/M INF	U/U 1 CP/CP INF	M RHO/RHO INF	P1/P INF PTN/P INF	T T INF T1/T INF	H/H INF H1/H INF
80.000000	0.028059							
		0.167000	0.447936	0.375144	1.343495	2.786426	5.388875	7.754685
		1.267715	0.940185	1.439017	0.174468	2.701361	6.690886	9.628302
		0.500000	1.341125	0.321614	1.183163	2.266500	5.100399	7.020059
		1.280257	0.948278	1.376374	0.185922	2.253147	6.100905	8.397130
		0.830000	2.226268	0.237254	0.930741	1.699512	4.467141	5.707443
		1.303140	0.961321	1.277650	0.215198	1.699512	5.053686	6.456842
		1.167000	3.130186	0.148807	0.655524	1.318522	3.515553	4.127765
		1.332408	0.975385	1.174144	0.277449	1.318522	3.766634	4.422570
		1.500000	4.023376	0.080404	0.415985	1.122853	2.525577	2.763217
		1.359995	0.986548	1.094093	0.390623	1.122853	2.604242	2.849284
		1.830001	4.908521	0.037538	0.231318	1.037421	1.766995	1.844619
		1.380136	0.993674	1.043929	0.562353	1.037421	1.784967	1.863379
100.000000	0.034262							
		0.167000	0.628718	0.237910	0.932721	1.703016	4.473011	5.718377
		1.302944	0.961218	1.278418	0.214893	1.703016	5.062449	6.471925
		0.500000	1.882389	0.203962	0.829407	1.535770	4.147358	5.137293
		1.313434	0.966567	1.238690	0.233056	1.535770	4.594478	5.691135
		0.830000	3.124765	0.150463	0.660908	1.324197	3.536523	4.159237
		1.331800	0.975118	1.176081	0.275728	1.324197	3.792798	4.460637
		1.167000	4.393495	0.094371	0.468534	1.156960	2.748434	3.051970
		1.353942	0.984248	1.110439	0.358112	1.156960	2.855209	3.170537
		1.500000	5.647167	0.050991	0.294413	1.060825	2.017764	2.138169
		1.373544	0.991427	1.059672	0.491349	1.060825	2.050430	2.172785
		1.830001	6.889546	0.023806	0.159094	1.017662	1.498255	1.539995
		1.387140	0.995979	1.027859	0.664760	1.017662	1.505596	1.547541

AERONAUTICAL RESEARCH ASSOCIATES OF PRINCETON, INC. -- GENERAL TURBULENT EXHAUST MIXING PROGRAM --
TEST 6

DEVELOPED REGION

X/R 1	K	R/R 5 GAMMA	R/R 1 M/M INF	U/U 1 CP/CP INF	M RHO/RHO INF	P'/P INF P'N/P INF	T T INF T'/T INF	H/H INF H'/H INF
120.000000	0.039379							
		0.167000	0.847946	0.158625	0.687272	1.352889	3.638041	4.313381
		1.328837	0.973804	1.185633	0.267673	1.352889	3.920580	4.648368
		0.500000	2.538760	0.135991	0.613360	1.276187	3.348654	3.881574
		1.337205	0.977458	1.159144	0.291896	1.276187	3.561060	4.127783
		0.830000	4.214341	0.100320	0.490188	1.172370	2.839958	3.173370
		1.351434	0.983272	1.117400	0.346228	1.172370	2.959867	3.307357
		1.167000	5.925465	0.062921	0.345922	1.084317	2.230258	2.394482
		1.367911	0.989442	1.073634	0.443645	1.084317	2.279351	2.447190
		1.500000	7.616281	0.033998	0.213580	1.031881	1.698961	1.766558
		1.381913	0.994268	1.039786	0.585221	1.031881	1.713761	1.781946
		1.830001	9.291866	0.015873	0.112201	1.008783	1.336882	1.361714
		1.391321	0.997316	1.018575	0.746002	1.008783	1.340176	1.365069
160.000000	0.044712							
		0.167000	1.365153	0.084532	0.431792	1.132632	2.592635	2.849112
		1.358181	0.985867	1.098925	0.380257	1.132632	2.679205	2.944245
		0.500000	4.087285	0.072470	0.384872	1.104785	2.393875	2.596899
		1.363539	0.987859	1.084809	0.412661	1.104785	2.458331	2.666821
		0.830000	6.784893	0.053461	0.305378	1.065498	2.062518	2.191558
		1.372361	0.991016	1.062564	0.480488	1.065498	2.098330	2.229609
		1.167000	9.539722	0.033531	0.211202	1.031169	1.689938	1.756251
		1.382149	0.994346	1.039240	0.588392	1.031169	1.704342	1.771220
		1.500000	12.261856	0.018118	0.125947	1.011068	1.383012	1.412335
		1.390127	0.996938	1.021202	0.720845	1.011068	1.387292	1.416706
		1.830001	14.959472	0.008459	0.063541	1.002818	1.181896	1.193595
		1.395322	0.998568	1.009898	0.844886	1.002818	1.182839	1.194548

AERONAUTICAL RESEARCH ASSOCIATES OF PRINCETON, INC. -- GENERAL TURBULENT EXHAUST MIXING PROGRAM --
TEST 6

DEVELOPED REGION

X/R 1	K	R/R 5 GAMMA	R/R 1 M/M INF	U/U 1 CP/CP INF	M RHO/RHO INF	P'/P INF P'N/P INF	T T INF T'/T INF	H/H INF H'/H INF
200.000000	0.046172							
		0.167000	1.932570	0.054548	0.310148	1.067580	2.082076	2.214986
		1.371844	0.990834	1.063835	0.475888	1.067580	2.119312	2.254600
		0.500000	5.786138	0.046764	0.275243	1.053102	1.940280	2.046466
		1.375587	0.992132	1.054727	0.511334	1.053102	1.967885	2.075582
		0.830000	9.604988	0.034498	0.216120	1.032646	1.708630	1.777609
		1.381661	0.994184	1.040371	0.581860	1.032646	1.723859	1.793453
		1.167000	13.504844	0.021637	0.146721	1.015024	1.454595	1.491426
		1.388273	0.996345	1.025321	0.684964	1.015024	1.460673	1.497660
		1.500000	17.358414	0.011691	0.085429	1.005096	1.249973	1.267076
		1.393566	0.998021	1.013681	0.798434	1.005096	1.251770	1.268896
		1.830001	21.177261	0.005458	0.042144	1.001236	1.118002	1.125143
		1.396967	0.999076	1.006387	0.893626	1.001236	1.118397	1.125540

NSTOP

TABLES FOR

THE MEAN FLOW PARAMETERS OF

THE HIGH CHAMBER PRESSURE ENGINE

AERONAUTICAL RESEARCH ASSOCIATES OF PRINCETON, INC. -- GENERAL TURBULENT EXHAUST MIXING PROGRAM --
TEST RUN (SET A) (APRIL 6 72)

BASIC INPUTS -	M 1	GAMMA 1	GAMMA INF	M 1/M INF	H'1/H INF	XC	PHI BREAK	M* BREAK
	4.049999	1.181999	1.400000	0.431000	49.500000	49.185394	0.010000	0.010000
RUN CONSTANTS -	(U 1)2/2H 1	H'1/H 1	P*	M*	A	B	KC*XC	SOLUTION
	1.492620	2.492620	3.305288	1.320185	48.500000	29.641357	0.611202	X
OUTPUT AT X=	5.000000	10.000000	15.000000	20.000000	25.000000	30.000000	35.000000	40.000000
OUTPUT AT R/RS=	0.167000	0.500000	0.830000	1.167000	1.500000	1.830001	0.000000	0.000000
INTEGRATION DATA	DX MINIMUM	DX INITIAL	DX MAXIMUM	DX MAX RATIO	RI ERROR	UC ERROR		
	0.001000	0.010000	10.000000	2.000000	0.000100	0.000100		

TABLE OF POLYNOMIALS USED FOR INTERPOLATION

INDEX	IND. VARIABLE	A0	A1	A2
1	0.000000	0.47450E-01	0.20080E-02	-0.50024E-01
2	0.200000	0.46873E-01	0.77651E-02	-0.62529E-01
3	0.300000	0.49951E-01	-0.14511E-01	-0.24984E-01
4	0.400000	0.53989E-01	-0.34948E-01	-0.56980E-04
5	0.500000	0.56886E-01	-0.47103E-01	0.12368E-01
6	0.600000	0.65719E-01	-0.77073E-01	0.37365E-01
7	0.700000	0.60075E-01	-0.60026E-01	0.24686E-01
8	0.800000	0.48654E-01	-0.31897E-01	0.75283E-02
9	0.900000	0.56962E-01	-0.50371E-01	0.17722E-01
10	1.000000	0.48903E-01	-0.33938E-01	0.94003E-02
11	1.099998	0.40455E-01	-0.18803E-01	0.26543E-02
12	1.200000	0.39909E-01	-0.17800E-01	0.22010E-02
13	1.299998	0.31001E-01	-0.41294E-02	-0.30254E-02
14	1.400000	0.31550E-01	-0.50842E-02	-0.26257E-02
15	1.500000	0.41048E-01	-0.17876E-01	0.16708E-02
16	1.599998	0.51620E-01	-0.31080E-01	0.57814E-02
17	1.700000	0.27603E-01	-0.25530E-02	-0.26701E-02
18	1.799998	0.27220E-01	-0.24546E-02	-0.26066E-02
19	1.900000	0.93207E-01	-0.72162E-01	0.15771E-01
20	2.000000	0.58643E-01	-0.38185E-01	0.74519E-02
21	2.200000	0.33152E-01	-0.15344E-01	0.23576E-02

CORE REGION

X/R 1	RI	R/R 5 GAMMA	R/R 1 M/M INF	U/U 1 CP/CP INF	M RHO/RHO INF	P1/P INF PIN/P INF	T T INF T1/T INF	H/H INF H1/H INF
10.000000	0.916642							
		0.930535	0.957458	0.784513	3.013241	48.875168	5.790582	20.805801
		1.193141	0.491231	3.593041	0.084833	10.857887	10.867916	39.048874
		0.958321	0.986048	0.657714	2.513500	18.852097	6.325469	20.076630
		1.202187	0.535245	3.173935	0.084617	7.750813	10.365410	32.899139
		0.986107	1.014637	0.548560	2.120646	9.286160	6.642218	18.685547
		1.212292	0.579979	2.813148	0.087317	5.700233	9.812906	27.605164
		1.013892	1.043226	0.455153	1.801578	5.441816	6.761783	16.934296
		1.223445	0.624654	2.504413	0.092380	4.290426	9.213711	23.074936
		1.041678	1.071816	0.375696	1.536899	3.623600	6.707806	15.037440
		1.235579	0.668455	2.241782	0.099653	3.297456	8.574087	19.221237
		1.069465	1.100407	0.308505	1.314279	2.656142	6.506601	13.141365
		1.248563	0.710589	2.019697	0.109210	2.590790	7.903407	15.962489
20.000000	0.815754							
		0.846462	0.896978	0.809948	3.121155	60.323486	5.666750	20.837280
		1.191588	0.483260	3.677113	0.085280	11.601958	10.954923	40.282486
		0.907877	0.962058	0.674284	2.575735	21.171875	6.264452	20.226059
		1.200863	0.529050	3.228703	0.084453	8.107327	10.438490	33.702789
		0.969292	1.027138	0.554186	2.140282	9.609475	6.630012	18.774506
		1.211703	0.577491	2.831745	0.087103	5.794539	9.844825	27.878036
		1.030707	1.092218	0.449670	1.783170	5.283860	6.763257	16.815399
		1.224193	0.627492	2.486287	0.092780	4.216126	9.173910	22.808975
		1.092122	1.157298	0.360212	1.485628	3.364248	6.675888	14.624229
		1.238315	0.677715	2.190604	0.101517	3.124084	8.431589	18.470276
		1.153536	1.222380	0.284869	1.235565	2.398501	6.392105	12.410747
		1.253916	0.726702	1.941574	0.113687	2.370585	7.631001	14.816155

CORE REGION

X/R 1	RI	R/R 5 GAMMA	R/R 1 M/M INF	U/U 1 CP/CP INF	M RHO/RHO INF	P1/P INF PIN/P INF	T T INF T1/T INF	H/H INF H1/H INF
30.000000	0.686662							
		0.738885	0.807444	0.841065	3.257463	78.809509	5.508956	20.823639
		1.189789	0.473853	3.779961	0.086015	12.578934	11.056101	41.791626
		0.843331	0.921581	0.696026	2.658646	24.744843	6.179977	20.397430
		1.199196	0.521137	3.300567	0.084327	8.595793	10.530690	34.757248
		0.947777	1.035718	0.561783	2.166887	10.067767	6.612741	18.891647
		1.210922	0.574166	2.856855	0.086827	5.923701	9.887260	28.246475
		1.052222	1.149854	0.442242	1.758283	5.078934	6.764135	16.651535
		1.225225	0.631376	2.461739	0.093342	4.116929	9.119061	22.448746
		1.156669	1.263991	0.339545	1.417207	3.054421	6.620456	14.050551
		1.242193	0.690483	2.122293	0.104295	2.902504	8.230683	17.467926
		1.261114	1.378128	0.254262	1.132870	2.113558	6.202653	11.415421
		1.261600	0.748687	1.840409	0.120704	2.108363	7.243883	13.331711
40.000000	0.500356							
		0.583630	0.659124	0.882957	3.449360	115.038116	5.286464	20.714630
		1.187522	0.461752	3.918428	0.087346	14.024972	11.183928	43.823425
		0.750178	0.847215	0.729014	2.787409	31.609909	6.042913	20.603928
		1.196810	0.509572	3.409601	0.084325	9.384852	10.663176	36.357178
		0.916726	1.035306	0.573791	2.209162	10.846749	6.583653	19.069839
		1.209716	0.568987	2.896544	0.086424	6.132065	9.952843	28.828842
		1.083273	1.223396	0.430520	1.719092	4.775195	6.762818	16.386261
		1.226901	0.637606	2.422993	0.094281	3.963589	9.030245	21.880219
		1.249822	1.411489	0.307931	1.312370	2.649455	6.504118	13.124005
		1.248688	0.710972	2.017799	0.109311	2.585273	7.897037	15.934636
		1.416369	1.599580	0.209959	0.981705	1.780349	5.830277	9.876342
		1.274561	0.782972	1.693974	0.134294	1.780349	6.601644	11.183016

AERONAUTICAL RESEARCH ASSOCIATES OF PRINCETON, INC. -- GENERAL TURBULENT EXHAUST MIXING PROGRAM --
TEST RUN A

DEVELOPED REGION

X/R 1	K	R/R 5 GAMMA	R/R 1 M/M INF	U/U 1 CP/CP INF	M RHO/RHO INF	P1/P INF PIN/P INF	T T INF T1/T INF	H/H INF H1/H INF
49.185394	0.012426							
		0.167000	0.195285	0.980854	3.944042	305.801270	4.727530	20.054214
		1.182830	0.435747	4.242006	0.092172	18.131363	11.450107	48.571426
		0.500000	0.584685	0.840896	3.256712	78.692535	5.509827	20.823868
		1.189798	0.473903	3.779405	0.086010	12.573551	11.055567	41.783463
		0.830000	0.970577	0.620327	2.375835	14.633493	6.451602	19.679703
		1.205360	0.549769	3.050359	0.085214	6.992894	10.190882	31.085846
		1.167000	1.364654	0.389074	1.581236	3.868749	6.729220	15.383000
		1.233322	0.660656	2.286000	0.098177	3.452426	8.692061	19.870056
		1.500000	1.754054	0.210225	0.982623	1.782103	5.832906	9.885918
		1.274476	0.782757	1.694853	0.134197	1.782103	6.605824	11.195900
		1.830001	2.139947	0.098148	0.568993	1.231993	4.133655	5.474640
		1.322196	0.885290	1.324407	0.214166	1.231993	4.349251	5.760177
60.000000	0.016445							
		0.167000	0.239398	0.786070	3.019766	49.499130	5.783138	20.808823
		1.193044	0.490735	3.598188	0.084856	10.902195	10.873362	39.124405
		0.500000	0.716762	0.673906	2.574306	21.115341	6.265876	20.222824
		1.200892	0.529190	3.227453	0.084456	8.099001	10.436846	33.684433
		0.830000	1.189824	0.497139	1.943557	6.866026	6.728791	17.785446
		1.218083	0.603750	2.643186	0.089726	4.889318	9.500362	25.111221
		1.167000	1.672921	0.311809	1.325253	2.695112	6.520602	13.240851
		1.247851	0.708393	2.030618	0.108639	2.622758	7.939814	16.122726
		1.500000	2.150285	0.168477	0.835744	1.535596	5.350350	8.329767
		1.289220	0.818050	1.556864	0.152896	1.535596	5.890765	9.171120
		1.830001	2.623348	0.078657	0.487020	1.167814	3.675826	4.631482
		1.333879	0.905927	1.259984	0.246455	1.167814	3.821375	4.814872

DEVELOPED REGION

X/R 1	K	R/R 5 GAMMA	R/R 1 M/M INF	U/U 1 CP/CP INF	M RHO/RHO INF	P1/P INF PIN/P INF	T T INF T1/T INF	H/H INF H1/H INF
70.000000	0.019998							
		0.167000	0.290692	0.622180	2.382578	14.814468	6.445745	19.701324
		1.205196	0.549030	3.056485	0.085177	7.029034	10.199869	31.175751
		0.500000	0.870336	0.533402	2.068012	8.478280	6.672521	18.436478
		1.213920	0.586790	2.763045	0.087941	5.451843	9.724764	26.869965
		0.830000	1.444757	0.393489	1.595881	3.954266	6.735102	15.494738
		1.232598	0.658121	2.300594	0.097715	3.504634	8.730010	20.084213
		1.167000	2.031363	0.246799	1.107649	2.051368	6.148620	11.164306
		1.263620	0.754250	1.815742	0.122670	2.048574	7.142951	12.969753
		1.500000	2.611007	0.133350	0.706675	1.368706	4.817178	6.940405
		1.304153	0.850307	1.440762	0.176515	1.368706	5.183022	7.467499
		1.830001	3.185430	0.062258	0.413091	1.119728	3.238244	3.904608
		1.344862	0.924051	1.205779	0.285356	1.119728	3.333528	4.019499
80.000000	0.022781							
		0.167000	0.350636	0.488796	1.915180	6.549591	6.738246	17.624619
		1.219100	0.607792	2.615609	0.090200	4.765983	9.445820	24.706573
		0.500000	1.049808	0.419049	1.680842	4.499672	6.758180	16.118790
		1.228598	0.643823	2.385078	0.095266	3.817343	8.940537	21.323883
		0.830000	1.742680	0.309132	1.316360	2.663466	6.509294	13.160286
		1.248427	0.710171	2.021769	0.109101	2.596833	7.910343	15.992884
		1.167000	2.450250	0.193889	0.925799	1.678703	5.661254	9.289329
		1.279910	0.796198	1.640861	0.140640	1.678703	6.340355	10.403640
		1.500000	3.149423	0.104762	0.595728	1.255572	4.275264	5.755658
		1.318528	0.878499	1.346270	0.205484	1.255572	4.516909	6.080977
		1.830001	3.842297	0.048911	0.348011	1.084549	2.841836	3.301259
		1.354709	0.939346	1.161564	0.330542	1.084549	2.902878	3.372169

AERONAUTICAL RESEARCH ASSOCIATES OF PRINCETON, INC. -- GENERAL TURBULENT EXHAUST MIXING PROGRAM --
TEST RUN A

DEVELOPED REGION

X/R 1	K	R/R 5 GAMMA	R/R 1 M/M INF	U/U 1 CP/CP INF	M RHO/RHO INF	P'/P INF PTN/P INF	T T INF T'/T INF	H/H INF H'/H INF
100.000000	0.028002							
		0.167000	0.492954	0.307208	1.309970	2.641056	6.500977	13.102143
		1.248845	0.711455	2.015411	0.109438	2.578318	7.889011	15.899605
		0.500000	1.475911	0.263373	1.163553	2.193175	6.264294	11.717503
		1.259216	0.742005	1.870522	0.118450	2.183622	7.363494	13.773582
		0.830000	2.450012	0.194289	0.927199	1.681119	5.665706	9.304122
		1.279772	0.795863	1.642182	0.140470	1.681119	6.347062	10.423035
		1.167000	3.444776	0.121860	0.662869	1.320966	4.612285	6.470028
		1.309661	0.861418	1.402781	0.186766	1.320966	4.926067	6.910196
		1.500000	4.427733	0.065843	0.429743	1.129789	3.338363	4.064893
		1.342361	0.920027	1.217630	0.275592	1.129789	3.443900	4.193398
		1.830001	5.401837	0.030740	0.248059	1.042789	2.235737	2.462900
		1.369651	0.961000	1.101605	0.429836	1.042789	2.261164	2.490911
120.000000	0.033543							
		0.167000	0.666175	0.200582	0.949166	1.719919	5.734076	9.535654
		1.277636	0.790636	1.662980	0.137884	1.719919	6.451199	10.728216
		0.500000	1.994535	0.171961	0.848229	1.554030	5.396389	8.463586
		1.287876	0.814983	1.568379	0.151024	1.554030	5.955253	9.340096
		0.830000	3.310928	0.126855	0.682028	1.341327	4.703383	6.675473
		1.307225	0.856552	1.419291	0.182114	1.341327	5.039463	7.152468
		1.167000	4.655245	0.079564	0.490960	1.170631	3.698566	4.671225
		1.333304	0.904945	1.262982	0.244674	1.170631	3.847139	4.858870
		1.500000	5.983606	0.042990	0.317194	1.070122	2.653234	3.030244
		1.359369	0.946293	1.142095	0.356656	1.070122	2.701200	3.085027
		1.830001	7.300003	0.020071	0.179142	1.022308	1.839470	1.961500
		1.379384	0.974187	1.066339	0.529602	1.022308	1.850668	1.973441

AERONAUTICAL RESEARCH ASSOCIATES OF PRINCETON, INC. -- GENERAL TURBULENT EXHAUST MIXING PROGRAM --
TEST RUN A

DEVELOPED REGION

X/R 1	K	R/R 5 / GAMMA	R/R 1 / M/M INF	U/U 1 / CP/CP INF	M / RHO/RHO INF	P'/P INF / P'N/P INF	T T INF / T'/T INF	H/H INF / H'/H INF
160.000000	0.041770							
		0.167000	1.107635	0.097223	0.565214	1.228769	4.113309	5.435114
		1.322721	0.886249	1.321348	0.215459	1.228769	4.325348	5.715291
		0.500000	3.316275	0.083350	0.507255	1.182562	3.791894	4.836541
		1.330939	0.900871	1.275495	0.237578	1.182562	3.953341	5.042466
		0.830000	5.505015	0.061487	0.409470	1.117600	3.216382	3.870054
		1.345407	0.924921	1.203232	0.287565	1.117600	3.309518	3.982118
		1.167000	7.740183	0.038565	0.293160	1.059834	2.506785	2.826321
		1.362981	0.951554	1.127468	0.379591	1.059834	2.545885	2.870405
		1.500000	9.948824	0.020837	0.184465	1.023653	1.869021	1.997747
		1.378658	0.973228	1.068873	0.520715	1.023653	1.881063	2.010618
		1.830001	12.137570	0.009728	0.099011	1.006827	1.423258	1.469024
		1.389600	0.987320	1.032155	0.693704	1.006827	1.425977	1.471829
200.000000	0.045187							
		0.167000	1.631144	0.056948	0.387834	1.105306	3.085137	3.665853
		1.348675	0.930075	1.188230	0.301470	1.105306	3.166039	3.761982
		0.500000	4.883664	0.048822	0.347560	1.084328	2.839075	3.297221
		1.354776	0.939449	1.161371	0.330900	1.084328	2.899912	3.367875
		0.830000	8.106883	0.036016	0.278866	1.054120	2.420216	2.708324
		1.365113	0.954611	1.119042	0.394432	1.054120	2.454575	2.746774
		1.167000	11.398471	0.022589	0.196386	1.026807	1.935919	2.080463
		1.377016	0.971042	1.074664	0.501592	1.026807	1.949994	2.095590
		1.500000	14.650993	0.012206	0.119883	1.010002	1.525991	1.587554
		1.387077	0.984142	1.040342	0.644920	1.010002	1.530236	1.591970
		1.830001	17.874207	0.005698	0.061909	1.002670	1.251834	1.275412
		1.393809	0.992534	1.018834	0.792864	1.002670	1.252779	1.276375

AERONAUTICAL RESEARCH ASSOCIATES OF PRINCETON, INC. -- GENERAL TURBULENT EXHAUST MIXING PROGRAM --
TEST RUN A

DEVELOPED REGION

X/R 1	K	R/R 5 GAMMA	R/R 1 M/M INF	U/U 1 CP/CP INF	M RHO/RHO INF	P'/P INF P'N/P INF	T T INF T'/T INF	H/H INF H'/H INF
240.000000	0.046253							
		0.167000	2.191142	0.038506	0.292832	1.059702	2.504791	2.823584
		1.363029	0.951624	1.127273	0.379922	1.059702	2.543779	2.867534
		0.500000	6.560308	0.033011	0.261538	1.047576	2.316045	2.568753
		1.367677	0.958239	1.109112	0.413739	1.047576	2.345169	2.601055
		0.830000	10.890111	0.024352	0.208060	1.030088	2.002343	2.163514
		1.375385	0.968852	1.080491	0.483859	1.030088	2.018613	2.181093
		1.167000	15.311756	0.015274	0.144122	1.014449	1.650546	1.733874
		1.384021	0.980234	1.050485	0.593885	1.014449	1.657130	1.740790
		1.500000	19.680923	0.008253	0.085925	1.005146	1.361116	1.398246
		1.391126	0.989223	1.027278	0.726773	1.005146	1.363082	1.400265
		1.830001	24.010727	0.003853	0.043293	1.001307	1.171511	1.186431
		1.395782	0.994940	1.012735	0.849279	1.001307	1.171946	1.186872

NSTOP

TABLES FOR
THE LOCAL NOISE EMISSION SPECTRA
AT VARIOUS ANGLES — THE F-1 ENGINE

FOR THE STRIP AT X= 5.0000

A1= 0.073

FREQUENCY	1/3 OCT.DB OVER ALL	1/3 OCT.DB 60 DEGREE	1/3 OCT.DB 90 DEGREE	1/3 OCT.DB 120 DEGREE	1/3 OCT.DB 150 DEGREE	A1*FREQ
0.00125	-165.73160	-188.33139	-200.54025	-187.95099	-185.94232	0.00009
0.00250	-156.70100	-179.30074	-191.50975	-178.92049	-176.91167	0.00018
0.00500	-147.67041	-170.27008	-182.47910	-169.88983	-167.88116	0.00037
0.01000	-138.63980	-161.23956	-173.44858	-160.85931	-158.85049	0.00073
0.02000	-129.60921	-152.20900	-164.41792	-151.82872	-149.82005	0.00147
0.04000	-120.57861	-143.17845	-155.38727	-142.79813	-140.78941	0.00293
0.08000	-111.54803	-134.14781	-146.35675	-133.76752	-131.75894	0.00587
0.16000	-102.51929	-125.11725	-137.32620	-124.73738	-122.73225	0.01173
0.32000	-93.54419	-116.08740	-128.29576	-115.72118	-113.82077	0.02347
0.64000	-85.62320	-107.08073	-119.27071	-107.06723	-107.33470	0.04694
1.28000	-82.11125	-98.75195	-110.34293	-103.51585	-112.64626	0.09388
2.56000	-80.65253	-98.03125	-101.89426	-113.86444	-130.54202	0.18775
5.12000	-78.42752	-112.67928	-98.77281	-133.69563	-151.46663	0.37551

POWER=0.1145E-09

FOR THE STRIP AT X= 10.0000

A1= 0.147

FREQUENCY	1/3 OCT.DB OVER ALL	1/3 OCT.DB 60 DEGREE	1/3 OCT.DB 90 DEGREE	1/3 OCT.DB 120 DEGREE	1/3 OCT.DB 150 DEGREE	A1*FREQ
0.00125	-156.28229	-178.91153	-191.07446	-178.50534	-176.49545	0.00018
0.00250	-147.25169	-169.88087	-182.04396	-169.47484	-167.46480	0.00037
0.00500	-138.22110	-160.85037	-173.01331	-160.44418	-158.43434	0.00073
0.01000	-129.19049	-151.81978	-163.98279	-151.41364	-149.40372	0.00147
0.02000	-120.15990	-142.78918	-154.95213	-142.38304	-140.37312	0.00293
0.04000	-111.12935	-133.75859	-145.92160	-133.35249	-131.34267	0.00587
0.08000	-102.10062	-124.72803	-136.89101	-124.32234	-122.31607	0.01173
0.16000	-93.12639	-115.69817	-127.86063	-115.30667	-113.40681	0.02347
0.32000	-85.21075	-106.69089	-118.83717	-106.65918	-106.93675	0.04694
0.64000	-81.69336	-98.34482	-109.92632	-103.11984	-112.25652	0.09388
1.28000	-80.21176	-97.46609	-101.49423	-113.47557	-130.14868	0.18775
2.56000	-78.01149	-111.90059	-98.37221	-133.30446	-151.07240	0.37551
5.12000	-80.33109	-132.53520	-108.82843	-154.33147	-172.14000	0.75101

POWER=0.1589E-09

FOR THE STRIP AT X= 15.0000

A1= 0.220

FREQUENCY	1/3 OCT.DB OVER ALL	1/3 OCT.DB 60 DEGREE	1/3 OCT.DB 90 DEGREE	1/3 OCT.DB 120 DEGREE	1/3 OCT.DB 150 DEGREE	A1*FREQ
0.00125	-150.55886	-173.21436	-185.32449	-172.78055	-170.76898	0.00028
0.00250	-141.52829	-164.18385	-176.29384	-163.74989	-161.73843	0.00055
0.00500	-132.49768	-155.15326	-167.26318	-154.71936	-152.70784	0.00110
0.01000	-123.46709	-146.12270	-158.23267	-145.68877	-143.67723	0.00220
0.02000	-114.43648	-137.09204	-149.20210	-136.65816	-134.64665	0.00440
0.04000	-105.40636	-128.06151	-140.17151	-127.62772	-125.61700	0.00880
0.08000	-96.38994	-119.03102	-131.14095	-118.60086	-116.61714	0.01760
0.16000	-87.72580	-110.00581	-122.11270	-109.67789	-108.39148	0.03520
0.32000	-82.14561	-101.14375	-113.14018	-102.78001	-107.80908	0.07041
0.64000	-80.45467	-95.58170	-104.40120	-106.98050	-121.44749	0.14082
1.28000	-78.33240	-103.51976	-97.96410	-124.29347	-141.92557	0.28163
2.56000	-77.98277	-122.68680	-102.14366	-145.17717	-162.97792	0.56326
5.12000	-84.76988	-143.66817	-119.68723	-166.24355	-184.04979	1.12652

POWER=0.1803E-09

FOR THE STRIP AT X= 20.0000

A1= 0.293

FREQUENCY	1/3 OCT.DB OVER ALL	1/3 OCT.DB 60 DEGREE	1/3 OCT.DB 90 DEGREE	1/3 OCT.DB 120 DEGREE	1/3 OCT.DB 150 DEGREE	A1*FREQ
0.00125	-146.31912	-169.01758	-181.06454	-168.55341	-166.53970	0.00037
0.00250	-137.28853	-159.98700	-172.03389	-159.52284	-157.50911	0.00073
0.00500	-128.25793	-150.95639	-163.00339	-150.49225	-148.47852	0.00147
0.01000	-119.22733	-141.92580	-153.97282	-141.46162	-139.44791	0.00293
0.02000	-110.19682	-132.89519	-144.94223	-132.43109	-130.41745	0.00587
0.04000	-101.16811	-123.86464	-135.91164	-123.40100	-121.39113	0.01173
0.08000	-92.19656	-114.83473	-126.88148	-114.38707	-112.48872	0.02347
0.16000	-84.29510	-105.82594	-117.86467	-105.75803	-106.06444	0.04694
0.32000	-80.73866	-97.43781	-109.00446	-102.25314	-111.40623	0.09388
0.64000	-79.16835	-96.12526	-100.61691	-112.62758	-129.28770	0.18775
1.28000	-77.08443	-109.49971	-97.49402	-132.44980	-150.20895	0.37551
2.56000	-79.48581	-129.05434	-107.80539	-153.47627	-171.27657	0.75101
5.12000	-88.07309	-150.02879	-127.76555	-174.54723	-192.34889	1.50203

POWER=0.2028E-09

FOR THE STRIP AT X= 25.0000

A1= 0.367

FREQUENCY	1/3 OCT.DB OVER ALL	1/3 OCT.DB 60 DEGREE	1/3 OCT.DB 90 DEGREE	1/3 OCT.DB 120 DEGREE	1/3 OCT.DB 150 DEGREE	A1*FREQ
0.00125	-142.21056	-165.61240	-173.66449	-163.69812	-162.08333	0.00046
0.00250	-133.17995	-156.58180	-164.63383	-154.66753	-153.05273	0.00092
0.00500	-124.14937	-147.55121	-155.60335	-145.63693	-144.02214	0.00183
0.01000	-115.11874	-138.52060	-146.57275	-136.60632	-134.99156	0.00367
0.02000	-106.08885	-129.49001	-137.54216	-127.57605	-125.96249	0.00733
0.04000	-97.07916	-120.45946	-128.51175	-118.55464	-116.98055	0.01467
0.08000	-88.45079	-111.43083	-119.48729	-109.78314	-108.88821	0.02934
0.16000	-81.97061	-102.46367	-110.64075	-102.93301	-105.71751	0.05867
0.32000	-79.65523	-95.06294	-104.03069	-103.58748	-115.95995	0.11735
0.64000	-77.86287	-97.87387	-98.21538	-118.32774	-135.74229	0.23469
1.28000	-76.56248	-112.86205	-98.60976	-138.96262	-156.76703	0.46938
2.56000	-81.36049	-128.05174	-113.28094	-160.02061	-177.83784	0.93877
5.12000	-90.58263	-148.30562	-133.95518	-181.09264	-198.91032	1.87753

POWER=0.2314E-09

FOR THE STRIP AT X= 30.0000

A1= 0.440

FREQUENCY	1/3 OCT.DB OVER ALL	1/3 OCT.DB 60 DEGREE	1/3 OCT.DB 90 DEGREE	1/3 OCT.DB 120 DEGREE	1/3 OCT.DB 150 DEGREE	A1*FREQ
0.00125	-139.21317	-162.66039	-170.43817	-160.69646	-159.10353	0.00055
0.00250	-130.18262	-153.62979	-161.40758	-151.66586	-150.07292	0.00110
0.00500	-121.15196	-144.59920	-152.37698	-142.63527	-141.04234	0.00220
0.01000	-112.12144	-135.56859	-143.34637	-133.60469	-132.01186	0.00440
0.02000	-103.09261	-126.53799	-134.31583	-124.57494	-122.98544	0.00880
0.04000	-94.11552	-117.50754	-125.28592	-115.57007	-114.08022	0.01760
0.08000	-85.80745	-108.48161	-116.27667	-107.13724	-106.68501	0.03520
0.16000	-80.42995	-99.59814	-107.80634	-101.30540	-106.40050	0.07041
0.32000	-78.60023	-93.63519	-102.21259	-105.64006	-120.20012	0.14082
0.64000	-76.57388	-99.46625	-96.64868	-123.05476	-140.69728	0.28163
1.28000	-76.53740	-114.24919	-100.42087	-143.94431	-161.75040	0.56326
2.56000	-83.01115	-122.18832	-117.85860	-165.01085	-182.82213	1.12652
5.12000	-92.35889	-128.28694	-138.76521	-186.08302	-203.89445	2.25304

POWER=0.2678E-09

FOR THE STRIP AT X= 35.0000

A1= 0.513

FREQUENCY	1/3 OCT.DB OVER ALL	1/3 OCT.DB 60 DEGREE	1/3 OCT.DB 90 DEGREE	1/3 OCT.DB 120 DEGREE	1/3 OCT.DB 150 DEGREE	A1*FREQ
0.00125	-136.42072	-159.92210	-167.29745	-157.89865	-156.33891	0.00064
0.00250	-127.39012	-150.89151	-158.26692	-148.86804	-147.30833	0.00128
0.00500	-118.35957	-141.86092	-149.23633	-139.83746	-138.27774	0.00257
0.01000	-109.32906	-132.83031	-140.20572	-130.80695	-129.24745	0.00513
0.02000	-100.30283	-123.79971	-131.17522	-121.77850	-120.22705	0.01027
0.04000	-91.39056	-114.76939	-122.14714	-112.81447	-111.47615	0.02054
0.08000	-83.47807	-105.74811	-113.19481	-104.87675	-104.91428	0.04107
0.16000	-79.05548	-97.00349	-105.61617	-100.30203	-107.59711	0.08214
0.32000	-77.27412	-92.58585	-100.23662	-107.98602	-123.89336	0.16428
0.64000	-75.36087	-99.32660	-95.63184	-126.96342	-144.68440	0.32857
1.28000	-76.75214	-117.62416	-102.49130	-147.94928	-165.74774	0.65714
2.56000	-84.33354	-138.57057	-121.51622	-169.01888	-186.81978	1.31427
5.12000	-93.49854	-159.63908	-142.51003	-190.09120	-207.89226	2.62855

POWER=0.3213E-09

FOR THE STRIP AT X= 40.5493

A1= 0.595

FREQUENCY	1/3 OCT.DB OVER ALL	1/3 OCT.DB 60 DEGREE	1/3 OCT.DB 90 DEGREE	1/3 OCT.DB 120 DEGREE	1/3 OCT.DB 150 DEGREE	A1*FREQ
0.00125	-132.40704	-156.06616	-161.81636	-153.86954	-152.45998	0.00074
0.00250	-123.37645	-147.03558	-152.78577	-144.83894	-143.42938	0.00149
0.00500	-114.34590	-138.00499	-143.75517	-135.80840	-134.39883	0.00297
0.01000	-105.31584	-128.97437	-134.72470	-126.77820	-125.36955	0.00595
0.02000	-96.30304	-119.94382	-125.69754	-117.76170	-116.38029	0.01190
0.04000	-87.59158	-110.91432	-116.75690	-109.05237	-108.08363	0.02379
0.08000	-80.18372	-101.91087	-108.60632	-101.89218	-102.65390	0.04758
0.16000	-76.15721	-93.31567	-104.05132	-98.95535	-108.52570	0.09517
0.32000	-74.13562	-89.67181	-97.25264	-109.89998	-126.59869	0.19033
0.64000	-73.39459	-94.48521	-93.95528	-129.80487	-147.52269	0.38066
1.28000	-76.40823	-104.21346	-103.26897	-150.83350	-168.59030	0.76133
2.56000	-84.15066	-123.13829	-123.17453	-171.90446	-189.66249	1.52265
5.12000	-94.81339	-144.12303	-144.20634	-192.97679	-210.73497	3.04531

POWER=0.5206E-09

FOR THE STRIP AT X= 50.0000

A1= 0.733

FREQUENCY	1/3 OCT.DB OVER ALL	1/3 OCT.DB 60 DEGREE	1/3 OCT.DB 90 DEGREE	1/3 OCT.DB 120 DEGREE	1/3 OCT.DB 150 DEGREE	A1*FREQ
0.00125	-124.77042	-149.78807	-152.64789	-145.31317	-144.30232	0.00092
0.00250	-115.73982	-140.75748	-143.61729	-136.28258	-135.27173	0.00183
0.00500	-106.70927	-131.72688	-134.58670	-127.25204	-126.24127	0.00366
0.01000	-97.68095	-122.69626	-125.55650	-118.22279	-117.21548	0.00733
0.02000	-88.71674	-113.66600	-116.53745	-109.23216	-108.32521	0.01465
0.04000	-80.60303	-104.64357	-107.65121	-100.96132	-101.37628	0.02930
0.08000	-74.53526	-95.68219	-99.61703	-96.15167	-99.14503	0.05861
0.16000	-71.65466	-87.93034	-95.54686	-97.07314	-109.87770	0.11722
0.32000	-70.10863	-86.96294	-92.11168	-112.32504	-129.84303	0.23443
0.64000	-69.97456	-101.58772	-91.30997	-133.02505	-150.87535	0.46887
1.28000	-74.38335	-122.32748	-105.43399	-154.08514	-171.94662	0.93774
2.56000	-83.60500	-143.38914	-126.08138	-175.15718	-193.01897	1.87547
5.12000	-91.98236	-164.46117	-147.13985	-196.22951	-214.09129	3.75094

POWER=0.1249E-08

FOR THE STRIP AT X= 60.0000

A1= 0.909

FREQUENCY	1/3 OCT.DB OVER ALL	1/3 OCT.DB 60 DEGREE	1/3 OCT.DB 90 DEGREE	1/3 OCT.DB 120 DEGREE	1/3 OCT.DB 150 DEGREE	A1*FREQ
0.00125	-120.60701	-144.28514	-148.81961	-141.75723	-140.59645	0.00114
0.00250	-111.57640	-135.25455	-139.78902	-132.72664	-131.56584	0.00227
0.00500	-102.54608	-126.22395	-130.75861	-123.69627	-122.53586	0.00455
0.01000	-93.52406	-117.19348	-121.73300	-114.67371	-113.52362	0.00909
0.02000	-84.66968	-108.16641	-112.79611	-105.80199	-104.88324	0.01818
0.04000	-76.83759	-99.15714	-104.31198	-98.39047	-98.50465	0.03637
0.08000	-71.44229	-90.32317	-98.08180	-93.57205	-99.21274	0.07274
0.16000	-68.90944	-84.11754	-94.18019	-98.70721	-113.26663	0.14548
0.32000	-67.48082	-85.37787	-89.15424	-116.28020	-133.78368	0.29095
0.64000	-68.82358	-90.96463	-94.30626	-137.17868	-154.83730	0.58190
1.28000	-76.00417	-98.78186	-112.29440	-158.24545	-175.90903	1.16380
2.56000	-85.44344	-115.56853	-133.23137	-179.31764	-196.98137	2.32761
5.12000	-99.64677	-136.40620	-154.29942	-200.39012	-218.05385	4.65522

POWER=0.1990E-08

FOR THE STRIP AT X= 70.0000

A1= 1.112

FREQUENCY	1/3 OCT.DB OVER ALL	1/3 OCT.DB 60 DEGREE	1/3 OCT.DB 90 DEGREE	1/3 OCT.DB 120 DEGREE	1/3 OCT.DB 150 DEGREE	A1*FREQ
0.00125	-115.93790	-141.20529	-142.81462	-136.43515	-135.62024	0.00139
0.00250	-106.90736	-132.17470	-133.78403	-127.40460	-126.58974	0.00278
0.00500	-97.87805	-123.14424	-124.75444	-118.37515	-117.56157	0.00556
0.01000	-88.88120	-114.11681	-115.74974	-109.37326	-108.59482	0.01112
0.02000	-80.36749	-105.11479	-106.88708	-100.74045	-100.69009	0.02224
0.04000	-73.75287	-96.14114	-98.64433	-95.21049	-97.57234	0.04447
0.08000	-69.45847	-87.43584	-93.20009	-94.54919	-102.88416	0.08895
0.16000	-67.05089	-81.54939	-91.84277	-103.91811	-119.62778	0.17790
0.32000	-66.41977	-87.40486	-91.38339	-123.12636	-140.46185	0.35580
0.64000	-70.88432	-106.51028	-102.15335	-144.12502	-161.52644	0.71159
1.28000	-80.24492	-127.50896	-121.98486	-165.19522	-182.59863	1.42319
2.56000	-87.80470	-148.57896	-143.01241	-186.26741	-203.67113	2.84638
5.12000	-95.52936	-169.65129	-164.08336	-207.33989	-224.74345	5.69275

POWER=0.2420E-08

FOR THE STRIP AT X= 80.0000

A1= 1.341

FREQUENCY	1/3 OCT.DB OVER ALL	1/3 OCT.DB 60 DEGREE	1/3 OCT.DB 90 DEGREE	1/3 OCT.DB 120 DEGREE	1/3 OCT.DB 150 DEGREE	A1*FREQ
0.00125	-112.26474	-138.43683	-138.19307	-132.32620	-131.75502	0.00168
0.00250	-103.23433	-129.40630	-129.16266	-123.29579	-122.72475	0.00335
0.00500	-94.20975	-120.37740	-120.13878	-114.27080	-113.70348	0.00671
0.01000	-85.23235	-111.37476	-111.18472	-105.31714	-104.85513	0.01341
0.02000	-77.43417	-102.39690	-102.45840	-97.21086	-98.49690	0.02682
0.04000	-71.91856	-93.49060	-94.65840	-94.69966	-99.87968	0.05364
0.08000	-67.78185	-84.83559	-91.14676	-99.06520	-109.36018	0.10729
0.16000	-65.71947	-80.04338	-93.20871	-112.12721	-128.02948	0.21458
0.32000	-67.43130	-85.43008	-98.93661	-132.26309	-148.99477	0.42916
0.64000	-75.17645	-91.64886	-113.72672	-153.30196	-170.06374	0.85832
1.28000	-84.16493	-98.17448	-134.33585	-174.37338	-191.13608	1.71664
2.56000	-94.19115	-110.69571	-155.39293	-195.44572	-212.20842	3.43328
5.12000	-101.22456	-130.83888	-176.46480	-216.51820	-233.28062	6.86656

POWER=0.2601E-08

FOR THE STRIP AT X= 100.0000

A1= 1.882

FREQUENCY	1/3 OCT.DB OVER ALL	1/3 OCT.DB 60 DEGREE	1/3 OCT.DB 90 DEGREE	1/3 OCT.DB 120 DEGREE	1/3 OCT.DB 150 DEGREE	A1*FREQ
0.00125	-106.39944	-132.56671	-130.58115	-126.37401	-126.35962	0.00235
0.00250	-97.37436	-123.54099	-121.55832	-117.34920	-117.33583	0.00471
0.00500	-88.41119	-114.56152	-112.59758	-108.38048	-108.40472	0.00941
0.01000	-80.05695	-105.65364	-103.86394	-99.93712	-100.78363	0.01882
0.02000	-74.00768	-96.86760	-96.06638	-95.92032	-100.86028	0.03765
0.04000	-67.89827	-88.32616	-92.72787	-100.45122	-107.51897	0.07530
0.08000	-63.97212	-80.74313	-97.34590	-111.08936	-122.42612	0.15059
0.16000	-66.08954	-78.70546	-108.46750	-130.52332	-143.01259	0.30118
0.32000	-74.26227	-85.76228	-128.13242	-151.53230	-164.06862	0.60236
0.64000	-83.28073	-93.46021	-149.15218	-172.60280	-185.14049	1.20473
1.28000	-92.68657	-102.65999	-170.22299	-193.67514	-206.21283	2.40946
2.56000	-102.99574	-121.06250	-191.29533	-214.74748	-227.28517	4.81891
5.12000	-113.63240	-142.01793	-212.36781	-235.81969	-248.35753	9.63783

POWER=0.3193E-08

FOR THE STRIP AT X= 120.0000

A1= 2.539

FREQUENCY	1/3 OCT.DB OVER ALL	1/3 OCT.DB 60 DEGREE	1/3 OCT.DB 90 DEGREE	1/3 OCT.DB 120 DEGREE	1/3 OCT.DB 150 DEGREE	A1*FREQ
0.00125	-106.29567	-132.08942	-129.32573	-126.44740	-126.91505	0.00317
0.00250	-97.31612	-123.12111	-120.35605	-117.46913	-117.94775	0.00635
0.00500	-88.68042	-114.28564	-111.60924	-108.85139	-109.64043	0.01269
0.01000	-81.93370	-105.65393	-103.82848	-103.16933	-106.66309	0.02539
0.02000	-76.06403	-97.58127	-100.61963	-106.01094	-111.52696	0.05078
0.04000	-69.46138	-91.32423	-105.06483	-112.67226	-119.74382	0.10155
0.08000	-69.65047	-92.45311	-112.97699	-126.74690	-137.11909	0.20310
0.16000	-77.69594	-108.39093	-129.94179	-147.23637	-158.00084	0.40620
0.32000	-86.79813	-129.19412	-150.79240	-168.28920	-179.06709	0.81240
0.64000	-95.75858	-150.25783	-171.85756	-189.36107	-200.13927	1.62481
1.28000	-105.14862	-171.33002	-192.92975	-210.43341	-221.21176	3.24961
2.56000	-114.38495	-192.40236	-214.00224	-231.50572	-242.28404	6.49922
5.12000	-120.95433	-213.47469	-235.07457	-252.57823	-263.35620	12.99845

POWER=0.9677E-09

FOR THE STRIP AT X= 160.0000

A1= 4.087

FREQUENCY	1/3 OCT.DB OVER ALL	1/3 OCT.DB 60 DEGREE	1/3 OCT.DB 90 DEGREE	1/3 OCT.DB 120 DEGREE	1/3 OCT.DB 150 DEGREE	A1*FREQ
0.00125	-106.36958	-131.31158	-128.21107	-126.76889	-127.90552	0.00511
0.00250	-98.07999	-122.79507	-119.79282	-118.63942	-120.18242	0.01022
0.00500	-92.33139	-115.43169	-113.87137	-115.35387	-119.07724	0.02044
0.01000	-88.18076	-112.06509	-115.70110	-119.86388	-124.39444	0.04087
0.02000	-86.85220	-116.11380	-121.51305	-126.07222	-130.93871	0.08175
0.04000	-96.58813	-122.73610	-129.10240	-136.52011	-143.75658	0.16349
0.08000	-115.44923	-136.30875	-145.37483	-155.85641	-163.97531	0.32698
0.16000	-136.29114	-156.70354	-166.16048	-176.86162	-185.01820	0.65397
0.32000	-157.35506	-177.75301	-187.22368	-197.93199	-206.08965	1.30793
0.64000	-178.42708	-198.82472	-208.29585	-219.00432	-227.16197	2.61586
1.28000	-199.49957	-219.89706	-229.36819	-240.07651	-248.23422	5.23172
2.56000	-220.57191	-240.96935	-250.44054	-261.14893	-269.30664	10.46345
5.12000	-241.64415	-262.04175	-271.51270	-282.22119	-290.37891	20.92690

POWER=0.1616E-10

FOR THE STRIP AT X= 200.0000

A1= 5.786

FREQUENCY	1/3 OCT.DB OVER ALL	1/3 OCT.DB 60 DEGREE	1/3 OCT.DB 90 DEGREE	1/3 OCT.DB 120 DEGREE	1/3 OCT.DB 150 DEGREE	A1*FREQ
0.00125	-107.23773	-130.68872	-128.50647	-127.95103	-129.70038	0.00723
0.00250	-101.92834	-124.06343	-123.24564	-124.63416	-127.92929	0.01447
0.00500	-101.15306	-123.89966	-126.03819	-129.09805	-133.03755	0.02893
0.01000	-105.64639	-129.31497	-131.90341	-135.10439	-139.11273	0.05786
0.02000	-113.12715	-135.48166	-138.45917	-142.42506	-147.26935	0.11572
0.04000	-127.41513	-144.82806	-151.19400	-158.12134	-164.57123	0.23145
0.08000	-147.38998	-163.33078	-171.38422	-178.84775	-185.45160	0.46289
0.16000	-168.41634	-184.29021	-192.42589	-199.90895	-206.51799	0.92578
0.32000	-189.48717	-205.35905	-213.49733	-220.98100	-227.59019	1.85156
0.64000	-210.55965	-226.43138	-234.56966	-242.05330	-248.66243	3.70313
1.28000	-231.63199	-247.50351	-255.64194	-263.12573	-269.73462	7.40625
2.56000	-252.70421	-268.57593	-276.71436	-284.19800	-290.80713	14.81250
5.12000	-273.77661	-289.64844	-297.78687	-305.27051	-311.87939	29.62500

POWER=0.6788E-12

TABLES FOR

THE LOCAL NOISE EMISSION SPECTRA AT

VARIOUS ANGLES — THE HIGH CHAMBER PRESSURE ENGINE

FOR THE STRIP AT X= 5.0000

A1= 0.059

FREQUENCY	1/3 OCT.DB OVER ALL	1/3 OCT.DB 60 DEGREE	1/3 OCT.DB 90 DEGREE	1/3 OCT.DB 120 DEGREE	1/3 OCT.DB 150 DEGREE	A1*FREQ
0.00125	-174.28827	-196.78644	-211.25665	-196.39536	-194.31726	0.00007
0.00250	-165.25761	-187.75594	-202.22600	-187.36470	-185.28676	0.00015
0.00500	-156.22713	-178.72528	-193.19550	-178.33405	-176.25610	0.00030
0.01000	-147.19652	-169.69476	-184.16483	-169.30353	-167.22543	0.00059
0.02000	-138.16594	-160.66411	-175.13432	-160.27287	-158.19493	0.00119
0.04000	-129.13533	-151.63345	-166.10367	-151.24237	-149.16437	0.00238
0.08000	-120.10481	-142.60297	-157.07300	-142.21179	-140.13391	0.00475
0.16000	-111.07675	-133.57243	-148.04250	-133.18163	-131.10814	0.00951
0.32000	-102.12482	-124.54424	-139.01196	-124.16533	-122.22974	0.01902
0.64000	-94.63527	-115.58841	-129.98154	-115.56805	-116.51080	0.03804
1.28000	-92.10101	-108.49042	-120.95714	-113.08832	-124.74225	0.07608
2.56000	-91.50294	-113.36313	-112.11685	-126.12033	-144.17558	0.15216
5.12000	-89.76170	-131.53987	-106.48193	-146.57024	-165.18581	0.30432

POWER=0.9884E-11

FOR THE STRIP AT X= 10.0000

A1= 0.119

FREQUENCY	1/3 OCT.DB OVER ALL	1/3 OCT.DB 60 DEGREE	1/3 OCT.DB 90 DEGREE	1/3 OCT.DB 120 DEGREE	1/3 OCT.DB 150 DEGREE	A1*FREQ
0.00125	-164.92000	-187.41388	-201.88791	-187.03378	-184.95447	0.00015
0.00250	-155.88940	-178.38338	-192.85741	-178.00328	-175.92397	0.00030
0.00500	-146.85881	-169.35272	-183.82675	-168.97263	-166.89331	0.00059
0.01000	-137.82820	-160.32205	-174.79623	-159.94211	-157.86279	0.00119
0.02000	-128.79761	-151.29156	-165.76558	-150.91153	-148.83220	0.00238
0.04000	-119.76711	-142.26099	-156.73492	-141.88092	-139.80174	0.00475
0.08000	-110.73901	-133.23047	-147.70444	-132.85078	-130.77605	0.00951
0.16000	-101.78780	-124.20221	-138.67384	-123.83466	-121.89909	0.01902
0.32000	-94.30504	-115.24646	-129.64349	-115.24132	-116.19305	0.03804
0.64000	-91.77431	-108.14781	-120.61937	-112.77405	-124.42928	0.07608
1.28000	-91.16516	-113.00986	-111.78647	-125.80658	-143.85626	0.15216
2.56000	-89.42146	-131.16975	-106.17751	-146.25398	-164.86589	0.30432
5.12000	-89.83589	-152.11345	-113.57553	-167.30525	-185.93639	0.60863

POWER=0.1435E-10

FOR THE STRIP AT X= 15.0000

A1= 0.178

FREQUENCY	1/3 OCT.DB OVER ALL	1/3 OCT.DB 60 DEGREE	1/3 OCT.DB 90 DEGREE	1/3 OCT.DB 120 DEGREE	1/3 OCT.DB 150 DEGREE	A1*FREQ
0.00125	-159.27991	-181.76950	-196.24826	-181.40283	-179.32184	0.00022
0.00250	-150.24931	-172.73885	-187.21761	-172.37233	-170.29118	0.00045
0.00500	-141.21872	-163.70834	-178.18695	-163.34167	-161.26068	0.00089
0.01000	-132.18811	-154.67776	-169.15643	-154.31113	-152.23010	0.00178
0.02000	-123.15756	-145.64717	-160.12578	-145.28053	-143.19955	0.00357
0.04000	-114.12752	-136.61662	-151.09528	-136.25003	-134.17015	0.00713
0.08000	-105.11644	-127.58656	-142.06468	-127.22292	-125.17703	0.01426
0.16000	-96.60768	-118.57384	-133.03412	-118.30191	-117.19910	0.02853
0.32000	-91.94324	-110.08197	-124.00516	-111.83461	-118.64113	0.05706
0.64000	-91.02641	-108.55884	-115.02586	-118.35562	-134.97884	0.11412
1.28000	-89.84494	-122.42912	-107.23326	-137.24631	-155.79123	0.22824
2.56000	-88.51744	-142.97853	-108.05193	-158.23015	-176.85533	0.45647
5.12000	-93.49225	-164.03362	-123.98076	-179.29973	-197.92735	0.91295

POWER=0.1617E-10

FOR THE STRIP AT X= 20.0000

A1= 0.238

FREQUENCY	1/3 OCT.DB OVER ALL	1/3 OCT.DB 60 DEGREE	1/3 OCT.DB 90 DEGREE	1/3 OCT.DB 120 DEGREE	1/3 OCT.DB 150 DEGREE	A1*FREQ
0.00125	-155.16003	-177.63467	-192.11893	-177.28433	-175.20135	0.00030
0.00250	-146.12944	-168.60417	-183.08827	-168.25368	-166.17070	0.00059
0.00500	-137.09885	-159.57358	-174.05777	-159.22319	-157.14020	0.00119
0.01000	-128.06825	-150.54297	-165.02710	-150.19258	-148.10959	0.00238
0.02000	-119.03775	-141.51237	-155.99660	-141.16200	-139.07918	0.00475
0.04000	-110.00977	-132.48183	-146.96596	-132.13185	-130.05359	0.00951
0.08000	-101.06073	-123.45361	-137.93539	-123.11613	-121.18076	0.01902
0.16000	-93.59863	-114.49788	-128.90501	-114.53352	-115.50879	0.03804
0.32000	-91.08202	-107.39706	-119.88176	-112.09872	-123.75679	0.07608
0.64000	-90.33897	-112.21555	-111.06992	-125.13211	-143.16722	0.15216
1.28000	-88.64571	-130.32483	-105.52637	-145.57272	-164.17578	0.30432
2.56000	-89.18146	-151.26482	-112.79689	-166.62370	-185.24614	0.60863
5.12000	-96.60658	-172.33302	-132.09865	-187.69542	-206.31847	1.21727

POWER=0.1776E-10

FOR THE STRIP AT x= 25.0000

A1= 0.297

FREQUENCY	1/3 OCT.DB OVER ALL	1/3 OCT.DB 60 DEGREE	1/3 OCT.DB 90 DEGREE	1/3 OCT.DB 120 DEGREE	1/3 OCT.DB 150 DEGREE	A1*FREQ
0.00125	-151.84511	-174.30826	-188.79907	-173.97821	-171.89264	0.00037
0.00250	-142.81456	-165.27760	-179.76857	-164.94756	-162.86211	0.00074
0.00500	-133.78392	-156.24707	-170.73792	-155.91704	-153.83151	0.00149
0.01000	-124.75336	-147.21646	-161.70740	-146.88643	-144.80090	0.00297
0.02000	-115.72295	-138.18587	-152.67679	-137.85583	-135.77081	0.00594
0.04000	-106.70058	-129.15550	-143.64619	-128.82671	-126.75584	0.01189
0.08000	-97.90923	-120.13210	-134.61565	-119.84218	-118.19531	0.02377
0.16000	-91.86891	-111.32626	-125.58577	-112.05945	-115.93317	0.04755
0.32000	-90.47556	-106.68054	-116.57936	-114.27625	-129.08389	0.09510
0.64000	-89.48558	-116.66885	-108.18250	-131.11577	-149.52754	0.19020
1.28000	-87.80075	-136.50702	-105.63634	-151.96799	-170.57867	0.38040
2.56000	-90.70236	-157.53465	-117.96864	-173.03346	-191.65041	0.76079
5.12000	-98.75755	-178.60561	-138.38374	-194.10564	-212.72273	1.52158

POWER=0.1946E-10

FOR THE STRIP AT X= 30.0000

A1= 0.357

FREQUENCY	1/3 OCT.DB OVER ALL	1/3 OCT.DB 60 DEGREE	1/3 OCT.DB 90 DEGREE	1/3 OCT.DB 120 DEGREE	1/3 OCT.DB 150 DEGREE	A1*FREQ
0.00125	-149.02162	-171.46921	-185.96857	-171.16525	-169.07648	0.00045
0.00250	-139.99103	-162.43864	-176.93791	-162.13470	-160.04588	0.00089
0.00500	-130.96043	-153.40805	-167.90741	-153.10411	-151.01529	0.00178
0.01000	-121.92982	-144.37746	-158.87674	-144.07350	-141.98473	0.00357
0.02000	-112.89992	-135.34685	-149.84624	-135.04300	-132.95537	0.00713
0.04000	-103.89005	-126.31680	-140.81563	-126.01613	-123.96460	0.01426
0.08000	-95.40425	-117.30417	-131.78511	-117.10201	-116.03052	0.02853
0.16000	-90.78391	-108.81314	-122.75664	-110.69991	-117.53400	0.05706
0.32000	-89.86400	-107.72316	-113.79198	-117.25380	-133.84146	0.11412
0.64000	-88.55762	-120.88673	-106.14200	-136.11992	-154.64503	0.22824
1.28000	-87.38795	-141.39914	-106.83409	-157.10135	-175.70868	0.45647
2.56000	-92.36571	-162.45287	-122.61644	-178.17079	-196.78087	0.91295
5.12000	-100.24813	-183.52473	-143.41075	-199.24312	-217.85320	1.82590

POWER=0.2155E-10

FOR THE STRIP AT X= 35.0000

A1= 0.416

FREQUENCY	1/3 OCT.DB OVER ALL	1/3 OCT.DB 60 DEGREE	1/3 OCT.DB 90 DEGREE	1/3 OCT.DB 120 DEGREE	1/3 OCT.DB 150 DEGREE	A1*FREQ
0.00125	-146.48608	-168.93182	-183.12082	-168.61566	-166.54001	0.00052
0.00250	-137.45549	-159.90129	-174.09032	-159.58517	-157.50948	0.00104
0.00500	-128.42491	-150.87068	-165.05966	-150.55458	-148.47888	0.00208
0.01000	-119.39433	-141.84007	-156.02913	-141.52396	-139.44836	0.00416
0.02000	-110.36543	-132.80949	-146.99858	-132.49373	-130.42108	0.00832
0.04000	-101.38487	-123.78014	-137.96822	-123.47495	-121.48970	0.01664
0.08000	-93.38382	-114.78838	-128.94514	-114.73372	-114.59137	0.03328
0.16000	-89.95537	-106.84958	-120.05675	-110.22960	-119.70215	0.06657
0.32000	-89.14644	-108.37549	-111.36031	-120.41568	-137.93024	0.13314
0.64000	-87.57938	-124.41641	-104.77437	-140.31215	-158.87386	0.26628
1.28000	-87.32838	-145.19415	-108.64590	-161.34177	-179.94223	0.53255
2.56000	-93.73691	-166.25703	-126.57829	-182.41273	-201.01442	1.06511
5.12000	-101.68774	-187.32921	-147.51796	-203.48506	-222.08675	2.13021

POWER=0.2425E-10

FOR THE STRIP AT X= 40.0000

A1= 0.475

FREQUENCY	1/3 OCT.DB OVER ALL	1/3 OCT.DB 60 DEGREE	1/3 OCT.DB 90 DEGREE	1/3 OCT.DB 120 DEGREE	1/3 OCT.DB 150 DEGREE	A1*FREQ
0.00125	-144.14862	-166.55405	-180.70245	-166.28793	-164.20798	0.00059
0.00250	-135.11798	-157.52357	-171.67195	-157.25735	-155.17738	0.00119
0.00500	-126.08743	-148.49298	-162.64130	-148.22675	-146.14679	0.00238
0.01000	-117.05692	-139.46237	-153.61078	-139.19620	-137.11641	0.00475
0.02000	-108.02972	-130.43182	-144.58023	-130.16643	-128.09271	0.00951
0.04000	-99.09756	-121.40367	-135.55060	-121.16113	-119.25871	0.01902
0.08000	-91.71129	-112.44904	-126.54819	-112.67081	-113.74680	0.03804
0.16000	-89.20964	-105.33525	-117.78773	-110.37140	-122.04192	0.07608
0.32000	-88.28973	-109.59375	-109.19307	-123.41193	-141.39108	0.15216
0.64000	-86.59116	-126.47125	-103.88271	-143.82747	-162.39513	0.30432
1.28000	-87.49774	-147.23486	-110.68379	-164.87723	-183.46533	0.60863
2.56000	-94.75627	-168.29698	-129.87788	-185.94896	-204.53767	1.21727
5.12000	-103.22937	-189.36900	-150.88023	-207.02144	-225.61015	2.43453

POWER=0.2777E-10

FOR THE STRIP AT X= 49.1854

A1= 0.585

FREQUENCY	1/3 OCT.DB OVER ALL	1/3 OCT.DB 60 DEGREE	1/3 OCT.DB 90 DEGREE	1/3 OCT.DB 120 DEGREE	1/3 OCT.DB 150 DEGREE	A1*FREQ
0.00125	-138.26546	-161.98930	-169.44238	-159.73488	-158.15169	0.00073
0.00250	-129.23486	-152.95871	-160.41188	-150.70428	-149.12109	0.00146
0.00500	-120.20432	-143.92812	-151.38129	-141.67374	-140.09059	0.00292
0.01000	-111.17540	-134.89749	-142.35077	-132.64406	-131.06393	0.00585
0.02000	-102.19496	-125.86710	-133.32365	-123.64262	-122.14960	0.01169
0.04000	-93.80106	-116.84233	-124.38351	-115.20604	-114.51929	0.02339
0.08000	-87.96733	-107.99358	-116.21608	-108.71817	-112.57700	0.04677
0.16000	-86.23305	-102.33051	-111.77554	-110.90840	-125.54605	0.09355
0.32000	-84.73401	-104.57239	-105.14540	-127.58940	-145.89738	0.18710
0.64000	-84.15199	-120.33646	-102.08643	-148.41182	-166.94469	0.37420
1.28000	-87.05383	-141.14478	-112.66442	-169.47607	-188.01627	0.74840
2.56000	-95.22746	-162.20872	-132.88892	-190.54826	-209.08861	1.49679
5.12000	-104.61284	-183.28090	-153.93199	-211.62059	-230.16100	2.99359

POWER=0.4942E-10

FOR THE STRIP AT X= 60.0000

A1= 0.717

FREQUENCY	1/3 OCT.DB OVER ALL	1/3 OCT.DB 60 DEGREE	1/3 OCT.DB 90 DEGREE	1/3 OCT.DB 120 DEGREE	1/3 OCT.DB 150 DEGREE	A1*FREQ
0.00125	-131.91222	-155.05362	-164.17841	-153.73991	-151.95103	0.00090
0.00250	-122.88161	-146.02301	-155.14780	-144.70932	-142.92044	0.00179
0.00500	-113.85117	-136.99242	-146.11722	-135.67882	-133.89012	0.00358
0.01000	-104.82463	-127.96182	-137.08771	-126.65125	-124.86897	0.00717
0.02000	-95.89192	-118.93172	-128.08881	-117.70044	-116.05908	0.01434
0.04000	-87.73921	-109.91647	-119.45926	-109.44620	-108.81140	0.02867
0.08000	-83.11748	-101.30304	-112.90147	-103.67761	-110.69856	0.05734
0.16000	-81.58177	-97.99020	-106.25464	-110.50612	-127.02983	0.11468
0.32000	-80.29413	-102.12260	-99.38382	-129.36827	-147.80824	0.22936
0.64000	-80.25716	-107.94189	-99.40115	-150.34435	-168.87080	0.45873
1.28000	-84.51996	-115.30898	-114.74362	-171.41364	-189.94299	0.91745
2.56000	-95.31758	-131.14229	-135.51668	-192.48598	-211.01534	1.83491
5.12000	-109.74316	-151.88472	-156.57939	-213.55830	-232.08775	3.66982

POWER=0.1288E-09

FOR THE STRIP AT X= 70.0000

A1= 0.870

FREQUENCY	1/3 OCT.DB OVER ALL	1/3 OCT.DB 60 DEGREE	1/3 OCT.DB 90 DEGREE	1/3 OCT.DB 120 DEGREE	1/3 OCT.DB 150 DEGREE	A1*FREQ
0.00125	-127.17233	-150.31216	-159.75983	-149.25124	-147.34770	0.00109
0.00250	-118.14177	-141.28157	-150.72923	-140.22066	-138.31712	0.00218
0.00500	-109.11160	-132.25098	-141.69896	-131.19046	-129.28754	0.00435
0.01000	-100.09363	-123.22046	-132.67850	-122.17244	-120.28540	0.00870
0.02000	-91.25815	-114.19254	-123.85841	-113.34731	-111.67854	0.01741
0.04000	-83.71590	-105.21669	-116.01575	-105.28706	-105.97395	0.03481
0.08000	-80.31926	-97.22601	-109.71989	-102.18100	-112.15643	0.06963
0.16000	-78.81630	-95.74542	-101.71335	-113.08496	-130.45125	0.13925
0.32000	-77.75331	-106.69603	-96.60356	-133.02089	-151.39162	0.27851
0.64000	-79.15921	-126.50037	-102.28825	-154.05116	-172.45982	0.55701
1.28000	-86.24329	-147.52539	-120.91769	-175.12213	-193.53201	1.11403
2.56000	-95.81587	-168.59636	-141.89226	-196.19447	-214.60435	2.22806
5.12000	-105.29523	-189.66869	-162.96153	-217.26695	-235.67662	4.45611

POWER=0.2090E-09

FOR THE STRIP AT X= 80.0000

A1= 1.050

FREQUENCY	1/3 OCT.DB OVER ALL	1/3 OCT.DB 60 DEGREE	1/3 OCT.DB 90 DEGREE	1/3 OCT.DB 120 DEGREE	1/3 OCT.DB 150 DEGREE	A1*FREQ
0.00125	-123.02954	-146.26833	-152.67976	-144.53294	-143.10268	0.00131
0.00250	-113.99899	-137.23772	-143.64922	-135.50244	-134.07222	0.00262
0.00500	-104.97073	-128.20714	-134.62010	-126.47397	-125.04672	0.00525
0.01000	-95.99855	-119.17735	-125.62921	-117.49715	-116.14546	0.01050
0.02000	-87.61838	-110.16150	-116.89954	-109.16148	-108.59435	0.02100
0.04000	-81.40443	-101.24556	-109.28120	-102.99580	-106.17009	0.04199
0.08000	-78.68683	-94.38383	-105.17711	-103.91229	-116.02293	0.08398
0.16000	-77.08075	-94.36705	-99.18672	-117.86453	-135.55988	0.16797
0.32000	-76.43024	-103.63997	-97.86906	-138.37169	-156.57335	0.33594
0.64000	-80.49573	-123.08861	-109.48894	-159.42500	-177.64384	0.67188
1.28000	-89.54413	-144.09995	-129.63936	-180.49673	-198.71619	1.34375
2.56000	-102.84053	-165.17046	-150.67979	-201.56923	-219.78868	2.68750
5.12000	-121.10092	-186.24278	-171.75105	-222.64156	-240.86095	5.37501

POWER=0.2659E-09

FOR THE STRIP AT X= 100.0000

A1= 1.476

FREQUENCY	1/3 OCT.DB OVER ALL	1/3 OCT.DB 60 DEGREE	1/3 OCT.DB 90 DEGREE	1/3 OCT.DB 120 DEGREE	1/3 OCT.DB 150 DEGREE	A1*FREQ
0.00125	-117.16631	-141.61769	-144.50806	-138.20776	-137.22891	0.00184
0.00250	-108.13722	-132.58727	-135.47943	-129.17897	-128.20099	0.00369
0.00500	-99.14143	-123.56219	-126.49844	-120.18773	-119.23245	0.00738
0.01000	-90.53195	-114.57219	-117.72525	-111.55179	-111.13200	0.01476
0.02000	-83.54898	-105.61394	-109.64516	-105.53310	-107.57089	0.02952
0.04000	-78.80087	-96.82152	-104.44244	-104.67670	-112.31544	0.05904
0.08000	-75.97713	-90.42009	-102.44756	-112.37209	-126.92654	0.11807
0.16000	-75.20621	-94.12241	-101.78494	-130.08041	-147.50691	0.23615
0.32000	-79.65697	-109.92194	-110.14067	-150.98940	-168.56310	0.47229
0.64000	-88.51996	-130.67416	-128.50804	-172.05653	-189.63496	0.94458
1.28000	-97.91689	-151.73605	-149.46188	-193.12872	-210.70731	1.88916
2.56000	-106.43924	-172.80824	-170.53041	-214.20122	-231.77965	3.77833
5.12000	-115.46974	-193.88057	-191.60274	-235.27354	-252.85191	7.55666

POWER=0.3057E-09

FOR THE STRIP AT X= 120.0000

A1= 1.995

FREQUENCY	1/3 OCT.DB OVER ALL	1/3 OCT.DB 60 DEGREE	1/3 OCT.DB 90 DEGREE	1/3 OCT.DB 120 DEGREE	1/3 OCT.DB 150 DEGREE	A1*FREQ
0.00125	-110.58279	-136.34373	-135.59218	-130.73138	-130.51064	0.00249
0.00250	-101.57140	-127.32541	-126.58997	-121.72060	-121.50591	0.00499
0.00500	-92.74203	-118.35641	-117.70070	-112.86005	-112.84581	0.00997
0.01000	-85.38373	-109.44482	-109.19957	-105.53247	-108.16695	0.01995
0.02000	-79.55190	-100.64127	-102.29800	-105.97324	-112.40752	0.03989
0.04000	-74.50287	-92.14520	-101.83897	-112.90886	-122.59473	0.07978
0.08000	-73.30150	-86.56554	-108.24271	-128.59999	-141.66339	0.15956
0.16000	-77.97255	-92.15710	-123.09348	-149.31798	-162.65019	0.31913
0.32000	-86.80658	-100.15417	-143.70439	-170.37889	-183.71996	0.63825
0.64000	-96.31767	-116.09413	-164.76146	-191.45091	-204.79228	1.27650
1.28000	-103.48518	-136.84637	-185.83350	-212.52325	-225.86462	2.55300
2.56000	-111.35895	-157.90834	-206.90584	-233.59557	-246.93712	5.10601
5.12000	-118.98558	-178.98036	-227.97813	-254.66808	-268.00928	10.21202

POWER=0.4071E-09

FOR THE STRIP AT X= 160.0000

A1= 3.316

FREQUENCY	1/3 OCT.DB OVER ALL	1/3 OCT.DB 60 DEGREE	1/3 OCT.DB 90 DEGREE	1/3 OCT.DB 120 DEGREE	1/3 OCT.DB 150 DEGREE	A1*FREQ
0.00125	-110.78159	-136.00920	-133.69057	-131.21260	-131.85851	0.00415
0.00250	-102.18942	-127.22444	-125.02275	-122.67950	-123.62265	0.00829
0.00500	-95.39006	-118.69035	-117.50310	-117.24123	-120.69649	0.01658
0.01000	-89.35886	-111.00490	-115.10492	-120.23689	-125.49586	0.03316
0.02000	-82.91005	-106.44994	-119.89165	-126.45959	-132.48358	0.06633
0.04000	-82.89360	-110.60750	-127.02199	-137.92542	-147.30568	0.13265
0.08000	-90.97594	-126.22951	-142.23105	-157.72501	-167.91193	0.26530
0.16000	-99.78781	-146.96233	-162.88930	-178.75096	-188.96886	0.53060
0.32000	-108.53612	-168.02370	-183.94807	-199.82195	-210.04076	1.06121
0.64000	-117.77953	-189.09572	-205.02010	-220.89427	-231.11308	2.12241
1.28000	-125.25868	-210.16806	-226.09244	-241.96640	-252.18539	4.24483
2.56000	-133.00813	-231.24034	-247.16466	-263.03882	-273.25781	8.48966
5.12000	-139.49779	-252.31285	-268.23706	-284.11133	-294.33008	16.97931

POWER=0.4486E-10

FOR THE STRIP AT X= 200.0000

A1= 4.884

FREQUENCY	1/3 OCT.DB OVER ALL	1/3 OCT.DB 60 DEGREE	1/3 OCT.DB 90 DEGREE	1/3 OCT.DB 120 DEGREE	1/3 OCT.DB 150 DEGREE	A1*FREQ
0.00125	-111.54477	-136.43376	-133.42944	-132.24817	-133.73871	0.00610
0.00250	-105.19476	-128.77121	-126.82956	-127.56578	-130.86633	0.01221
0.00500	-100.89285	-124.18419	-127.25980	-131.14293	-135.61005	0.02442
0.01000	-99.04597	-127.37616	-132.82999	-137.13019	-141.75864	0.04884
0.02000	-106.53853	-133.58241	-139.42726	-145.12900	-151.34315	0.09767
0.04000	-124.11035	-144.84401	-152.41501	-162.19070	-170.13077	0.19535
0.08000	-144.63411	-164.56293	-172.66275	-183.05185	-191.10818	0.39069
0.16000	-165.68150	-185.58553	-193.70656	-204.11748	-212.17747	0.78139
0.32000	-186.75325	-206.65620	-214.77815	-225.18968	-233.24983	1.56277
0.64000	-207.82558	-227.72868	-235.85042	-246.26180	-254.32210	3.12554
1.28000	-228.89792	-248.80087	-256.92285	-267.33423	-275.39453	6.25108
2.56000	-249.97032	-269.87305	-277.99512	-288.40674	-296.46680	12.50217
5.12000	-271.04248	-290.94556	-299.06738	-309.47900	-317.53931	25.00433

POWER=0.9396E-12

FOR THE STRIP AT X= 240.0000

A1= 6.560

FREQUENCY	1/3 OCT.DB OVER ALL	1/3 OCT.DB 60 DEGREE	1/3 OCT.DB 90 DEGREE	1/3 OCT.DB 120 DEGREE	1/3 OCT.DB 150 DEGREE	A1*FREQ
0.00125	-114.05963	-137.13278	-135.35736	-135.85271	-138.70642	0.00820
0.00250	-111.62808	-134.58134	-135.66809	-138.54182	-142.55214	0.01640
0.00500	-114.48169	-139.12434	-141.20522	-144.39590	-148.50029	0.03280
0.01000	-120.93050	-145.13673	-147.35628	-150.79100	-155.19424	0.06560
0.02000	-132.77925	-152.53638	-156.48320	-162.46114	-168.70686	0.13121
0.04000	-151.33667	-168.34869	-174.85291	-182.33200	-189.08920	0.26241
0.08000	-172.24893	-189.08502	-195.80545	-203.36084	-210.13818	0.52482
0.16000	-193.31593	-210.14653	-216.87413	-224.43181	-231.20992	1.04965
0.32000	-214.38829	-231.21858	-237.94612	-245.50398	-252.28206	2.09930
0.64000	-235.46053	-252.29085	-259.01855	-266.57642	-273.35449	4.19859
1.28000	-256.53296	-273.36328	-280.09106	-287.64868	-294.42700	8.39719
2.56000	-277.60522	-294.43555	-301.16333	-308.72119	-315.49927	16.79437
5.12000	-298.67749	-315.50806	-322.23584	-329.79370	-336.57153	33.58875

POWER=0.5381E-13

END OF JOB

N*EXIT*